REAL-TIME POWER SYSTEM OPERATIONAL RELIABILITY TOOLS

BY

KAI EMERSON VAN HORN

DISSERTATION

Submitted in partial fulfillment of the requirements
for the degree of Doctor of Philosophy in Electrical and Computer Engineering
in the Graduate College of the
University of Illinois at Urbana-Champaign, 2015

Urbana, Illinois

Doctoral Committee:

Associate Professor Alejandro Domínguez-García, Co-Chair
Professor Peter Sauer, Co-Chair
Professor Venugopal Veeravalli
Assistant Professor Hao Zhu

ABSTRACT

The primary goal of power system operators is to effectively and economically maintain *operational reliability*—a power system is said to be in an operationally reliable state if the supply-demand balance is met, and the system can tolerate the failure of a small number of components without jeopardizing continued operation. In pursuit of this goal, operators rely on so-called *operational reliability tools* to schedule resources and manage uncertainty. Conventional operational reliability tools include market-scheduling tools, e.g., the real-time security-constrained economic dispatch (SCED), and system-monitoring tools, e.g., real-time contingency analysis (RTCA).

Due to the stringent computational speed requirements of real-time operations, conventional operational reliability tools make extensive use of power flow sensitivities to simplify the mathematical representation of the physical electricity system. Moreover, the computation of such sensitivities requires a model of the system, which is typically obtained offline. As such, the effectiveness of these tools is highly dependent on the accuracy of the model from which such sensitivities are computed, which may be compromised due to erroneous input parameters, undetected topology changes, and changes in ambient conditions. Inaccurate sensitivities are an impediment to effective electricity market operation and price formation, as well as compromising system operational reliability.

The 2011 San Diego blackout brought to light an additional shortcoming of conventional operational reliability tools: they do not provide system operators the ability to predict the angle of the voltage across the breaker of a transmission line that will arise in the event of the line's outage—which we refer to as the *outage angle*—or means by which to mitigate such angles. Indeed, the conventional SCED process does not include any means by which to bring outage angle considerations to bare on the generator dispatch, which determines if the system will be in an operationally reliable state.

In this thesis, we address the aforementioned shortcomings of conventional operational reliability tools by formulating a set of measurement-based operational reliability tools and deriving a sensitivity-based approach to monitoring and mitigating line outage angles. To this end, we provide: (i) a measurement-based approach to marginal loss factor (LF) estimation, which harnesses phasor measurement unit (PMU) measurements to estimate the LFs online rather than computing them from a power flow model; (ii) a formulation of the line outage angle factor (LOAF), the computation of which requires only existing sensitivities, the angle factors (AFs) and injection shift factors (ISFs), and which can be deployed to formulate a tool for outage angle monitoring and an angle-constrained SCED; and (iii) a measurement-based formulation of the SCED, which utilizes the measurement-based LFs along with measurement-based ISFs to decouple the SCED process and underlying RTCA from the vulnerabilities associated with a system model. Our hope is that the proposed tools will enhance the real-time operational reliability process and contribute to more effective and efficient power system operations.

To the universe, in homage to the endless stream of confounding and inspiring questions that spring forth from its infinite depths.

ACKNOWLEDGMENTS

First and foremost, I'd like to thank advisers, Professors Alejandro Domíguez-García and Peter Sauer; you gave me that latitude to explore and it was through the time I spent with you fine gentlemen that I learned to find joy in the pursuit of ideas. Alejandro, you have become both my mentor and my friend and I feel very fortunate to have had the opportunity to complete this journey with your guidance; I will cherish alike the memories of our technical discussions and off-hand lunch conversations. Pete, your sound judgment, kind words, and sense of humor have been a source of strength and I am equally grateful to have had your steady hand propelling me forward. Thank you both.

Of course, none of this would have been possible without the amazing group of friends I found here at the University of Illinois, both in the Power Group and outside of it—you folks supported me academically and emotionally in various ways known and unknown throughout the years. I will fondly remember all of the Saturday morning brunches, latté Wednesday walks, group lunches in Everitt and then in Beckman after the Big Move, game nights, MAC nights, and potlucks at 407 S Birch St. Matt, Stanton, Tutku, Tim, Trevor, Raj, Dimitra, Christine, Shamina, Enver, Giang-Chau, Xichen, Jiangmeng, and everyone else who has been a part of this hubbub called graduate school: you are like family and I couldn't have done it without your company and your counsel. Let this be just the beginning for our friendships.

I'd also like to thank Joyce and Robin for your help throughout the years in all things Power Group-related. You endured my trivial and repetitive questions about travel reimbursements with patience and humor and for that I am grateful.

I would be remiss not to mention the people who made this possible in a very literal sense: my family. Mom, Dad, Annette, Hans, Galen, and

Katherine, you collectively raised me, taught me to always question and to be kind and compassionate in words and actions above all else. Your high expectations and ceaseless support endowed me with the self-confidence and enthusiasm for learning that carried me through this endeavor. I love you guys.

I owe special thanks to one Miriam Axelbaum; your tireless and loving support during our past two years together (despite my repeated and prolonged absences) gave me the energy to make it to the end of this long road.

TABLE OF CONTENTS

LIST OF ABBREVIATIONS

AF	Angle Factor
ED	Economic Dispatch
ISO	Independent System Operator
ISF	Injection Shift Factor
LF	Marginal Loss Factor
LMP	Locational Marginal Price
LOAF	Line Outage Angle Factor
LODF	Line Outage Distribution Factor
LSE	Least-Squared-Error Estimation
OPF	Optimal Power Flow
PMU	Phasor Measurement Unit
PTDF	Power Transfer Distribution Factor
RTCA	Real-Time Contingency Analysis
RTO	Regional Transmission Organization
SCED	Security-Constrained Economic Dispatch
UC	Unit Commitment
WLSE	Weighted Least-Squared-Error Estimation

CHAPTER 1

INTRODUCTION

In this chapter, we set the stage for the thesis. To begin, we describe the role of operational reliability tools in the power systems operational context and motivate the need for new operational reliability tools. Next, we describe existing work related to the operational reliability tools we propose and the shortcomings of existing approaches. Then, we describe our contributions and the manner in which they address the identified shortcomings. We close the chapter with a brief outline of the thesis.

1.1 Motivation

Reliable access to electricity is fundamentally important to a functioning modern society and economy. This fact is derived from electricity's status as a key input to numerous processes relied on by its consumers on a day-to-day basis so as to maintain their standard of living and create economic opportunities. As such, consumers require electricity system operators to ensure access to electricity is maintained except under extreme circumstances, which is reflected in power system reliability standards [1]. On the other hand, there are limits to how much consumers can, or are willing to, pay for electricity access. Thus, they further require that system operators supply electricity in the most economic manner possible.

Meeting such requirements is a challenging task for system operators; the electricity system is a complex network composed of tens of thousands of thermal, hydro, and renewable generation resources, loads, and transmission elements, and operating the system is subject to numerous sources of uncertainty, e.g., load uncertainty, equipment outage uncertainty, and the uncertainty associated with renewable generator outputs, such as wind and solar photovoltaic generators. As an additional layer of complexity, system

operators must also schedule resources to meet the supply-demand balance considering multiple decision-making time horizons, from day-ahead (DA) scheduling, with horizons of days to weeks, and based on forecast system conditions; to real-time (RT) scheduling, with horizons of minutes to hours, and based on a combination of measured or estimated system conditions and forecast system conditions. To manage such uncertainty and economically and reliably deliver on-demand access to electricity, system operators rely on operational reliability tools. These tools enable them to strike a balance between consumers' competing requirements of high reliability and economic electricity access. The work presented in this thesis provides an enhanced set of operational reliability tools aimed at assisting system operators in more effectively meeting these requirements.

The majority of the uncertainty faced by system operators comes to bear on real-time scheduling processes, during which the actual operation of the system takes place. Thus, real-time operational reliability tools play the largest role in maintaining operational reliability. Conventional real-time operational reliability tools include market-scheduling tools, e.g., the real-time security-constrained economic dispatch (SCED), and system-monitoring tools, e.g., real-time contingency analysis (RTCA). Furthermore, due to the short time horizons in the real-time operational context, which translate into strict computational requirements, such tools have typically been based on sensitivities derived from a linearized representation of the power system, e.g., marginal loss factors (LFs) and injection shift factors (ISFs), which we will introduce in Section 1.2 and discuss in detail in Chapters 3 and 5, respectively. These tools enable system operators to simultaneously optimize the dispatch of system resources to meet the load and requirements of reliability standards while taking into due consideration the costs of doing so.

System operators, guided by existing real-time operational reliability tools, generally have a long track record of success in maintaining reliable and economic access to electricity. However, a number of high-impact events, e.g., the 2003 Northeast Blackout [2] and the 2011 San Diego Blackout [3], have exposed weaknesses in operational reliability processes that stem primarily from: (i) a lack of adequate tools for monitoring and controlling pre- and post-outage voltage angles at the terminal buses of outaged transmission lines; and (ii) the widespread dependance of conventional tools on a model of the internal system and that of neighboring systems, which may

be out of date or contain erroneous data. Furthermore, real-time operational processes, such as state estimation,[1] the results of which are required to perform conventional RTCA and formulate the SCED, are built around measurements obtained from the telemetry system, primarily the supervisory control and data acquisition system (SCADA). However, SCADA provides non-time-synchronized measurements every two to four seconds [4], which limits its usefulness in the development of next-generation operational tools.

Until recently, there were no readily available means of addressing these weaknesses. However, the rapidly expanding deployment of phasor measurement units (PMUs), which provide time-synchronized measurements at a rate of 30-120 measurements per second [5], is facilitating the proliferation of a new generation of operational tools that harness the very high frequency and time synchronicity of their measurements (see, e.g., [6], [7]). Indeed, thousands of PMUs have been installed in North America over the past decade and many relays come equipped with PMU functionality (see, e.g., [8]). The use of PMU data in real-time operations has been promoted as a means by which to circumvent the shortcomings of the existing telemetry system, and reduce the frequency of occurrence and the magnitude of the impact of preventable outages. In the context of the work we present in this thesis, PMUs enable the estimation of power system sensitivities from measurements collected throughout the system rather than the computation of those sensitivities from a model of the system obtained offline. Such sensitivities play a key role in the development of operational reliability tools.

In this thesis, we address the shortcomings of conventional operational reliability tools and propose a set of enhanced ones, which harness power system sensitivities, both (i) those estimated from PMU measurements, as well as (ii) those derived from a power flow model. To this end, we propose: (i) a measurement-based approach to the estimation of marginal loss factors (LFs), which are a key input for electricity market scheduling processes, e.g., SCED; (ii) a set of line angle monitoring tools based on a proposed generalized approach to the computation of line outage angle factors (LOAFs), which provide system operators a pre-outage mean to manage the post-outage angle

[1] State estimation is a process which utilizes measurements, e.g., voltage, active power flow, from throughout the system and an assumed model of the system to estimate the system state. The system state typically consists of the voltages and voltage angles at each bus, however, it may also include active and reactive power flow and power injection measurements as well as transformer tap positions and switch and breaker statuses [4].

that will arises between the terminal buses of a transmission line if its outage occurs; and (iii) a measurement-based approach to the real-time SCED, which requires sensitivity-based flow constraints and reliability constraints identified using RTCA.

1.2 Background and Related Work

In this section, we provide context for the topics discussed in the thesis and describe the existing work on operational reliability tools while pointing out the shortcomings of such tools. We begin by providing some the background on LFs and LOAFs. Then, we give an overview of the SCED.

1.2.1 Marginal Loss Factors

Transmission losses are an unavoidable result of the physics that governs power transfer over an electric power system. Effectively modeling losses so as to capture their economic and physical impacts has been a goal of power engineers since the emergence of electricity scheduling algorithms [9]. Over the subsequent half century, numerous methods, e.g., penalty factors and the B-coefficients method, have been proposed to represent total and marginal transmission losses—the incremental losses resulting from an incremental increase in the load—in the electricity scheduling problem (see, e.g., [10, 11, 12, 13]).

The emergence of competitive electricity markets based on marginal pricing principles over the past two decades has driven the need to associate a location-specific price with losses. To meet this need, the so-called *marginal loss factors* (LFs) emerged as a mean by which to capture the dependence of system-wide losses on the location of active power injections [13, 14]. Loss factors are linear sensitivities of the system-wide losses with respect to power injections, assuming the change in injection is balanced by a single slack bus or set of slack buses. Conventionally, model-based LFs are derived from the power flow Jacobian [13]; furthermore, the LF computation requires the *a priori* specification of *distributed slack weights*, which define the distribution of the active power mismatch and losses among the buses in the system necessary to maintain the system-wide power balance. Such distributed slack

weights are typically selected based on the bus load distribution or generator output distribution (see, e.g., [15, 16]).

Loss factors are principally used in: (i) market scheduling procedures for setting generator dispatch targets, e.g. SCED, and (ii) the computation of locational marginal prices (LMPs) (see, e.g., [15, 16]). The LFs, through the dispatch targets and LMPs, also impact the distribution of payments among market participants. The losses for large interconnected power systems are substantial and the associated costs are non-trivial. Indeed, the total losses in the PJM Interconnection[2] for 2014 were 17,150 GWh, and the cost of those losses was in excess of $1.4 billion [17]. The economic impacts of inaccuracy in the LFs may likewise be substantial and, as such, accurate LFs are a critical component of efficient and effective electricity market operation.

Existing Approaches and Shortcomings. As stated above, LFs are a necessary component of the real-time market scheduling procedure, and play a key role in the assignment of a location-specific price to losses. The conventional approach to computing LFs relies on the power flow Jacobian, which in turn relies on the availability of an accurate model of the system (see, e.g., [14]). As such, the conventional LFs are vulnerable to undetected changes in the model topology and erroneous model data. Measurement-based approaches to sensitivity estimation that overcome the challenges associated with computing sensitivities from a model have been proposed in [18] and [19]. However, this previous work has not addressed the use of PMU measurements for the estimation of LFs.

1.2.2 Line Outage Angle Factors

It has long been known that a transmission line breaker that has tripped open can be safely reclosed only if the outage angle—the voltage angle difference between the terminal buses of a transmission line after it is outaged—is sufficiently small (see, e.g., [20]). In fact, the failure to reclose a breaker due to a large line outage angle was a contributing factor in the chain of events that ultimately resulted in the 2011 San Diego blackout [3]. More-

[2]The PJM Interconnection is a U.S.-based regional transmission organization which oversees market scheduling processes to serve some 60 million customers and schedules 167 GW of generating capacity.

over, in the case of the San Diego blackout, the system operator did not have in place a systematic mean by which to determine the appropriate actions, e.g., generation redispatch, so as to bring the outage angle within a range that permitted the line breakers to be successfully reclosed. Indeed, the after-the-fact assessment of the blackout event concluded that "underlying factors that contributed to the event... [included] not providing effective tools and operating instructions for use when reclosing lines with large phase angle differences across the reclosing breakers [3]." Furthermore, the report recommended that "transmission operators should have: (1) the tools necessary to determine phase angle differences following the loss of lines; and (2) mitigation and operating plans for reclosing lines with large phase angle differences [3]." The line outage angle factors (LOAFs) are one potential mean of addressing these identified needs.

A LOAF provides the ratio of the difference between the line angle and outage angle, and the flow through the line before the outage occurs. The LOAFs can be used to formulate accurate and computationally efficient tools for assessing the impacts of line outages on voltage angles and appropriate responses by system operators to mitigating reliability issues arising from large line outage angles. However, LOAFs have received scant attention in the academic literature and system operators have yet to recognize their utility and embrace LOAF-based tools.

Existing Approaches and Shortcomings. Formulations of angle-based dispatch tools go back to the 1980s (see, e.g., [21]); the LOAFs were first proposed in [22]. However, such tools focused on the control of phase-shifting transformers and did not address the issue of large line outage angles. Additionally, the derivation of the LOAFs in [22] utilizes the dc assumptions[3] and, as such, the LOAFs remain fixed for all operating points under a specific topology; the derivation also requires the computation of the bus impedance matrix for each outage topology—a computationally burdensome requirement for online applications. Finally, the integration of LOAFs into the SCED and other operational reliability processes and the impact of angle constraints on LMPs remains an unexplored area of research.

[3]The dc assumptions can be stated as follows: (i) the system is lossless, (ii) the voltage at each bus is approximately equal to one p.u., (iii) the difference in the voltage angles between each pair of connected buses is small [13].

1.2.3 The Security-Constrained Economic Dispatch

The majority of electricity consumers in the United States are served by entities that procure energy in Independent System Operator (ISO)- or Regional Transmission Organization (RTO)-run markets [23]. ISO/RTOs oversee reliability-focused scheduling procedures consisting of a sequence of forward markets based on security-constrained unit commitment- and economic dispatch-based algorithms (see, e.g., [24], [25]). The goal of these processes is to schedule resources on various time-scales such that the system operator can maintain the supply-demand balance around the clock, including the impacts of losses, and satisfy operational and physical constraints imposed by the electricity network and reliability standards. Moreover, the market outcomes include resource dispatch targets and the prices for energy, the locational marginal prices (LMPs), and ancillary services [26].[4]

The so-called real-time markets are the final stage in the market scheduling process, and real-time SCED and the underlying RTCA are key components of that stage and key operational reliability tools. Typically, the real-time SCED is formulated using model-based LFs to capture system losses and model-based ISFs to represent network flows [13].

In the power system real-time operational context, system operators are primarily concerned with economically maintaining *operational reliability*. The system is said to be in an operationally reliable state if generator dispatch targets and other controllable system resources are set such that the supply-demand balance is met and so that the system can tolerate the failure of a small number of components without jeopardizing continued operation, known, for a single component failure, as the (N-1)-*reliability criterion* [1]. To achieve operational reliability, system operators have conventionally undertaken three reliability functions: (i) system monitoring, (ii) contingency analysis, and (iii) security-constrained optimal power flow (SCOPF) [13]. System monitoring consists of collecting and processing measurements, e.g., voltages, power injections, or breaker statuses, for use in real-time applications, e.g., state estimation. Contingency analysis harnesses the data from system monitoring along with a system model to perform model-based dc and ac power flow analyses to identify outages in the system that may cause

[4]Ancillary services are reliability products, e.g., spinning reserve, regulating reserve, non-spinning reserve, the provision of which are intended to assists the system operator with managing uncertainty in real-time operations (see, e.g. [25]).

overloads on system equipment and thus compromise operational reliability. The overloads identified by contingency analysis are utilized with system operational constraints, LFs, and system model data to formulate the real-time SCED—the formulation of the SCOPF used in real-time operations.

The SCED was first formulated more than 40 years ago [27]. Over the years, SCED research has focused on improving computational speed and incorporating additional system and reliability information, e.g., transient stability constraints and remedial actions, into the problem formulation (see, e.g., [28]). More recent developments in methods for improving SCED solution computational time have focused on reducing the size of the problem, e.g., by eliminating unnecessary constraints (see e.g., [29]), or by decomposing the problem into a series of less computationally burdensome subproblems via methods such as Benders' decomposition (see, e.g., [30]). Furthermore, the introduction of market-based scheduling for electricity and reserves necessitates more complex formulations of the SCED (see, e.g., [31]). Also, in the past two decades, improvements in optimization methods and the availability and economy of computational resources have driven a surge in the exploration of probabilistic methods, e.g. stochastic OPF, for incorporating reliability considerations into the SCED (see, e.g., [32]). In practical settings, e.g., ISO/RTO operations, the deterministic, single-stage, linear formulation of the SCED is in widespread use (see, e.g. [24, 25]).

Existing Approaches and Shortcomings. In order to perform conventional contingency analysis, compute LFs, and formulate power flow, network flow, and security constraints in the real-time SCED, the system operator requires an up-to-date model of the ISO/RTO's electricity system and that of neighboring systems, which is typically derived from the output of a state estimator. The state estimator-based model is vulnerable to errors due to numerous phenomena, e.g., undetected changes in the internal system topology and erroneous model parameters [33], as well as inaccurate representations of neighboring systems [34]. Further, model line parameters errors can arise as a result of assumptions made when computing model parameter values, e.g., the extent of line transposition and non-homogeneity in conductor material due to partial facility upgrades/reconductoring [35]. Also, model parameter values are impacted dynamically by natural phenomena, e.g., mutual conductance, temperature, humidity, and ground conductance [36].

The accuracy of conventional operational reliability processes, e.g., the security constraints identified through contingency analysis and the dispatch targets and LMPs determined in the model-based real-time SCED, are coupled with the accuracy of the system model and the sensitivities computed from that system model and, as such, subject to the same vulnerabilities. Inaccurate LFs and ISFs, contingency analysis, dispatch targets, and LMPs have economic implications, e.g., sending incorrect local price signals and over/under payment to resources, as well as system reliability implications, e.g., failure to operate the system in an N-1 secure state which can lead to unintended equipment overloads and outages [3].

Several approaches to identifying and handling erroneous data in state estimation have been proposed (see, e.g., [4]). There has also been a great deal of work on identifying topology errors using various means (e.g., state estimation), see, e.g., [37, 38, 39]. Further, ISOs/RTOs update system model data periodically as erroneous data is identified through ex-post analysis, e.g., the analysis of non-convergent state-estimator solutions, and reporting by market participants (see, e.g., [40]). However, even with these error detection and correction algorithms and processes in place, the potential for erroneous model data and topological errors persists in real-time operations due to continued reliance of many processes on a system model, and presents a challenge to reliable and economic power system operations (see, e.g., [41]).

1.3 Contributions of the Thesis

In this thesis, we develop a set of measurement-based real-time operational reliability tools aimed at eradicating the model-dependance of the conventional real-time SCED and contingency analysis—the cornerstones of operational reliability. To fully eradicate the model-dependence of the SCED, we develop a measurement-based approach to estimating LFs. Furthermore, to extend the scope and effectiveness of operational reliability tools, we propose a generalized formulation of the line outage angle factors (LOAFs), which form the basis of an operational reliability tool used to assess whether tripped transmission lines can be safely reclosed, and, if necessary, to determine a set of least-cost redispatch actions to take to make reclosure possible. In what follows, we describe the details of each of these contributions.

1.3.1 Measurement-Based Marginal Loss Factors

We propose a measurement-based approach to the computation of LFs. Unlike conventional LF computation approaches, ours does not rely on a model of the system obtained offline. Instead, we estimate the LFs using load and generation measurements obtained from PMUs. Furthermore, the LFs estimated using our approach do not depend on arbitrarily selected distributed slack weights, i.e., our approach will produce LFs consistent with the responses of generators to load changes in real-time. In fact, our estimated LFs enable us to learn the "true" distributed slack weights, which may be useful for determining resource performance when providing ancillary services, e.g., regulating reserves. In addition, our approach harnesses the existing practice to collect load and generator output measurements for use in market settlements, although its implementation would require the frequency with which such measurement are collected to be increased.

The deployment of our measurement-based LF approach in the real-time SCED can eliminate the impacts of erroneous data on computed losses, which can significantly improve the accuracy of the dispatch and LMPs resulting from the market.

1.3.2 Outage Angle Monitoring Tools

We develop a set of effective and computationally efficient tools for use by system operators in addressing the challenge of large line outage angle monitoring and control. To develop these tools, we derive the LOAFs using a linearized power flow model (computed without the dc assumptions) taking a sensitivity-focused approach based on the angle factors (AFs) and ISFs. Our approach harnesses the concept of the flow-canceling transaction (FCT) used in the formulation of the sensitivity-based quantities commonly utilized in contingency analysis, e.g., the line outage distribution factors (LODFs) [42]. However, we generalize the FCT concept by including the impacts of line losses in its derivation. Using our proposed approach, we are able to compute the LOAF of any line from a single system topology—the outage-free topology. In addition, we show how the LOAFs can be estimated using PMU measurements. Finally, we show how the LOAFs can be used for (i) online angle monitoring, (ii) representing angle-reliability considerations in the

SCED via outage angle constraints, and (iii) to derive an angle component of the LMP, which provides economic signals as to the buses at which active power injections relieve and exacerbate large line outage angles. Such information can be used to incentivize reliability-preserving behavior from market participants. LOAFs can be deployed in both the real-time and day-ahead market contexts.

1.3.3 Measurement-Based Real-Time Security-Constrained Economic Dispatch

We propose a measurement-based approach to the real-time SCED with the goal of overcoming the shortcomings of the model-based SCED described in Section 1.2.3. The crux of our approach is the reformulation of the SCED constraints using more accurate data—removing model-based quantities and replacing them with measurement-based estimates of the same quantities. Specifically, we reformulate three types of constraints: (i) the power balance constraint; (ii) network flow constraints, and (iii) security constraints. In the model-based SCED, (i) depends on the the model-based LFs and (ii) and (iii) depend on model-based ISFs and sensitivities derived from ISFs. Instead of relying on model-based LFs and ISFs, our approach utilizes our proposed LF estimation approach, and a measurement-based method for estimating ISFs similar to that described in [18] and [43]. Furthermore, we propose an extended SCED which includes outage angle constraints, which, using our estimation approach, can be formulated using sensitivities estimated from PMU measurements.

By moving away from a model-based representation of the network, our approach virtually eliminates the impacts of phenomena such as undetected changes in system topology and erroneous model parameters on the real-time SCED outcomes. Furthermore, by computing sensitivities directly from measurements, the measurement-based SCED can be formulated without the output of a topology processor and state estimator, which may be advantageous for cases in which the state estimator fails to converge (see, e.g., [2, 41]). Our measurement-based approach also removes the requirement to define an arbitrary distributed slack bus policy in order to compute the ISFs, which is a fundamental limitation of model-based ISFs. Finally, the measurement-

based sensitivities can be used to enhance contingency selection, which, as we show, can improved contingency analysis by identifying potential cases of security constraint omission and commission due to model errors that will subsequently impact the SCED formulation and solution.

1.4 Thesis Organization

In this section, we give an overview of the structure of the thesis; it is organized as follows:

Chapter 2. The model-based operational reliability tools presented throughout the thesis make extensive use of: (i) the distributed slack bus power flow; (ii) the generalized power flow sensitivities; and (iii) both linearized ac- and dc-based active power flow sensitivities. Furthermore, these tools are implemented primarily via variants of the real-time economic dispatch (ED) process. Hence, in this chapter, we introduce these concepts as well as providing an introduction to the notation used throughout the thesis.

Chapter 3. The accurate representation of losses in the (typically linear) real-time ED is of central importance to maintaining operational reliability and ensuring accurate economic incentives are provided to market participants. Conventionally, losses have been represented using LFs computed from a model of the system obtained offline and with respect to a pre-specified distributed slack policy. However, owing to the dependence of such LFs on a model of the system, which may contain errors, and the underlying slack policy selection, the LFs computed with conventional methods may not be accurate. In this chapter, we give an overview of the conventional approach to computing LFs based on the distributed slack bus power flow, illustrating the dependence of the computation on the distributed slack policy selection. Then, we formulate a measurement-based approach to estimating the LFs, which harnesses PMU measurements at loads and generators. Moreover, we provide the results of case studies carried out to demonstrate the impacts on market outcomes of erroneous LFs and the adaptability of the proposed measurement-based LFs.

The work presented in this chapter was submitted for publication in [44].

Chapter 4. The 2011 San Diego blackout brought to light the shortcomings of existing operational reliability tools with regard to identifying and mitigating large line outage angles. However, since the blackout, no new approaches to assessing line outage angles have appeared in the literature to address the gaps in existing operational reliability tools exposed by the blackout. To the contrary, the needs have only grown, with system operators echoing the calls in the San Diego blackout after-the-fact assessment report to develop the needed tools to assess the potential impacts of line outages on line outage angles (see, e.g., [45]). In this chapter, we describe a generalized approach to computing LOAFs based on existing power flow sensitivities that heeds these calls. We demonstrate how our proposed LOAFs can be used to formulate tools for monitoring outage angles, as well as those for mitigating them via manual dispatch decisions and systematically and economically via an extended real-time ED. Furthermore, we show how the measurement-based approach used to compute LFs can likewise be used to compute LOAFs from PMU measurements alone, i.e., without the need of a system model.

The work presented in this chapter was published in [46] and has been submitted for publication in [47].

Chapter 5. The real-time SCED is the primary tool used by system operators to maintain operational reliability. Via the SCED, system operators determine generator set points and LMPs that, in theory, meet the N-1 security criterion in the most economic manner possible. However, the conventional SCED formulation depends heavily on sensitivities computed from a model of the system: LFs and ISFs, as well as sensitivities derived from ISFs. Furthermore, the process of contingency analysis, which drives the construction of the set of reliability constraints that will be included in each SCED formulation, also depends on the availability of an accurate system model. If the system model proves to be inaccurate, the dispatch targets and LMPs may also be inaccurate, which can cause reliability issues, e.g., a failure to achieve the N-1 security criterion, and economic issues, e.g., the inappropriate distribution of payments among market participants.

In this chapter we address these issues by bringing together the LF estimation approach proposed in this thesis with an approach to estimating ISFs in order to formulate a measurement-based SCED. The formulation of our

measurement-based SCED does not require access to an accurate model of the system, rather we estimate the sensitivities used in the SCED formulation via PMU measurements. In doing so, we overcome the challenges with the conventional SCED described above. We demonstrate the extent to which modeling errors can impact the SCED and that to which our measurement-based SCED can alleviate those impacts with a series of case studies.

The work presented in this chapter was published in [48] and [49].

Chapter 6. In this chapter, we conclude the thesis with a summary of the contributions.

CHAPTER 2

PRELIMINARIES

In this chapter, we give an overview of some power system modeling fundamentals that will be used in the subsequent chapters to derive model-based operational reliability tools, which we will use as a basis of comparison for our proposed tools. First, we introduce the distributed slack bus power flow. Then, using the distributed slack bus power flow, we derive the fundamental power flow sensitivities relating the changes in bus voltages, voltage angles and system-wide active power mismatch to changes in the active and reactive power injections. Additionally, we derived the injection shift factor (ISF) matrix, which is used extensively in real-time operations to represent active power flows. We also introduce the basic real-time economic dispatch (ED) formulation and the notation that we use throughout the thesis.

2.1 Introduction

The operational reliability tools presented in this thesis rely heavily on two fundamental power system concepts. The first concept is the the distributed slack bus power flow formulation (see, e.g., [50]). In this power flow formulation, the active power balance is maintained by distributing the slack, i.e., the mismatch between total active power generation and total active power load plus losses, among several buses.[1] The second concept is the fundamental power flow sensitivities. These sensitivities provide the total variation in the power system state vector (i.e., the vector of voltage angles, voltage magnitudes, and active power mismatch) with respect to active and reactive power bus injections and are the basis for the derivation of other widely used sensitivities, e.g., marginal loss factors (LFs) and ISFs.

[1] We will show that the conventional single slack-bus formulation is a particular case of the more general one presented here.

Furthermore, as stated previously, market scheduling tools are critically important to system operators in their pursuit of operational reliability. To this end, we give an overview of the basic scheduling problem solved by system operators in the real-time setting: the so-called real-time ED. We build on this basic market scheduling problem throughout the thesis to formulate our proposed operational reliability tools.

2.2 Distributed Slack Bus Power Flow Formulation

Consider a system with N buses indexed by $\mathcal{N} = \{1, \ldots, N\}$. Let V_n and θ_n denote the voltage magnitude and angle, respectively, at a bus n, and define $V = [V_1, \ldots, V_N]^T$ and $\theta = [\theta_1, \ldots, \theta_N]^T$, with $\theta_1 = 0$ (i.e., we take bus 1 to be the angle reference bus). Additionally, let $\mathcal{L} = \{\ell_1, \ldots, \ell_L\}$, $|\mathcal{L}| = L$, where each ℓ_l is an ordered pair (n, m), $n, m \in \mathcal{N}$, representing a transmission line between buses n and m, with the convention that positive active power flow on such a line is in the direction *from n to m*. Moreover, assume that there are G generators indexed by $\mathcal{G} = \{1, \ldots, G\}$, D loads indexed by $\mathcal{D} = \{1, \ldots, D\}$, and let $\mathcal{G}_n \subseteq \mathcal{G}$ denote the subset of generators at bus $n \in \mathcal{N}$, and let $\mathcal{D}_m \subseteq \mathcal{D}$ denote the subset of loads at bus $m \in \mathcal{N}$.

Throughout the thesis, we use the terms *pre-allocation* and *schedule* to make a distinction between the generator (load) output (demand) before and after, respectively, the system-wide losses (which are not known *a priori*) have been allocated to generators and loads. Let $\tilde{P}_i^g$ (P_i^g) denote the pre-allocation (schedule) output of generator $i \in \mathcal{G}$, with the convention that $\tilde{P}_i^g, P_i^g > 0$ if the generator injects active power into the system. Similarly, let $\tilde{P}_v^d$ (P_v^d) denote the pre-allocation (schedule) demand, with the convention that $\tilde{P}_v^d, P_v^d > 0$ if the load withdraws active power from the system. Further, let $\tilde{Q}_i^g$ (Q_i^g) denote the pre-allocation (schedule) reactive output of generator $i \in \mathcal{G}$, with the convention that $\tilde{Q}_i^g$, $Q_i^g > 0$ if the generator injects reactive power into the system, and $\tilde{Q}_v^d$ (Q_v^d) denote the pre-allocation (schedule) reactive consumption of load $v \in \mathcal{D}$, with the convention that $\tilde{Q}_v^d$ (Q_v^d) if the load withdraws reactive power from the system.

Then, define, for each bus $n \in \mathcal{N}$, the pre-allocation and schedule net

active power injections, respectively, as

$$\tilde{P}_n = \sum_{i \in \mathcal{G}_n} \tilde{P}_i^g - \sum_{v \in \mathcal{D}_n} \tilde{P}_v^d, \tag{2.1}$$

$$P_n = \sum_{i \in \mathcal{G}_n} P_i^g - \sum_{v \in \mathcal{D}_n} P_v^d, \tag{2.2}$$

and the pre-allocation and schedule reactive power injections as

$$\tilde{Q}_n = \sum_{i \in \mathcal{G}_n} \tilde{Q}_i^g - \sum_{v \in \mathcal{D}_n} \tilde{Q}_v^d, \tag{2.3}$$

$$Q_n = \sum_{i \in \mathcal{G}_n} Q_i^g - \sum_{v \in \mathcal{D}_n} Q_v^d. \tag{2.4}$$

Moreover, define the vector of pre-allocation (schedule) net injections at all buses as $\tilde{P} = [\tilde{P}_1, \ldots, \tilde{P}_N]^T$ ($P = [P_1, \ldots, P_N]^T$) and those of pre-allocation (schedule) reactive net injections as $\tilde{Q} = [\tilde{Q}_1, \ldots, \tilde{Q}_N]^T$ ($Q = [Q_1, \ldots, Q_N]^T$).

The distributed slack bus power flow formulation requires the selection of a distributed slack *policy* [14], which consists of specifying a vector of *distributed slack weights*, $\alpha = [\alpha_1, \ldots, \alpha_N]^T$, $\alpha_i \in \mathbb{R}$, satisfying $\mathbb{1}_N^T \alpha = 1$, where $\mathbb{1}_N$ is the N-dimensional all-ones vector. These weights determine the manner in which the active power mismatch due to losses and discrepancies between total pre-allocation generation and load—the so-called *slack*, which we denote by p_m— will be balanced at each bus $n \in \mathcal{N}$. Then, we have that the relationship between the pre-allocation and scheduled net active and reactive power injection vectors is given by

$$P = \tilde{P} + p_m \alpha, \tag{2.5}$$

and

$$Q = \tilde{Q} + q_m, \tag{2.6}$$

where q_m defines the allocation of reactive power at voltage-controlled buses that adhere to some specified voltage control policy, which is typically determined implicitly in the power flow problem by making the conventional assumption that the voltages remain constant at such buses (see, e.g., [13]).

Utilizing the quantities defined in (2.1)–(2.6), the steady-state behavior of the power system can be described by the distributed slack bus power flow

equations as follows:

$$\begin{bmatrix} \tilde{P} \\ \tilde{Q} \end{bmatrix} - \begin{bmatrix} p(\theta, V) - p_m \alpha \\ q(\theta, V) - q_m \end{bmatrix} = 0, \tag{2.7}$$

where

$$p(\theta, V) = [p_1(\theta, V), \ldots, p_N(\theta, V)]^T,$$
$$q(\theta, V) = [q_1(\theta, V), \ldots, q_N(\theta, V)]^T,$$

with

$$p_n(\theta, V) = \sum_{j \in \mathcal{N}} V_n V_j (G[n, j] \cos(\theta_n - \theta_j) + B[n, j] \sin(\theta_n - \theta_j)),\ n = 1, \ldots, N,$$

$$q_n(\theta, V) = \sum_{j \in \mathcal{N}} V_n V_j (G[n, j] \sin(\theta_n - \theta_j) - B[n, j] \cos(\theta_n - \theta_j)),\ n = 1, \ldots, N,$$

where $B[n, j] = B[j, n]$,[2] and $B[n, j]$ and $G[n, j]$ are, respectively, the real and imaginary parts of the (n, j)th entry of the bus admittance matrix. Moreover, summing the active power equations in (2.7) yields the following expression for the active power mismatch:

$$p_m = \sum_{n \in \mathcal{N}} \alpha_n p_m = P^\ell(\theta, V) - \sum_{n \in \mathcal{N}} \tilde{P}_n, \tag{2.8}$$

where

$$P^\ell(\theta, V) = \sum_{n \in \mathcal{N}} p_n(\theta, V) = \sum_{n \in \mathcal{N}} \sum_{j \in \mathcal{N}} V_n V_j G[n, j] \cos(\theta_n - \theta_j)$$

are the system-wide losses.

We note that if α is selected such that $\alpha_n = 1$ for $n = 1$ and zero otherwise, i.e., bus 1 picks up the slack, then, from (2.5) and (2.7), we have that

$$P_n = \begin{cases} \tilde{P}_n + p_m = p_n(\theta, V) & \text{for } n = 1, \\ \tilde{P}_n = p_n(\theta, V) & \forall n \in \mathcal{N} \setminus \{1\}. \end{cases}$$

With such an α, $\tilde{P}_1$ can be selected arbitrarily and (2.7) is equivalent to the

[2]The assumption that $B[n, j] = B[j, n]$ is equivalent to assuming that there are no phase-shifting transformers in the system.

conventional single-slack-bus power flow formulation (see, e.g., [13]).

Finally, we can compactly write the power flow equations in (2.7) as follows:

$$g(x, \tilde{P}, \tilde{Q}) = \begin{bmatrix} \tilde{P} \\ \tilde{Q} \end{bmatrix} - \begin{bmatrix} p(\theta, V) - p_m \alpha \\ q(\theta, V) - q_m \end{bmatrix} = 0, \tag{2.9}$$

where $x = [\theta_2, \ldots, \theta_N, V_1, \ldots, V_N, p_m]^T$, and $g(\cdot, \cdot, \cdot)$ is assumed to be continuously differentiable with respect to x, $\tilde{P}$, and $\tilde{Q}$.

2.3 Fundamental Power Flow Sensitivities

The fundamental power flow sensitivities relate the changes in the state vector, x, to changes in the pre-allocation bus injections of active and reactive power, including the impacts of the distributed slack and voltage control policies applied in the system. As demonstrated throughout this thesis, these sensitivities are the basis for the derivation of the other widely used power flow sensitivities, e.g. LFs and ISFs.

Suppose the system defined in (2.9) is operating at the point (x_0, P_0, Q_0), i.e., $g(x_0, P_0, Q_0) = 0$, and, without loss of generality, assume that $p_m = 0$, $q_m = 0$ at (x_0, P_0, Q_0). Let $\tilde{P} = P_0 + \Delta P'$, $\tilde{Q} = Q_0 + \Delta Q'$, and $x = x_0 + \Delta x'$, where $\Delta P'$ ($\Delta Q'$) is an active (reactive) power perturbation in the pre-allocation quantities, which in this case happen to coincide with the scheduled quantities since $p_m = q_m = 0$, and $\Delta x'$ is the system response to such a perturbation prior to control actions, which we discuss below. Then, assuming $\Delta x'$, $\Delta P'$, and $\Delta Q'$ are sufficiently small, we can approximate $g(x, \tilde{P}, \tilde{Q})$ as

$$g(x, \tilde{P}, \tilde{Q}) \approx g(x_0, P_0, Q_0) + J\Delta x' + C\Delta P' + D\Delta Q', \tag{2.10}$$

with

$$J = \left.\frac{\partial g}{\partial x}\right|_{x_0} = \begin{bmatrix} -\frac{\partial p}{\partial \theta}|_{x_0} & -\frac{\partial p}{\partial V}|_{x_0} & \alpha \\ -\frac{\partial q}{\partial \theta}|_{x_0} & -\frac{\partial q}{\partial V}|_{x_0} & 0 \end{bmatrix},$$

$$C = \frac{\partial g}{\partial \tilde{P}} = \begin{bmatrix} I_{N\times N} \\ 0_{N\times N} \end{bmatrix}, \quad D = \frac{\partial g}{\partial \tilde{Q}} = \begin{bmatrix} 0_{N\times N} \\ I_{N\times N} \end{bmatrix},$$

where $I_{N\times N}$ ($0_{N\times N}$) is the $N \times N$ identity (all-zeros) matrix. By definition,

$g(x_0, P_0, Q_0) = 0$ and $g(x, \tilde{P}, Q) = 0$. Thus, from (2.10) we have that

$$0 \approx J\Delta x' + C\Delta P' + D\Delta Q'. \tag{2.11}$$

Next, assume that J, which is the Jacobian of the power flow equations, is invertible around (x_0, P_0, Q_0). Accordingly, we may solve (2.11) for $\Delta x'$ to arrive at

$$\Delta x' \approx -J^{-1}C\Delta P' - J^{-1}D\Delta Q', \tag{2.12}$$

which describes the *pre-control-response* change in x with respect to the perturbation $(\Delta P', \Delta Q')$. However, in a power system, a perturbation $(\Delta P', \Delta Q')$ provokes a response by the controls in order to: (i) maintain the active power balance and (ii) maintain the voltage-controlled bus voltages at constant values (under the conventional power flow assumptions). Let $\Delta P''$ and $\Delta Q''$ be, respectively, the allocations of active and reactive power to each bus to achieve (i) and (ii),[3] and let $\Delta x''$ be the additional change in x due to $\Delta P''$ and $\Delta Q''$, which, assuming $\Delta P''$ and $\Delta Q''$ are sufficiently small, is given by

$$\Delta x'' \approx -J^{-1}C\Delta P'' - J^{-1}D\Delta Q''. \tag{2.13}$$

Then, the total variation in x due to the perturbation and control response can be expressed as follows:

$$\Delta x = \Delta x' + \Delta x''. \tag{2.14}$$

By substituting (2.12) and (2.13) into (2.14), we arrive at

$$\Delta x \approx -J^{-1}C(\Delta P' + \Delta P'') - J^{-1}D(\Delta Q' + \Delta Q''). \tag{2.15}$$

Now, partition the inverse Jacobian as follows:

$$J^{-1} = \begin{bmatrix} -F & -M \\ -E & -H \\ -r^T & -w^T \end{bmatrix}, \tag{2.16}$$

where $F, M \in \mathbb{R}^{(N-1)\times N}$, $E, H \in \mathbb{R}^{N\times N}$, $r, w \in \mathbb{R}^N$; then, from (2.15) and

[3]We note that the selection of a voltage policy fully specifies the reactive power mismatch that will be allocated to each voltage-controlled bus, i.e., $q_m = \Delta Q''$.

(2.16) we conclude that

$$\Delta\theta \approx F(\Delta P' + \Delta P'') + M(\Delta Q' + \Delta Q''), \tag{2.17}$$

$$\Delta V \approx E(\Delta P' + \Delta P'') + H(\Delta Q' + \Delta Q''), \tag{2.18}$$

and

$$\Delta p_m \approx r^T(\Delta P' + \Delta P'') + w^T(\Delta Q' + \Delta Q''). \tag{2.19}$$

For notational simplicity and without loss of generality, suppose the buses are numbered such that voltage-controlled buses are numbered first followed by the non-voltage-controlled buses, and define N^c and N^u to be the number of voltage-controlled and non-voltage-controlled buses, respectively, with $N^c + N^u = N$. Then, partition E, H, and M as follows:

$$E = \begin{bmatrix} E_{cc} & E_{cu} \\ E_{uc} & E_{uu} \end{bmatrix},\ H = \begin{bmatrix} H_{cc} & H_{cu} \\ H_{uc} & H_{uu} \end{bmatrix}, \tag{2.20}$$

$$\text{and } M = \begin{bmatrix} M_{cc} & M_{cu} \\ M_{uc} & M_{uu} \end{bmatrix}, \tag{2.21}$$

where the subscripts c and u indicate those elements of the matrices associated with voltage-controlled and non-voltage-controlled buses, respectively, and E_{cc}, H_{cc}, $M_{cc} \in \mathbb{R}^{N^c \times N^c}$, E_{cu}, H_{cu}, $M_{cu} \in \mathbb{R}^{N^c \times N^u}$, E_{uc}, H_{uc}, $M_{uc} \in \mathbb{R}^{N^u \times N^c}$, and E_{uu}, H_{uu}, $M_{uu} \in \mathbb{R}^{N^u \times N^u}$.

Next, partition $\Delta V = [\Delta V_c^T,\ \Delta V_u^T]^T$ and $\Delta Q'' = [\Delta Q_c''^T,\ \Delta Q_u''^T]^T$ and observe that $\Delta V_c = 0_{N^c}$ and $\Delta Q_u'' = 0_{N^u}$ due to (ii) above, where 0_{N^c} and 0_{N^u} are N^c- and N^u-dimensional all-zeros vectors, respectively. Then, from (2.18), we have that

$$0_{N^c} \approx E_c(\Delta P' + \Delta P'') + H_c\Delta Q' + H_{cc}\Delta Q_c'', \tag{2.22}$$

where $E_c = \begin{bmatrix} E_{cc} & E_{cu} \end{bmatrix}$ and $H_c = \begin{bmatrix} H_{cc} & H_{cu} \end{bmatrix}$.

Furthermore, from (2.12), the we have that the active power mismatch that arises due to $\Delta P'$ and $\Delta Q'$ is given by

$$\Delta p_m' \approx r^T\Delta P' + w^T\Delta Q'. \tag{2.23}$$

However, by definition, the active power control response is given by

$$\Delta P'' = \Delta p'_m \alpha. \tag{2.24}$$

Thus, by substituting (2.23) into (2.24), we arrive at

$$\Delta P'' = \alpha(r^T \Delta P' + w^T \Delta Q'). \tag{2.25}$$

Moreover, by solving for $H_{cc}\Delta Q''_c$ in (2.22) we obtain

$$H_{cc}\Delta Q''_c \approx -E_c(\Delta P' + \Delta P'') - H_c \Delta Q'. \tag{2.26}$$

Then, by substituting (2.25) into (2.26) and rearranging, we obtain the reactive power control response required to meet the specified voltage policy

$$\Delta Q''_c \approx U\Delta P' + W\Delta Q', \tag{2.27}$$

where

$$U = -H_{cc}^{-1}(E_c + E_c \alpha r^T),$$

and

$$W = -H_{cc}^{-1}(H_c + E_c \alpha w^T),$$

and the existence of H_{cc}^{-1} is guaranteed by the invertibility of J and the matrix inversion lemma (see, e.g., [51]).

Now, by substituting (2.25) and (2.27) into (2.17) and rearranging, we arrive at

$$\Delta\theta \approx \Omega\Delta P' + \Omega^q \Delta Q', \tag{2.28}$$

where

$$\Omega = F + F\alpha r^T + M_{c^*}U, \tag{2.29}$$

$$\Omega^q = M + F\alpha w^T + M_{c^*}W), \tag{2.30}$$

and $M_{c^*} = [M_{cc}^T, M_{uc}^T]^T$; Ω (Ω^q) is the $N \times N$ matrix of model-based active (reactive) power angle factors (AFs), which will be utilized in Chapter 4 to derive the LOAFs. Furthermore, the components of Ω (Ω^q) have the following intuitive physical interpretation: (i) F (M) is the portion of $\Delta\theta$ attributable directly to the perturbation $\Delta P'$ ($\Delta Q'$); (ii) $F\alpha r^T$ ($F\alpha w^T$) is the portion of $\Delta\theta$ attributable to the system control response to the perturbation

$\Delta P'$ ($\Delta Q'$) to maintain the active power balance plus changes in the active power losses; and (iii) $M_{c^*}U$ ($M_{c^*}W$) is the portion of $\Delta\theta$ attributable to the system control response to the perturbation $\Delta P'$ ($\Delta Q'$) to maintain voltages according to the specified voltage policy, e.g., constant voltages, at voltage-controlled buses.

Additionally, by substituting (2.25) and (2.27) into (2.18) and rearranging, we arrive at

$$\Delta V \approx \Pi \Delta P' + \Pi^q \Delta Q', \tag{2.31}$$

where

$$\Pi = E + E\alpha r^T + H_{c^*}U,$$

$$\Pi^q = H + E\alpha w^T + H_{c^*}W,$$

and $H_{c^*} = [H_{cc}^T, H_{uc}^T]^T$; we note that $\Delta V_c = 0$ in (2.31) in accordance with the conventional power flow voltage assumption, a proof of which we provide in Appendix A. Moreover, as in the case of the AFs, the components of Π (Π^q) have the following intuitive physical interpretation: (i) E (H) is the portion of ΔV attributable directly to the perturbation $\Delta P'$ ($\Delta Q'$); (ii) $E\alpha r^T$ ($H\alpha w^T$) is the portion of ΔV attributable to the system control response to the perturbation $\Delta P'$ ($\Delta Q'$) to maintain the active power balance plus changes in the active power losses; and (iii) $H_{c^*}U$ ($H_{c^*}W$) is the portion of ΔV attributable to the system control response to the perturbation $\Delta P'$ ($\Delta Q'$) to maintain voltages according to the specified voltage policy at voltage-controlled buses.

Then, by substituting (2.25) and (2.27) into (2.19) and rearranging, we have also that

$$\Delta p_m \approx \gamma^T \Delta P' + (\gamma^q)^T \Delta Q', \tag{2.32}$$

where

$$\gamma^T = r^T + r^T \alpha r^T + w_c^T U,$$

$$(\gamma^q)^T = w^T + r^T \alpha w^T + w_c^T W,$$

and $w = [w_c^T, w_u^T]^T$. We note also that $\Delta p_m = 0$ in (2.32), as required by (2.5) after the active power control actions have taken place to update the pre-allocation quantities to schedule quantities, and a proof of which we provide in Appendix A. Moreover, the components of γ (γ^q) have an analogous physical interpretation to that given for (2.28) and (2.31).

Finally, by combining (2.28), (2.31), and (2.32), we have that the total variation in Δx with respect to a perturbation in the pre-allocation is given by:

$$\Delta x \approx \Theta \Delta P' + \Theta^q \Delta Q', \tag{2.33}$$

where

$$\Theta = \begin{bmatrix} \Omega \\ \Pi \\ \gamma^T \end{bmatrix}, \qquad \Theta^q = \begin{bmatrix} \Omega^q \\ \Pi^q \\ (\gamma^q)^T \end{bmatrix}.$$

The quantities Θ and Θ^q are the fundamental power flow sensitivities.

2.4 Line Flow Sensitivities

The computation of the impacts on line active power flows of changes in bus active power injections, represented by the ISFs, is of pivotal importance for online tools used to maintain operational reliability, e.g., the real-time ED. To derive the ISFs, define $P^f_{l,n} = h_{l,n}(x)$, where $h_{l,n} : \mathbb{R}^{2N} \to \mathbb{R}^L$, to be the active power flow injected into line ℓ_l at the bus n end, which, without loss of generality, we will assume is the *from* bus. Then, we can describe the variation in the active power flow, denoted by $\Delta P^f_{l,n}$, in terms of the variation in Δx, derived in (2.33), for Δx small, as follows:

$$\Delta P^f_{l,n} \approx s^T_{l,n} \Delta x, \tag{2.34}$$

where $s_{l,n} = \frac{\partial h_{l,n}}{\partial x}|_{x_0}$. Next, by substituting (2.33) into (2.34) and rearranging, we obtain

$$\Delta P^f_{l,n} \approx \Psi_l \Delta P' + \Psi^q_l \Delta Q', \tag{2.35}$$

where

$$\Psi_l = -s^T_{l,n}(J^{-1}C + J^{-1}C\alpha r^T + B_{c^*}U), \tag{2.36}$$

$$\Psi^q_l = -s^T_{l,n}(J^{-1}D + J^{-1}D\alpha w^T + B_{c^*}W), \tag{2.37}$$

and B_{c^*} is a matrix composed of the columns of $J^{-1}D$ corresponding to voltage-controlled buses. Furthermore, let Ψ denote the $L \times N$ ISF matrix, the rows of which are computed using (2.35). Each entry of Ψ, denoted by $\Psi[l, n]$, provides the sensitivity of the active power injected at the *from* end

of line $\ell_l \in \mathcal{L}$ to an injection at bus n that is withdrawn, along with the change in losses introduced by the injection, according to the distributed slack policy.

In the market context, the ISFs computed with (2.36) are typically further simplified using the dc assumptions. To derive these dc-model-based ISFs, let $A = [a_1, \ldots, a_n, \ldots, a_N]$ denote the transmission network incidence matrix, where a_n is an L-dimensional column vector the lth entry of which is equal to 1 if bus n is the *from* bus of line l, -1 if bus n is the *to* bus of line l, and zero otherwise. Further, let b denote the L-dimensional column vector of branch susceptances, and define the diagonal $L \times L$ branch susceptance matrix as $B_b = \text{diag}\{b\}$, where $\text{diag}\{\cdot\}$ denotes a diagonal matrix such that $B_b[l, l] = b_l$, $\forall l$. Then, define the $N \times N$ nodal susceptance matrix as $B = A^T B_b A$, and the augmented nodal susceptance matrix by $B_\alpha = [\tilde{B}\ \alpha]$, where $\tilde{B}$ is the nodal susceptance matrix absent the column corresponding to the specified angle reference bus and α is the vector of distributed slack weights. Furthermore, recall that θ_1 is the specified angle reference and define $\tilde{A} = [a_2, \ldots a_N, 0_L]$, where 0_L is the L-dimensional all-zeros vector.

Under the dc assumptions, Ψ, can be calculated directly from the network connectivity, parameters, and distributed slack weights as follows [13]:

$$\Psi = B_b \tilde{A} B_\alpha^{-1} (I_{N\times N} - \alpha \mathbb{1}_N^T). \tag{2.38}$$

With the dc assumptions and dc-model-based ISFs, we can also define the PTDFs and LODFs, which are used extensively to model outages in real-time operations. The $N \times N$ matrix of PTDFs for a line ℓ_l, denoted by Φ_l, provides the sensitivity of the active power flow on line ℓ_l to active power transactions between buses in the system, e.g., the (n, m)th element of Φ_l, denoted by $\Phi_l[n, m]$, gives us the proportion of a real power transaction injected at bus n and withdrawn at bus m that flows over line ℓ_l. The PTDF for a line ℓ_l with respect to an injection at a bus n that is withdrawn at a bus m is calculated directly from the ISFs as follows [13]:

$$\Phi_l[n, m] = \Psi[l, n] - \Psi[l, m]. \tag{2.39}$$

The $L \times L$ matrix of LODFs provides the proportion of the pre-outage active power flow on each line ℓ_l that flows on each in-service line ℓ_u in the

system in the event of the outage of line ℓ_l. The LODF for a line ℓ_u with respect to the outage of a separate line $\ell_l = (n, m)$ is calculated from the PTDFs in (2.39) of the respective lines by [13]

$$\Xi[u, l] := \frac{\Phi_u[n, m]}{1 - \Phi_l[n, m]}. \tag{2.40}$$

2.5 Real-Time Economic Dispatch

The real-time ED is a widely used, optimal power flow (OPF)-based market scheduling tool that has three primary components: (i) power flow and network flow constraints obtained from a model of the system; (ii) equipment constraints, e.g., generator power output limits; and (iii) the objective, typically the maximization of social surplus[4] or minimization of generator costs, commonly quadratic or piecewise-linear functions (see, e.g., [13], [27], [53]).

Consider the system defined in Section 2.2 and suppose it is operating with a nominal load, $P_0^d \in \mathbb{R}^D$, nominal dispatch, $P_0^g \in \mathbb{R}^G$, and corresponding nominal line flows, $P_0^f \in \mathbb{R}^L$, and losses, $P_0^\ell \in \mathbb{R}$. Furthermore, suppose we have a forecast change in each bus load, denoted by $\Delta P^d \in \mathbb{R}^D$, over the time horizon of interest for the real-time ED—typically five minutes. The aim of the real-time ED is to determine the changes in the generator dispatch targets, which we denote by $\Delta P^g \in \mathbb{R}^G$, required to economically meet the forecast changes in the loads plus the change in system-wide losses, which we denote by $\Delta P^\ell \in \mathbb{R}$, and ensure system equipment and transmission constraints are met [53].

For a number of computational and practical reasons, the conventional real-time ED is commonly formulated using a simplified OPF formulation, referred to as the dc-OPF [54]. The dc assumptions result in a linear approximation of the nonlinear power balance and network flow constraints.

There are two primary approaches to the representation of the network in the dc-OPF: (i) the conventional "B-θ" approach; and (ii) the ISF-based approach [54]. In this thesis, we focus on the ISF-based approach due to its

[4]The social surplus, also referred to as the *economic surplus*, is defined to be the sum of: (i) the consumer surplus, which is sum over all buyers of the difference between each buyer's willingness to pay and the price paid by that buyer; and (ii) the producer surplus, which is the sum over all sellers of the difference between the price received by each seller and that seller's offer price [52].

widespread use by ISOs/RTOs in practical market operations.

In the ISF-based network representation conventionally deployed to formulate the ED in a market setting, the voltage angles are not explicitly represented, rather the bus power balance and power flowing on each line are written in terms of the system-wide power balance, the linear flow sensitivities, and the bus injections. Under this representation, the system-wide power balance constraint is given by

$$\mathbb{1}_G^T \Delta P^g - \mathbb{1}_D^T \Delta P^d - \Delta P^\ell = 0, \tag{2.41}$$

where $\mathbb{1}_G$ and $\mathbb{1}_D$ are all-ones vectors of dimensions G and D, respectively; and ΔP^ℓ is the change in system-wide losses, which typically takes the form of an LF-based loss model [14]; we will derive such a model in Chapter 3.

The ISF matrix provides the basis of the ISF-based dc-OPF network flow representation. Denote by ΔP the vector of bus net active power injection changes and by P_0 the vector of nominal bus net active power injections, each defined according to (2.1) with ΔP^d, ΔP^g and P_0^d, P_0^g, respectively. Then, using the ISF matrix from (2.38), we define the vector of incremental line flows in terms of the bus injections as

$$\Delta P^f = \Psi \Delta P, \tag{2.42}$$

which are bounded above and below by the line upper and lower incremental limits, denoted by $\Delta \bar{P}^f = \bar{P}^f - P_0^f$ and $\Delta \underline{P}^f = \underline{P}^f - P_0^f$, respectively.

Denote by $\mathscr{O}_i(\cdot)$ the offer function of generator i and by $\mathscr{B}_v^d(\cdot)$ the bid function of demand v, the arguments of which are ΔP_i^g and ΔP_v^d, respectively. The objective of the real-time ED is the maximization of the social surplus, [53],[5] which is defined as

$$\mathscr{S}(\Delta P^g, \Delta P^d) = \sum_{v \in \mathcal{D}} \mathscr{B}_v(P_{v,0}^d + \Delta P_v^d) - \sum_{i \in \mathcal{G}} \mathscr{O}_i(P_{i,0}^g + \Delta P_i^g), \tag{2.43}$$

where $P_{v,0}^d$ and $P_{i,0}^g$ are, respectively, the vth and ith components of P_0^d and P_0^g.

Combining the objective in (2.43) with the constraints that result from the

[5] If we make the additional assumption that loads have an infinite willingness to pay, i.e., demand is completely inelastic, then the maximization of the social surplus is equivalent to the minimization of generator cost.

power balance and network flow expressions in (2.41) and (2.42), respectively, we formulate the real-time ED problem as follows:

$$\max_{\Delta P^g, \Delta P^d} \mathscr{S}(\Delta P^g, \Delta P^d) \tag{2.44a}$$

$$s.t.$$

$$\mathbb{1}_G^T \Delta P^g - \mathbb{1}_D^T \Delta P^d - \Delta P^\ell = 0 \leftrightarrow \lambda_r \tag{2.44b}$$

$$\underline{P}^g \leq P_0^g + \Delta P^g \leq \bar{P}^g \tag{2.44c}$$

$$\underline{P}^d \leq P_0^d + \Delta P^d \leq \bar{P}^d \tag{2.44d}$$

$$\Delta \underline{P}^f \leq \Psi \Delta P \leq \Delta \bar{P}^f \qquad \leftrightarrow \underline{\mu}^f, \bar{\mu}^f \tag{2.44e}$$

where $\underline{P}^g$ ($\bar{P}^g$) and $\underline{P}^d$, ($\bar{P}^d$) are the G- and D-dimensional vectors of generator and demand lower (upper) limits, respectively; $\Delta P^\ell = \Lambda^T \Delta P^g$, where $\Lambda \in \mathbb{R}^N$ is the vector of LFs and for notational simplicity we assume $G = N$; and λ_r, $\underline{\mu}^f$, and $\bar{\mu}^f$ are the dual variables of their respective constraints, also referred to as *shadow prices* due to their well-known economic interpretation [53].[6] We note that, in practical applications, the real-time ED also includes so-called *security constraints*, which enforce reliability standards. However, we leave the discussion of such security constraints for Chapter 5. The primary outcome of the real-time ED is the set of generator dispatch instructions, ΔP^g.

The LMPs are an important additional outcome of the real-time market clearing process and serve two primary functions: (i) they provide location-specific prices for energy supplied/consumed by resources in the system; (ii) they provide the system operator with an indication of the existence of localized scarcity due to network constraints. Though the LMPs are not a direct result of the solution to (2.44), they may be calculated from the ISFs, the LFs, and the shadow prices at the solution to (2.44) [50] as follows:

$$\lambda = \mathbb{1}_N \lambda_r + \Psi^T \left(\bar{\mu}^f - \underline{\mu}^f \right) + \Lambda \lambda_r. \tag{2.45}$$

Now, define

$$\lambda^c = \Psi^T \left(\bar{\mu}^f - \underline{\mu}^f \right) \text{ and } \lambda^\ell = \Lambda \lambda_r,$$

to be the N-dimensional vectors representing the congestion and loss com-

[6] The shadow price of the system-wide power balance constraint, λ_r, is often referred to as the system reference or energy price.

ponents of the LMPs. Then, for each bus n, the LMP can be decomposed into three components [50]:

$$\lambda_n = \lambda_r + \lambda_n^c + \lambda_n^\ell,$$

where λ_r is the *energy component*, which represents the cost to generate the next MW from those generators that provide it; λ_n^c is the *congestion component*, which captures the additional costs to deliver the next MW to bus n associated with transmission congestion-driven dispatch limitations; and λ_n^ℓ is the *loss component*, which accounts for the location-differentiated cost of losses associated with serving the next MW at bus n.

CHAPTER 3

MEASUREMENT-BASED LOSS FACTOR ESTIMATION

In this chapter, we propose a measurement-based approach to the estimation of marginal loss factors (LFs), which are conventionally computed from the power flow Jacobian. Our approach circumvents the shortcomings of model-based LF computation approaches by utilizing PMU measurements for online LF estimation so as to reflect real-time operating conditions and adapt to changing system conditions. These strengths of the proposed measurement-based LF estimation approach can be harnessed to enhance the real-time scheduling process and the computation of real-time locational marginal prices (LMPs).

3.1 Introduction

In a power system, the allocation of the additional energy that must be generated to account for losses and the costs associated with providing such energy are critical components of effective market-based electricity scheduling procedures. Conventionally, model-based approaches, e.g., penalty factors, the B-coefficients, and, more recently, LFs, have been used to represent losses in such scheduling procedures.

Loss factors are sensitivities of the system-wide active power losses to changes in the bus active power injections, assuming the change in injection is balanced by a single slack bus or set of slack buses. Model-based LFs are derived from the power flow Jacobian [13], the computation of which requires an up-to-date system model, typically obtained offline. As such, the accuracy of the LFs is coupled with the accuracy of the underlying system model and the inaccuracies in the system model extend to the model-based LFs. Furthermore, the LF computation requires the *a priori* specification of *distributed slack weights*, which define the distribution of the power mis-

match and losses among the buses in the system necessary to maintain the system-wide power balance. Such distributed slack weights are typically selected based on the bus load distribution or generator output distribution (see, e.g., [15, 16]).

Loss factors are primarily used in: (i) market scheduling procedures for setting generator dispatch targets, and (ii) the computation of locational marginal prices (LMPs) (see, e.g., [15, 16]). The LFs, through the dispatch targets and LMPs, also impact the distribution of payments among market participants. Inaccurate LFs have physical implications, e.g., changing the dispatch targets of generators which may raise reliability concerns, and economic implications, e.g., changing the LMPs and causing an incorrect distribution of market payments.

In this chapter, we propose a measurement-based approach to the computation of LFs. Unlike conventional LF computation approaches, ours does not rely on a model of the system obtained offline. Instead, we estimate the LFs using load and generation measurements obtained from PMUs. Furthermore, the LFs estimated using our approach do not depend on arbitrarily selected distributed slack weights, i.e., our approach will produce LFs consistent with the responses of generators to load changes in real-time. Indeed, our measurement-based estimation approach makes possible the calculation of the "true" distributed slack weights. In addition, our approach harnesses the existing practice to collect load and generator output measurements for use in market settlements.

3.2 Model-Based Loss Factor Computation

To derive conventional, model-based LFs, we focus on the active power mismatch, p_m, and consider again the power system outlined in (2.9). Suppose the system is operating at the point (x_0, P_0, Q_0), i.e., $g(x_0, P_0, Q_0) = 0$ and without loss of generality, assume that $p_m = 0$, $q_m = 0$ at (x_0, P_0, Q_0). Then, let $\tilde{P} = P_0 + \Delta P'$, $\tilde{Q} = Q_0 + \Delta Q'$, and $x = x_0 + \Delta x'$, where $\Delta P'$ ($\Delta Q'$) is an active (reactive) power perturbation in the pre-allocation quantities, which happen to coincide with the scheduled quantities, and $\Delta x'$ is the system response to such a perturbation prior to control actions. From (2.12), we have that the *pre-control-response* active power mismatch, that arises due to the

perturbation ($\Delta P'$, $\Delta Q'$) is given by

$$\Delta p'_m \approx r^T \Delta P' + w^T \Delta Q'. \tag{3.1}$$

However, to fully characterize the losses, we must also consider the loss impact of the voltage control policy. The voltage control policy impacts the losses that arise as a result of the perturbation ($\Delta P'$, $\Delta Q'$) via the provision of reactive power to meet the voltage control objective, which is not captured in (3.1). To capture these impacts on the losses, we define the *post-voltage-control* active power mismatch as follows:

$$\Delta \tilde{p}_m \approx r^T \Delta P' + w^T \Delta Q' + w_c^T \Delta Q''_c. \tag{3.2}$$

Then, by substituting (2.27) into (3.2), we arrive at the post-voltage-control active power mismatch with respect to the perturbation ($\Delta P'$, $\Delta Q'$):

$$\Delta \tilde{p}_m \approx y^T \Delta P' + (y^q)^T \Delta Q', \tag{3.3}$$

where $y = (r^T + w_c^T U)^T$ and $y^q = (r^T + w_c^T W)^T$.

Recall that the active (reactive) LFs are the sensitivities of the system-wide losses with respect to changes in the pre-allocation net active (reactive) power injection at each bus, assuming the change is balanced by a pre-specified bus, i.e., there is a single slack bus, or set of buses, i.e., the slack is distributed among several buses. Now, let ΔP^ℓ be the change in the system-wide losses, $P^\ell(\theta, V)$, due to the perturbation in the pre-allocation, ($\Delta P'$, $\Delta Q'$). Then, define the active and reactive power perturbation LFs for a bus n, respectively, by

$$\Lambda_n = \frac{\partial P^\ell(\theta, V)}{\partial \tilde{P}_n},$$

and

$$\Lambda_n^q = \frac{\partial P^\ell(\theta, V)}{\partial \tilde{Q}_n}.$$

Moreover, let $\Delta \tilde{p}_{m,n}$ ($\Delta \tilde{p}^q_{m,n}$) be the portion of the variation $\Delta \tilde{p}_m$ attributable to $\Delta P'_n$ ($\Delta Q'_n$) such that

$$\Delta \tilde{p}_m = \sum_{n \in \mathcal{N}} \Delta \tilde{p}_{m,n} + \Delta \tilde{p}^q_{m,n}. \tag{3.4}$$

Then, from (2.8) and (3.4), it follows that

$$\Delta P^{\ell} = \sum_{n \in \mathcal{N}} \left(\Delta P'_n + \Delta \tilde{p}_{m,n} + \Delta \tilde{p}^{q}_{m,n} \right). \tag{3.5}$$

Further, by rearranging the right side of (3.5) and assuming that $\Delta \tilde{p}_{m,n} \approx \frac{\partial \tilde{p}_m}{\partial \tilde{P}_n} \Delta P'_n$ ($\Delta \tilde{p}^{q}_{m,n} \approx \frac{\partial \tilde{p}_m}{\partial \tilde{Q}_n} \Delta Q'_n$) for $\Delta P'_n$ ($\Delta Q'_n$) small, we obtain

$$\Delta P^{\ell} \approx \sum_{n \in \mathcal{N}} \left(1 + \frac{\partial \tilde{p}_m}{\partial \tilde{P}_n} \right) \Delta P'_n + \frac{\partial \tilde{p}_m}{\partial \tilde{Q}_n} \Delta Q'_n. \tag{3.6}$$

From (3.3) and (3.6), we conclude that the active and reactive power model-based LF for each bus n with respect to a chosen α and voltage control policy are, respectively, given by

$$\Lambda_n \approx 1 + y_n, \tag{3.7}$$

and

$$\Lambda^{q}_n \approx y^{q}_n, \tag{3.8}$$

where y_n (y^{q}_n) is the nth element of the vector y (y^{q}). Current market scheduling practice is concerned only with the scheduling of active power. Thus, in practice, only the active power LFs are used. Moreover, in operations these LFs are recomputed periodically via (3.7) using an operator-selected α and an ac power flow solution based on state estimator output (see, e.g., [15, 16]).

3.3 Measurement-Based Loss Factor Estimation

The conventional, model-based LFs defined in (3.7) are not ideal because they depend on the availability of an up-to-date model of the system. Furthermore, they require the arbitrary selection of a distributed reference bus and a voltage policy in the system, which may not be consistent with actual operations.

In this section, we formulate our measurement-based approach to LF estimation, which does not carry the above requirements. To this end, we focus on the measured response of generators to changes in load injections (necessary to maintain the system-wide power balance, including losses). If the power system is to remain in operation, the power balance must be main-

tained around-the-clock and thus the losses manifest themselves as the difference between the load injection changes and their corresponding generator output changes.

3.3.1 Loss Factor Estimation

Suppose the active (reactive) power consumed by a load v at time t, $P_v^d(t)$ ($Q_v^d(t)$), varies by a small amount from time t to time $t+\Delta t$, $\Delta t > 0$ and small, to become $P_v^d(t+\Delta t)$ ($Q_v^d(t+\Delta t)$), and define $\Delta P_v^d(t) = P_v^d(t+\Delta t) - P_v^d(t)$ ($\Delta Q_v^d(t) = Q_v^d(t+\Delta t) - Q_v^d(t)$). Further, let $\Delta P_{i,v}^{g,p}(t) = P_{i,v}^{g,p}(t+\Delta t) - P_{i,v}^{g,p}(t)$ be the response of generator i to the load v active power consumption change $\Delta P_v^d(t)$; then, define

$$\Upsilon^p[v,i] = \frac{\partial P_i^g(t)}{\partial P_v^d(t)} \approx \frac{\Delta P_{i,v}^{g,p}(t)}{\Delta P_v^d(t)}. \tag{3.9}$$

Moreover, let $\Delta P_{i,v}^{g,q}(t) = P_{i,v}^{g,q}(t+\Delta t) - P_{i,v}^{g,q}(t)$ be the response of generator i to the load v reactive power consumption change $\Delta Q_v^d(t)$; then, define

$$\Upsilon^q[v,i] = \frac{\partial P_i^g(t)}{\partial Q_v^d(t)} \approx \frac{\Delta P_{i,v}^{g,q}(t)}{\Delta Q_v^d(t)}. \tag{3.10}$$

While $\Delta P_{i,v}^{g,p}(t)$ and $\Delta P_{i,v}^{g,q}(t)$ are not directly available through PMU measurements, we can, however, measure the total change in generator i output due to load changes at time t, $\Delta P_i^g(t)$. We observe that the variation in the generator i output is due to the generator's response to variations in the active and reactive power of each load v:

$$\Delta P_i^g(t) = \Delta P_{i,1}^{g,p}(t) + \cdots + \Delta P_{i,D}^{g,p}(t) + \Delta P_{i,1}^{g,q}(t) + \cdots + \Delta P_{i,D}^{g,q}(t). \tag{3.11}$$

Employing (3.9) and (3.10) together with (3.11) we obtain

$$\begin{aligned}\Delta P_i^g(t) \approx & \Delta P_1^d(t)\Upsilon^p[1,i] + \cdots + \Delta P_D^d(t)\Upsilon^p[D,i] \\ & + \Delta Q_1^d(t)\Upsilon^q[1,i] + \cdots + \Delta Q_D^d(t)\Upsilon^q[D,i].\end{aligned}$$

Now suppose we have $M+1$ sets of synchronized load and generation mea-

surements, and let

$$\Delta P_v^d[k] = P_v^d[(k+1)\Delta t] - P_v^d[k\Delta t],$$

$$\Delta Q_v^d[k] = Q_v^d[(k+1)\Delta t] - Q_v^d[k\Delta t],$$

$$\Delta P_i^g[k] = P_i^g[(k+1)\Delta t] - P_i^g[k\Delta t],$$

for $k = 1, \ldots, M$, and define

$$\Delta P_v^d = \left[\Delta P_v^d[1] \ \cdots \ \Delta P_v^d[k] \ \cdots \ \Delta P_v^d[M]\right]^T,$$

$$\Delta Q_v^d = \left[\Delta Q_v^d[1] \ \cdots \ \Delta Q_v^d[k] \ \cdots \ \Delta Q_v^d[M]\right]^T,$$

$$\Delta P_i^g = \left[\Delta P_i^g[1] \ \cdots \ \Delta P_i^g[k] \ \cdots \ \Delta P_i^g[M]\right]^T.$$

Furthermore, let

$$\Upsilon_i^p = [\Upsilon[1,i], \ldots, \Upsilon[v,i], \ldots, \Upsilon[D,i]]^T,$$

$$\Upsilon_i^q = [\Upsilon^q[1,i], \ldots, \Upsilon^q[v,i], \ldots, \Upsilon^q[D,i]]^T,$$

$$\Upsilon_i = [(\Upsilon_i^p)^T \ (\Upsilon_i^q)^T]^T.$$

Then, clearly,

$$\Delta P_i^g = \left[\Delta P_1^d \ \cdots \ \Delta P_v^d \ \cdots \ \Delta P_D^d \ \cdots \ \Delta Q_1^d \ \cdots \ \Delta Q_v^d \ \cdots \ \Delta Q_D^d\right] \Upsilon_i. \quad (3.12)$$

Define $\Delta P^d = \left[\Delta P_1^d \ \cdots \ \Delta P_v^d \ \cdots \ \Delta P_D^d\right]$, $\Delta Q^d = \left[\Delta Q_1^d \ \cdots \ \Delta Q_v^d \ \cdots \ \Delta Q_D^d\right]$, and $\Delta S^d = [(\Delta P^d)^T \ (\Delta Q^d)^T]^T$. Then, the system in (3.12) becomes

$$\Delta P_i^g = \Delta S^d \Upsilon_i. \quad (3.13)$$

If $M \geq 2D$, then (3.13) is an overdetermined system. Moreover, assuming Υ_i is approximately constant over the $M+1$ measurements,[1] we can obtain an estimate of Υ_i from least-squares error estimation (LSE) as follows:

$$\hat{\Upsilon}_i = ((\Delta S^d)^T \Delta S^d)^{-1} (\Delta S^d)^T \Delta P_i^g. \quad (3.14)$$

As an added benefit of the measurement-based estimation approach de-

[1] We provide an empirical analysis of this assumption in Appendix B.

scribed above, a measurement-based estimate of the actual distributed slack weight—sometimes referred to as the *participation factor*—for each generator i can be computed from the results of (3.14) as follows:

$$\hat{\alpha}_i = \frac{\hat{\Upsilon}[v,i]}{\sum_{i\in\mathcal{G}} \hat{\Upsilon}[v,i]}, \tag{3.15}$$

for an arbitrary $v \in \mathcal{D}$.

Let $\hat{\Upsilon} = [(\hat{\Upsilon}^p)^T\ (\hat{\Upsilon}^q)^T]^T$ be the $2D \times G$ matrix of generator output to load change sensitivity estimates, which we will use to derive the measurement-based LFs. Consider a change in the loads at instant t, $(\Delta P^d(t),\ \Delta Q^d(t))$, for which we can write the corresponding change in system-wide losses as

$$\Delta P^\ell(t) = \mathbb{1}_G^T \Delta P^g(t) - \mathbb{1}_D^T \Delta P^d(t), \tag{3.16}$$

where $\Delta P^g(t)$ is the *post-load-change response* of the generators to load change $(\Delta P^d(t),\ \Delta Q^d(t))$ and $\mathbb{1}_G$ ($\mathbb{1}_D$) is an all-ones vector of dimension G (D).

Now, by substituting (3.11) into (3.16) we arrive at

$$\Delta P^\ell(t) = \sum_{v\in\mathcal{D}}(-\Delta P^d(t) + \sum_{i\in\mathcal{G}} \Delta P^g_{i,v}(t) + \Delta P^{g,q}_{i,v}(t)). \tag{3.17}$$

For sufficiently small $\Delta P^d(t)$, $\Delta Q^d(t)$, and $\Delta P^g(t)$, we can substitute (3.9) and (3.10) into (3.17) and rearrange to obtain

$$\Delta P^\ell(t) \approx \sum_{v\in\mathcal{D}} \left(-1 + \sum_{i\in\mathcal{G}} \hat{\Upsilon}^p[v,i]\right) \Delta P^d_v(t) + \sum_{v\in\mathcal{D}} \hat{\Upsilon}^q[v,i])\Delta Q^d_v(t),$$

from which we conclude that the active power LFs are given by:

$$\frac{\partial P^\ell(t)}{\partial P^d(t)} \approx -\mathbb{1}_D + \hat{\Upsilon}^p \mathbb{1}_G. \tag{3.18}$$

Let Λ be the N-dimensional vector of active power LFs. Noting the relationship in (3.18) and the load injection sign convention adopted herein, and assuming we have active and reactive power load measurements at each bus

(i.e., $D = N$), an estimate of Λ, which we denote by $\hat{\Lambda}^g$, can be written as

$$\hat{\Lambda}^g = -(-\mathbb{1}_N + \hat{\Upsilon}^p \mathbb{1}_G). \tag{3.19}$$

The LF estimates computed with (3.19) have an implicit generator slack bus, i.e., they embody the responses of generators to changes in the loads in the system. However, market processes are by-and-large concerned with the selection of a least-cost generator dispatch to meet a fixed load forecast. Thus, the LFs used in the market context are typically computed with respect to a load slack bus. Suppose we have selected a distributed load slack weight vector, α, e.g., using the bus load distribution. Then, we can compute from the generator-referenced measurement-based LFs in (3.19) a close approximation of the desired load-referenced LFs as follows:

$$\hat{\Lambda} = \hat{\Lambda}^g - \mathbb{1}_N \alpha^T \hat{\Lambda}^g. \tag{3.20}$$

Unlike the model-based LFs computed with (3.7), the LFs computed with (3.19) and (3.20) are not affected by incorrect model data or undetected changes in system topology.

3.3.2 Practical Considerations for the LF Estimation

The estimation of the sensitivities in (3.14) used to compute the LFs requires a complete set of data, i.e., M sets of load active and reactive demand and generator output measurements, where $M > 2D$. Moreover, the LSE-based approach gives equal weight to all measurements, regardless of their acquisition time. In practice, these aspects of the approach above may prove to be impractical. To address this, similar to the ISF estimation approach in [18], we propose the deployment of a weighted least squares (WLS) formulation of (3.14) given by

$$\hat{\Upsilon}_i^T = ((\Delta S^d)^T W (\Delta S^d))^{-1} (\Delta S^d)^T W \Delta P_i^g, \tag{3.21}$$

where W is a weighting matrix that can be selected to give more weight to recent measurements so as to track changing operating conditions and minimize the impacts of erroneous measurements on the LF estimation.

The WLS approach in (3.21) may be further improved by implementing a recursive weighted least squares variant (see, e.g., [18]), which enables the computation of updated estimates of the $\hat{\Upsilon}_i$ as each set of measurements arrives. In this chapter, we adopt the WLS approach in (3.21) with a diagonal weighting matrix W, where $W[k,k] = f^{M-k}$, $f \in (0,1]$. Furthermore, our observations from a number of tests carried out on IEEE test systems of varying sizes, a subset of the results of which we furnish in Chapter 5, suggest that $M \approx 4D$ and $f \approx e^{\frac{-2.4}{M}}$ are appropriate selections to balance tracking changes in operating point and steady-state error, and to prevent singularity in the regressor matrix.

PMU Measurement Error Impacts. PMU measurement data may contain errors due to a host of issues, e.g., communication channel failure, inadequate maintenance and calibration of PMUs, and detection of such errors is an area of ongoing research [55]. The accuracy of measurement data used in conventional applications, e.g., state estimation, is commonly assessed via error residuals (see, e.g., [4]). Additionally, some erroneous data can be detected by analyzing: (i) measurement magnitude, e.g., are the measurements orders of magnitude too small or large to be plausible; and (ii) measurement consistency, e.g., do the measurements result in gross violations of Kirchhoff's laws. For the purposes of the work presented in this thesis, we assume that standard checks have been performed on the PMU measurements prior to their use in sensitivity estimation. Furthermore, the impacts of temporary errors in measured data are minimized through the use of weighted least squares with a sliding measurement window and by setting $f < 1$.

3.4 Measurement-Based Loss Factor Applications

In this section, we give an overview of two key applications for measurement-based LFs: (i) the market-based resource scheduling process known as the real-time economic dispatch (ED); and (ii) the computation of real-time LMPs.

3.4.1 Real-Time Economic Dispatch

Recall that the real-time ED is a widely used operational tool that aims to determine the change in the generator dispatch targets, ΔP^g, required to economically meet the forecast change in the load, ΔP^d, and ensure system physical constraints are met [53]. In this chapter, we assume the load has an infinite willingness to pay and thus the objective of the real-time ED reduces to the minimization of generator costs. We derived the real-time ED in Section 2.5. However, for completeness, we restate it here:

$$\min_{\Delta P^g} \sum_{i \in \mathcal{G}} \mathscr{C}_i(\Delta P_i^g + P_{i,0}^g) \tag{3.22a}$$

$$s.t.$$

$$\mathbb{1}_G^T \Delta P^g - \mathbb{1}_D^T \Delta P^d - \Delta P^\ell = 0 \leftrightarrow \lambda_r \tag{3.22b}$$

$$\underline{P}^g \leq P_0^g + \Delta P^g \leq \bar{P}^g \tag{3.22c}$$

$$\underline{P}^f \leq P_0^f + \Psi \Delta P \leq \bar{P}^f \qquad \leftrightarrow \underline{\mu}^f, \bar{\mu}^f \tag{3.22d}$$

where $\mathscr{C}_i(\cdot)$ is the cost function of generator i, and $\Delta P^\ell = \Lambda^T \Delta P^g$ when using the LF-based loss model commonly used in market applications. We note that to focus on LF impacts on the ED, we leave out the security constraints that would be present in a practical ED formulation—we will discuss in detail such security constraints in Chapter 5. The primary outcome of the real-time ED is the vector of generator dispatch instructions, ΔP^g, which depend on a system model via the LFs and ISFs in constraints (3.22b) and (3.22d) respectively.

We deploy the measurement-based LFs from (3.20) to reformulate the losses in (3.22b) as

$$\Delta \hat{P}^\ell = \hat{\Lambda}^T \Delta P^g, \tag{3.23}$$

which no longer depends on a system model. The measurement-based estimate of $\hat{\Lambda}$ is updated periodically via (3.19) and (3.20) as new measurements arrive, and applied in the real-time ED constraint (3.22b). The elimination of the real-time ED dependence on model-based ISFs in (5.9e) is the subject of Chapter 5. Thus, for the sake of brevity, we defer its discussion here.

3.4.2 Real-Time LMP Computation

As derived in Section 2.5, the so-called three-part LMP can be computed from the ISFs, the LFs, and the shadow prices [50] as follows:

$$\lambda = \mathbb{1}_N \lambda_r + \lambda^c + \lambda^\ell, \tag{3.24}$$

where the congestion and losses components are, respectively, given by

$$\lambda^c = \Psi^T \left(\bar{\mu}^f - \underline{\mu}^f \right) \text{ and } \lambda^\ell = \lambda_r \Lambda.$$

The congestion and loss components of the LMP depend on a system model directly via Ψ and Λ. As such, errors in the system model may propagate to the computation of the LMPs resulting in LMP errors. As above, we defer to Chapter 5 for a discussion of removing the ISF-based model dependence and the impacts of security constraints on the LMP. To address the LF-based model dependence, we modify the LMP computation by replacing Λ in (3.24) with its measurement-based estimate from (3.20), which is updated with new measurements as needed, e.g., before a real-time ED execution.

3.5 Case Studies

In the following case studies, we compare the model-based, measurement-based, and actual LFs and their resepective impacts when utilizing them to determine the generator dispatch and LMPs via the real-time ED.

We deploy (3.7) to compute the conventional, model-based LFs. Furthermore, we calculate the actual LFs used in our studies by (i) increasing the net injection at each bus by 0.01 p.u., and (ii) computing the change in losses via a solution to the full nonlinear ac power flow with the appropriate system model, and assuming the net injection change is balanced according to distributed load slack weights, α^d, defined $\forall n \in \mathcal{N}$ by

$$\alpha_n^d = \frac{\sum_{v \in \mathcal{D}_n} P_{v,0}^d}{\sum_{v \in \mathcal{D}} P_{v,0}^d}, \tag{3.25}$$

where $P_{v,0}^d$ is the case nominal load injection for load v; to compute the actual LFs, for each net injection increase and ac-power flow solution, we take the

ratio of the ac-power-flow-calculated change in the losses and the change in the net active power injection.

We compute the measurement-based LF estimates with (3.20) and (3.21), and carry out the estimation procedures with simulated PMU measurements (assumed to be collected at a measurement frequency of 30/s) of the random fluctuations in each load injection $v \in \mathcal{D}$, which are generated according to

$$P_v^d[k] = P_{v,0}^d[k] + \sigma_1 P_{v,0}^d[k]\nu_1 + \sigma_2\nu_2, \tag{3.26}$$

where $P_{v,0}^d[k]$ is the case nominal load injection for load v at instant k, and ν_1 and ν_2 are pseudorandom values drawn from a normal distribution with zero mean and standard deviations $\sigma_1, \sigma_2 = 0.01$, respectively ($\sigma_1 P_{v,0}^d[k]\nu_1$ represents random load fluctuations, whereas $\sigma_2\nu_2$ represents measurement noise). We compute simulated PMU measurements of generator injections $P_i^g[k]$ for each generator $i \in \mathcal{G}$ corresponding to the loads at instant k by solving (2.9) with pre-allocation generation outputs $P^g[k-1]$, and loads $P^d[k]$, nominal bus reactive power injections Q_0 and voltages V_0 and distributed generator slack weights, α^g, defined $\forall n \in \mathcal{N}$ by

$$\alpha_n^g = \frac{\sum_{i\in\mathcal{G}_n} \bar{P}_i^g}{\sum_{j\in\mathcal{G}} \bar{P}_i^g}. \tag{3.27}$$

For simplicity, we assume no variation in the load reactive power injections, i.e., $\Delta Q_v^d[k] = 0$, $\forall v \in D$. This assumption, however, does not impact the nature of the results we present.

3.5.1 Case Studies I: The 6-Bus Test System

In this section, we present the results of case studies carried out on a modified version of the 3-generator, 6-bus test system provided in the simulation package MATPOWER [56], the topology of which we show in Fig. 3.1; we modified the test system by moving the generator at bus 3 to bus 6 and moving the load at bus 6 to bus 3. We assume each load has an infinite willingness to pay, i.e., the demand is inelastic, and each generator, i, submits a quadratic offer function of the form $a_i(P_i^g)^2 + b_i P_i^g + c_i$, the parameters of which are provided in Table 3.1. Moreover, we select estimation parameter values of $M = 60$ and $f = 0.98$ and simulate system operation for 300 measurement

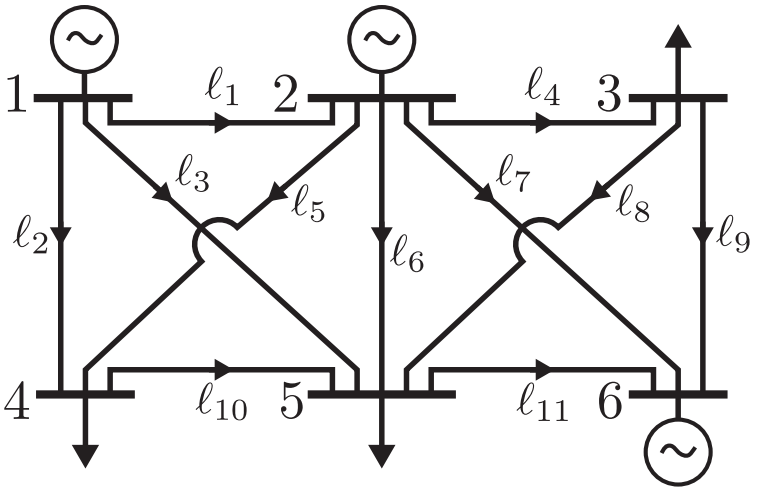

Figure 3.1: The 6-bus test system topology.

Table 3.1: The 6-bus test system generator cost function parameters.

generator	a_i [\$/MWh^2]	b_i [\$/MWh]	c_i [\$]
1	0.1100	5.0	150
2	0.0850	1.2	600
6	0.1225	1.0	335

intervals using the approach to synthesizing PMU measurements outlined in Section 3.5, and assume the nominal load at bus 3 increases linearly by 0.2 p.u. between intervals 100 and 200.

Impact on LFs of a Change in Operating Point. In this case, we demonstrate the impact on the LFs of a change in the system operating point. Do do so, we compare the pre-injection-change model-based LFs, computed at interval 75, and the measurement-based LFs computed at intervals 75 (pre-operating-point change) and 225 (post-operating-point change) with the actual LFs computed at the same intervals.

In Table 3.2, we show the actual LFs at the pre- and post-injection change intervals—75 and 225, respectively—and the error between the actual and the model- and measurement-based LFs, respectively. The LFs are sensitive to changes in the operating point as illustrated by the change in the actual LFs pre- and post-load increase. Prior to the operating point change, the mean squared error (MSE) of the model-based LFs compared to the actual LFs is 0.0055 MWh/MWh, whereas the post-change MSE is 0.0137 MWh/MWh, an increase of 97%. The measurement-based LFs compared to the actual LFs, on the other hand, have pre- and post-injection

Table 3.2: Pre- and post-load-change LFs.

			LF error			
	actual LFs		model-based		measurement-based	
bus	pre-change	post-change	pre-change	post-change	pre-change	post-change
1	0.0402	0.0481	-0.00179	-0.00973	0.0015	0.0020
2	0.0404	0.0426	-0.00258	-0.00473	0.0014	0.0014
3	0.0110	0.0047	-0.00243	0.00378	0.0004	0.0002
4	-0.0000	0.0045	0.00108	-0.00348	0.0003	-0.0000
5	-0.0093	-0.0078	-0.00155	-0.00303	0.0006	-0.0006
6	0.0333	0.0308	0.00329	0.00587	0.0013	0.0010
MSE:	-	-	0.0055	0.0137	0.0025	0.0028

[all values in MWh/MWh]

Table 3.3: Post-load-change LMPs.

	actual	model-based		measurement-based	
bus	LMP	LMP	error	LMP	error
1	22.27	22.34	-0.072	22.26	0.011
2	22.40	22.40	-0.003	22.40	-0.003
3	23.28	22.95	0.335	23.32	-0.034
4	23.29	22.97	0.315	23.33	-0.039
5	23.57	23.23	0.347	23.63	-0.051
6	22.67	22.55	0.124	22.68	-0.013
MSE:	-	-	0.594	-	0.075

[all values in $/MWh]

change MSEs of 0.0025 MWh/MWh and 0.0028 MWh/MWh, respectively. Thus, we conclude that the measurement-based LFs are a more accurate representation of the maginal losses than the model-based LFs and are able to track the changing operating point.

Impacts on Dispatch and LMPs of LF Errors. In this case, we demonstrate the impacts on the real-time ED-determined dispatch instructions and LMPs of model-based LF errors. We assume the real-time ED is executed using (3.22) with each of the model-based, measurement-based and actual LFs at interval 225—after the operating point change. Moreover, we assume that the forecast bus load changes, ΔP_v^d, $\forall v \in \mathcal{D}$, being balanced in the ED are equal in magnitude to 5% of each bus' load, i.e. $\Delta P_v^d = \xi P_{v,0}^d \ \forall v \in \mathcal{D}$, where $\xi = 0.05$. We compute the LMPs with (3.24) for each of the real-time ED solutions.

The deviations in the dispatch targets are negligible in this case due to the size of the system, so we do not report them; however, as we will show

in Section 3.5.2, in larger systems the dispatch impacts can be substantial. In Table 3.3, we report the LMPs computed with the ED solutions using the actual, model-based, and measurement-based LFs and model- and measurement-based LF LMP errors with respect to the LMPs computed from the solution to the ED with the actual LFs. The model-based LFs produce LMPs with a total MSE of \$0.594/MWh, while the measurement-based LFs closely track the actual LMPs and have an MSE of \$0.075/MWh—the LMP errors resulting from the use of erroneous model-based LFs are non-trivial, unlike those for the LMPs computed with the measurement-based LFs.

3.5.2 Case Studies II: IEEE 118-Bus Test System

In this section, we present the results of case studies carried out using the IEEE 54-generator, 186-line, 118-bus test system [57]. As before, when solving the real-time ED, we assume each load has an infinite willingness to pay, i.e., the demand is inelastic, and each generator, i, submits a quadratic offer function of the form $a_i(P_i^g)^2 + b_i P_i^g + c_i$, the parameters of which we take from the test case [57]. Moreover, in the LF estimations, we use the parameter values $M = 236$ and $f = 0.99$ and synthetic PMU measurements of load demand and generator outputs generated using the procedure outlined in Section 3.5. To isolate the LF impacts on the ED in the following cases, we have selected the line thermal limits such that there are no binding transmission constraints.

Undetected Line Outage. In this case, we investigate the impacts on LFs and real-time ED outcomes based on those LFs of an undetected line outage. We simulate 1200 measurement intervals using simulated PMU measurements of the load active power consumption and generator active power production, synthesized as outlined in Section 3.5. Further, we assume there is an undetected outage of the double circuit consisting of lines ℓ_{141} and ℓ_{142} at interval 600 and that the real-time ED in (3.22) is executed at interval 1100 assuming a forecast load increase of 5% at each load bus,.

In Fig. 3.2, we show the LF, dispatch target, and LMP absolute errors for: (i) the measurement-based quantities with respect to the actual quantities; (ii) the undetected outage model-based quantities with respect to the actual

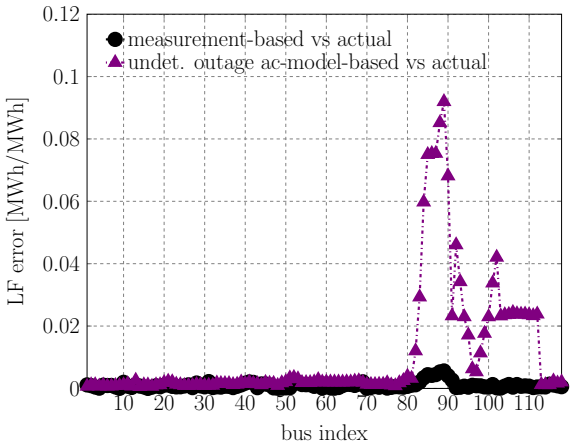

(a) LFs errors.

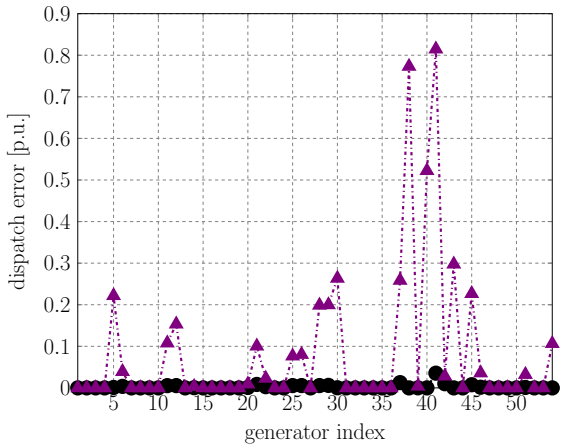

(b) Generator dispatch errors.

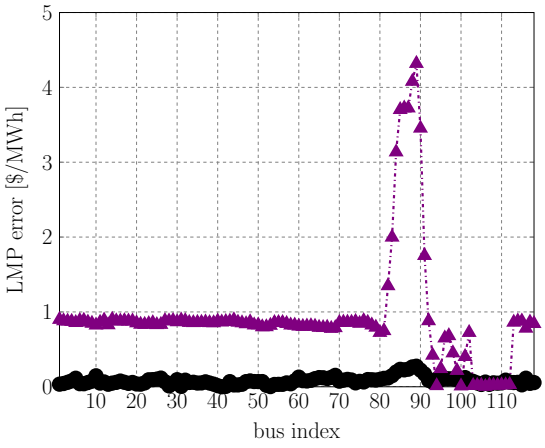

(c) LMP errors.

Figure 3.2: Absolute errors due to the undetected outage of double-circuit ℓ_{141}, ℓ_{142}.

Table 3.4: LFs, dispatch target, and LMP MSE across all buses/generators due to the undetected outage of ℓ_{141}, ℓ_{142}.

quantity	MSE	
	undet. outage model-based	measurement-based
LFs [MWh/MWh]	0.2374	0.0158
dispatch target [p.u.]	1.4189	0.0431
LMP [$/MWh]	13.1432	1.0340

quantities. The undetected line outage causes substantial model-based LF errors, shown in Fig. 3.2a. These LFs errors are primarily driven by the redistribution of line flows that takes place when the line outage occurs. Thus, they are higher at those buses that are electrically close to the outaged lines, e.g., buses 83–91, for which between 10 and 40% of the respective bus injections flow over ℓ_{141} and ℓ_{142} prior to their outage.

The generator dispatch is also significantly impacted by the undetected outage. The generator dispatch errors, shown in Fig. 3.2b, result in some generator outputs, e.g., generators 38 and 40, changing by more than 0.7 p.u. between the model-based and measurement-based LF real-time ED solutions. The generators for which the dispatch errors are the highest are those at buses with high LF errors, i.e., those at buses close the outaged facilities.

Finally, the LFs and dispatch errors contribute to LMP errors in the model-based ED, shown in Fig. 3.2c, particularly at those buses electrically close to the undetected outage. Our measurement-based approach, on the other hand, incorporates the impacts of the undetected outage and produces LFs, a generator dispatch, and LMPs that are very close to their actual values.

As evidenced by the LFs, dispatch, and LMP MSEs reported in Table 3.4, the model-based LF performance suffers considerably when there are undetected outages. The proposed measurement-based approach, on the other hand, accurately captures the LFs regardless of changes in the system topology resulting in MSEs that are an order of magnitude below those for the model-based LFs.

Incorrect Model Line Impedance Data. In this case, we investigate the impacts on the LFs and real-time ED outcomes based on those LFs of incorrect line impedance data in the model. To this end, we perturb

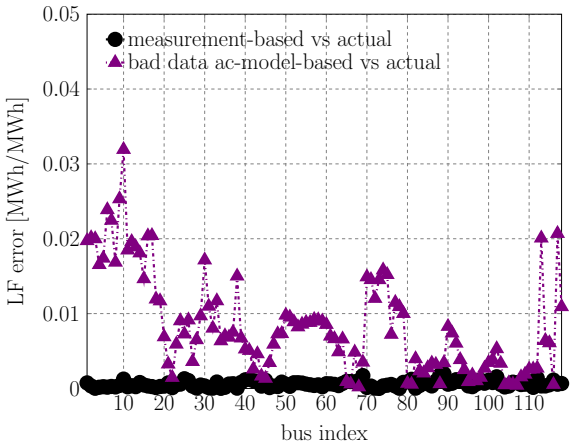

(a) LF errors.

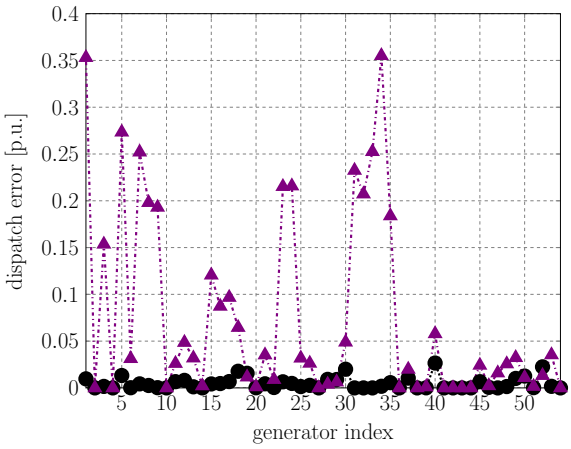

(b) Generator dispatch errors.

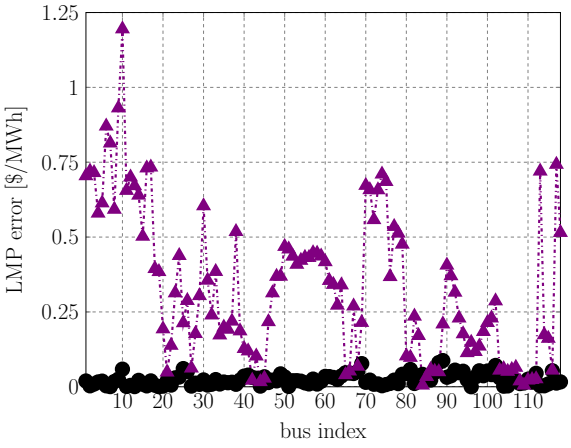

(c) LMP errors.

Figure 3.3: Absolute errors due to incorrect model line impedance data.

Table 3.5: LFs, dispatch target, and LMP MSE across all buses/generators due to incorrect line impedance data.

quantity	MSE	
	incorrect data model-based	measurement-based
LFs [MWh/MWh]	0.116	0.0078
dispatch target [p.u.]	0.911	0.0581
LMP [$/MWh]	4.52	0.337

the line impedance on each of the top 30% of loaded lines by a random multiple in $[0.7, 1.3]$ drawn from a uniform distribution. We simulate 600 PMU measurement intervals of load demand and generator output with the correct model data using the approach to synthesizing PMU measurements outlined above. We compute the model-based LFs using the incorrect model data and the actual LFs using the correct model data. Further, we assume the real-time ED in (3.22) is executed at interval 500 assuming a forecast load increase of 5% at each load bus.

In Fig. 3.3, we show the LF, dispatch target, and LMP absolute errors for: (i) the measurement-based quantities with respect to the actual quantities computed with correct data; (ii) the incorrect data model-based quantities with respect to the actual quantities computed with correct data. Incorrect line impedance data for a subset of the lines impacts results in LF errors at all buses, shown in Fig. 3.3a. Moreover, erroneous LFs cause substantial errors in the generator dispatch, shown in Fig. 3.3b, and LMPs, shown in Fig. 3.3c.

As shown in Table 3.5, the MSEs for the measurement-based LFs and the dispatch targets and LMPs computed with those LFs are an order of magnitude less than those for the respective model-based quantities. The deployment of measurement-based LFs in the real-time ED offers substantial enhancements compared to the model-based LFs, making the process robust to model errors.

3.6 Summary

In this chapter, we developed a measurement-based approach for estimating LFs. Our approach harnesses PMU measurements at the loads and generators to estimate the LFs without the use of a system model. Furthermore,

our approach does not rely on arbitrarily selecting a set of distributed slack weights.

As demonstrated in our case studies, our approach makes possible the computation of LFs with high accuracy despite the challenges posed by changes in the system operating point, undetected outages, and the existence of incorrect data in the system model. The resulting measurement-based LFs better reflect real-time system conditions and enhance the real-time ED and LMP calculation.

CHAPTER 4

GENERALIZED, SENSITIVITY-BASED LINE OUTAGE ANGLE FACTORS

In this chapter, we propose a model-based approach to the computation of line outage angle factors (LOAFs), which relies on the use of angle factors (AFs) and injection shift factors (ISFs). A LOAF provides the ratio of the difference between the outage angle and line angle, and the flow through the line before the outage occurs. The proposed LOAFs, along with the AFs and ISFs, enable a fast assessment of line outage angles, and, as we show, provide system operators with a systematic mean for determining the appropriate dispatch actions necessary to alleviate large outage angles. Additionally, using the sensitivity estimation approach described in Chapter 3, we formulate a PMU-measurement-based approach to computing LOAFs.

4.1 Introduction

System operators have long known that a transmission line breaker that has tripped open can be safely reclosed only if the outage angle—the voltage angle difference between the terminal buses of a transmission line after it is outaged—is sufficiently small (see, e.g., [20]). Indeed, as mentioned in Chapter 1, the failure to reclose a breaker due to a large line outage angle was a contributing factor in the chain of events that ultimately resulted in the 2011 San Diego blackout [3]. Furthermore, the blackout after-the-fact assessment report concluded that "underlying factors that contributed to the event... [included] not providing effective tools and operating instructions for use when reclosing lines with large phase angle differences across the reclosing breakers [3]." In this chapter, we introduce a sensitivity-based formulation of the LOAFs and propose a set of LOAF-based tools that enable operators to: (i) efficiently compute line outage angles; (ii) take effective action to reduce outage angles. Such tools address the needs identified in [3] by providing

effective means of preventing reliability issues that may result from a lack of operator awareness of large outage angles.

A LOAF provides the ratio of the difference between the outage angle and and line angle—the difference between the angle of the voltage at a line's terminal buses—and the flow through the line before the outage occurs. The LOAF derivation and deployment relies on: (i) the AFs, which provide the sensitivity of the bus voltage angles to changes in bus active power injections, assuming the injection changes are balanced by a single slack bus or set of slack buses; and (ii) the ISFs, which provide the sensitivity of line active power flows to bus active power injections assuming they are balanced by a single slack bus or set of slack buses. LOAFs, together with AFs and ISFs, can be used to quickly compute line outage angles, and ascertain the impact on line outage angles of line outages and active power injections.

Power system sensitivities, e.g., ISFs, are a critically important component of real-time operational reliability processes, e.g., security-constrained economic dispatch (SCED) (see, e.g., [25]). Conventional sensitivities and tools such as the SCED, however, have not, up to now, effectively captured outage angle impacts. Indeed, the need for angle-related reliability tools was recently made explicit in [45]. The LOAFs were first proposed in [22]. However, the derivation of the LOAFs in [22] utilizes the dc assumptions[1] and, as such, the LOAFs remain fixed for all operating points under a specific topology. Additionally, the derivation requires the computation of the bus impedance matrix for each outage topology—a computationally burdensome requirement for online applications.

In this chapter, we derive the LOAFs from a linearized power flow model—without the dc assumptions—making use of the AFs and ISFs. Our approach harnesses the concept of the flow-canceling transaction (FCT) used in the formulation of another sensitivity-based quantity commonly utilized in contingency analysis: the line outage distribution factors (LODFs) [42]. However, in this thesis, we generalize the FCT concept by removing the need of the dc assumptions in its derivation. Using our proposed approach, we are able to compute the LOAF of any line from a single system topology—the outage-free topology. Furthermore, we formulate a measurement-based LOAF using

[1]Recall that the dc assumptions are conventionally stated as follows: (i) the system is lossless, (ii) the voltage at each bus is approximately equal to one p.u., (iii) the difference in the voltage angles between each pair of connected buses is small [13].

the sensitivity estimation approach described in Chapter 3, which does not require a (potentially erroneous) model of the system. Our proposed LOAFs form the basis for effective and computationally efficient tools for use by system operators in addressing the challenge of large line outage angle monitoring and control.

4.2 Model-Based LOAF Computation

In this section, we describe our approach to the model-based LOAF computation. We begin with a brief review of the model-based AFs and ISFs derived in Sections 2.3 and 2.4, respectively. Then, we derive the generalized FCT, which we use along with the AFs to derive the LOAFs.

4.2.1 Model-Based AF and ISF Computation

Model-Based AFs. As mentioned above, the AFs are the sensitivities of the bus voltage angles with respect to the bus active power injections assuming the change is balanced by a pre-specified slack bus, or distributed slack bus. Let θ_n be the voltage angle at bus n, and let P_m be the net active power injection at a bus m. Then, we define the AF for bus n with respect to an injection at bus m that is withdrawn according to the distributed slack policy as

$$\Omega[n, m] = \frac{\partial \theta_n}{\partial P_m}.$$

As developed in Section 2.3, the change in the bus voltage angles with respect to active (reactive) power perturbations, $\Delta P'$ ($\Delta Q'$) is given by:

$$\Delta\theta \approx \Omega \Delta P' + \Omega^q \Delta Q', \tag{4.1}$$

where

$$\Omega = F + F\alpha r^T + M_{c^*} U, \tag{4.2}$$

$$\Omega^q = M + F\alpha w^T + M_{c^*} W), \tag{4.3}$$

are active and reactive power AFs, respectively.

Model-Based ISFs. As described previously, the ISFs are the sensitivities of line active power flows to bus active power injections assuming the change is balanced by a pre-specified slack bus, or distributed slack bus. In line with the derivation in Section 2.4, define $P^f_{l,n} = h_{l,n}(x)$, where $h_{l,n} : \mathbb{R}^{2N} \to \mathbb{R}^L$, to be the active power flow injected into line ℓ_l at the bus n end, which, without loss of generality, we will assume is the *from* bus. Then, the ISF for the active power injected at the *from* end of line $\ell_l \in \mathcal{L}$ with respect to an active power injection at bus n that is withdrawn according to the distributed slack policy is defined as follows:

$$\Psi[l, n] = \frac{\partial P^f_{l,n}}{\partial P_n}.$$

Then, we can describe the variation in the active power flow $\Delta P^f_{l,n}$ in terms of the variation in active and reactive power bus injections as follows:

$$\Delta P^f_{l,n} \approx \Psi_l \Delta P' + \Psi^q_l \Delta Q', \tag{4.4}$$

where

$$\Psi_l = -s^T_{l,n}(J^{-1}C + J^{-1}C\alpha r^T + B_{c^*}U), \tag{4.5}$$

$$\Psi^q_l = -s^T_{l,n}(J^{-1}D + J^{-1}D\alpha w^T + B_{c^*}W), \tag{4.6}$$

where $s_{l,n} = \frac{\partial h_{l,n}}{\partial x}|_{x_0}$ and B_{c^*} is a matrix composed of the columns of $J^{-1}D$ associated with voltage-controlled buses. In addition, recall that we denote by Ψ the $L \times N$ ISF matrix, the rows of which are computed using (2.35). Moreover, we define Ψ^r to be the matrix of sensitivities of the active power flow at the *to* end of each line to bus injections, which is computed for each line $\ell_l = (n, m)$ using $h_{l,m}(x)$ in a manner analogous to that used to compute Ψ.

4.2.2 Model-Based LOAF Computation

The LOAF for line $\ell_l = (n, m)$ provides the ratio of the difference between the outage angle and line angle of line ℓ_l to the flow on line ℓ_l before its outage occurs. Let $\Delta\theta_{n\text{-}m} = \Delta\theta_n - \Delta\theta_m$ be the change in the voltage angle across line ℓ_l in response to the outage of line ℓ_l, which has pre-outage flow, $P^f_{l,n}$, at bus n, i.e., at the *from* end of the line. Then, define the LOAF for

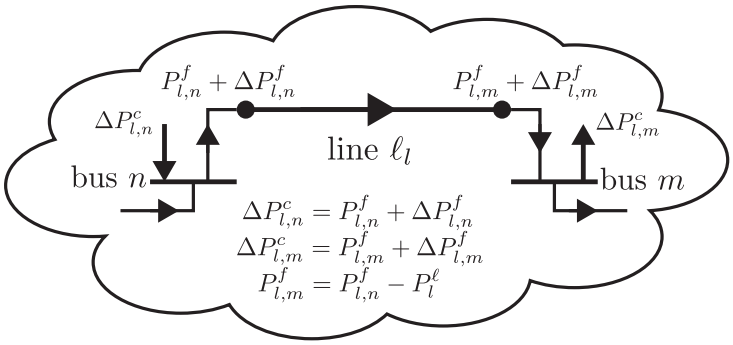

Figure 4.1: The flow-canceling transaction.

the outage of line ℓ_l as follows:

$$\Sigma_l = \frac{\Delta\theta_{n\text{-}m}}{P^f_{l,n}}.$$

To derive LOAFs using the outage-free topology, we simulate the outage of line $\ell_l = (n, m)$ by introducing active power injections $\Delta P^c_{l,n}$ and $\Delta P^c_{l,m}$ at buses bus n and m, respectively, that result in zero net injection at each end of line ℓ_l—a so-called *flow-canceling transaction* (FCT) [42]—as illustrated in Fig. 4.1. However, in this thesis, we introduce the notion of the generalized FCT, which does not, as is the case for the conventional notion of the FCT, rely on the dc assumptions.

In order to enforce the desired zero net injection condition, we select the magnitude of the generalized FCT injections such that

$$\Delta P^c_{l,n} = P^f_{l,n} + \Delta P^f_{l,n}, \tag{4.7}$$

and

$$\Delta P^c_{l,m} = P^f_{l,m} + \Delta P^f_{l,m}, \tag{4.8}$$

where $\Delta P^f_{l,n}$ and $\Delta P^f_{l,m}$ are the additional flow that appears at the respective ends of line ℓ_l in response to injections $\Delta P^c_{l,n}$ and $\Delta P^c_{l,m}$. For notational simplicity in what follows, let $P^f_{l,n} = P^f_l$ and $\Delta P^f_{l,n} = \Delta P^f_l$. Then, we relate the flow at each end of line $\ell_l = (n, m)$ including the impacts of the FCT by

$$P^f_{l,m} + \Delta P^f_{l,m} = P^f_l + \Delta P^f_l - P^\ell_l - \Delta P^\ell_l, \tag{4.9}$$

where P^ℓ_l is the active power losses on line ℓ_l due to the original flow P^f_l

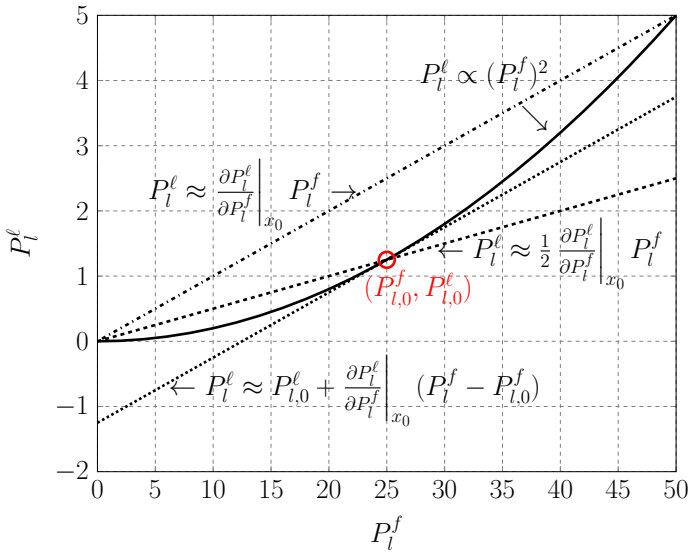

Figure 4.2: Affine and linear loss approximation functions.

and ΔP_l^ℓ is the change in losses due to the FCT. Moreover, we write ΔP_l^f in terms of ISFs as follows:

$$\Delta P_l^f \approx \Psi[l,n]\Delta P_{l,n}^c - \Psi[l,m]\Delta P_{l,m}^c, \tag{4.10}$$

and we compute ΔP_l^ℓ from the ISFs as follows:

$$\Delta P_l^\ell \approx (\Psi[l,n] - \Psi^r[l,n])\Delta P_{l,n}^c - (\Psi[l,m] - \Psi^r[l,m])\Delta P_{l,m}^c. \tag{4.11}$$

Next, we require a linear expression for P_l^ℓ in terms of P_l^f for which the approximated losses are: (i) zero when the line ℓ_l flow is zero, i.e., the relationship is strictly linear; and (ii) accurately represented around the nominal operating point. To obtain such an expression, we assume that $P_l^\ell \propto (P_l^f)^2$.[2] By linearizing this quadratic function about the operating point (P_0, Q_0, x_0), we can approximate the quadratic line ℓ_l losses as an affine function of the line ℓ_l flows as

$$P_l^\ell \approx P_{l,0}^\ell + a(P_l^f - P_{l,0}^f), \tag{4.12}$$

where $a = \frac{\partial P_l^\ell}{\partial P_l^f}\Big|_{x_0}$, and $P_{l,0}^f$ and $P_{l,0}^\ell$ are the nominal flow and line loss, respectively, on line ℓ_l. Furthermore, considering a change in the flow on a line ℓ_l as an equivalent injection at bus n, which we denote by $\Delta\tilde{P}_n$, we can

[2]The intuition behind this assumption, which we explore empirically in Appendix B, is thus: $\Delta P_l^f \propto \Delta P$ and $\Delta P_l^\ell \propto \Delta P^2$, hence $P_l^\ell \propto (P_l^f)^2$.

approximate a using the ISFs as follows:

$$\begin{aligned} a \approx & \frac{(\Psi[l,n] - \Psi^r[l,n])\Delta\tilde{P}_n}{\Psi[l,n]\Delta\tilde{P}_n} \\ = & \frac{(\Psi[l,n] - \Psi^r[l,n])}{\Psi[l,n]}. \end{aligned} \tag{4.13}$$

Additionally, we use (4.13) to approximate the nominal line ℓ_l losses as

$$P^{\ell}_{l,0} \approx aP^f_{l,0}. \tag{4.14}$$

Then, by substituting (4.13) and (4.14) into (4.12) and simplifying, we obtain the following linear relationship between P^{ℓ}_l and P^f_l:

$$P^{\ell}_l \approx aP^f_l. \tag{4.15}$$

Though the linear loss approximation in (4.15) meets criterion (i) above, this approach is not ideal for the derivation of the LOAFs owing to the fact that, as shown in Fig. 4.2, it grossly over-estimates the line losses at the nominal operating point, i.e., criterion (ii) is not met. To obtain a more appropriate linear representation of the line losses, we approximate the quadratic line loss function by the following function:

$$P^{\ell}_l \approx \frac{1}{2}aP^f_l, \tag{4.16}$$

which, as shown in Fig. 4.2, for a nominal flow and line loss on line ℓ_l, $P^f_{l,0}$ and $P^{\ell}_{l,0}$, respectively, is exact for the point $(P^f_{l,0}, P^{\ell}_{l,0})$ and strictly linear. The line loss representation in (4.16) is advantageous for deriving the LOAFs due to the fact that it meets criteria (i) and (ii) above, and its being computed from the ISFs, which are already computed periodically in the real-time operations context. These advantages, however, come at the expense of decreased loss approximation accuracy around the nominal operating point compared to the affine approximation in (4.12).

Now, by substituting (4.9), (4.10), (4.11), and (4.16) into (4.7) and (4.8) and rearranging, we obtain the desired FCT magnitudes at buses n and m in terms of the pre-injection flow into ℓ_l at bus n as

$$\Delta P^c_{l,n} = XP^f_l, \tag{4.17}$$

and

$$\Delta P^c_{l,m} = Y P^f_l, \tag{4.18}$$

where

$$X = \frac{1 - \Psi[l,m]Y}{1 - \Psi[l,n]},$$

and

$$Y = \frac{(\Psi^r[l,n] + \Psi[l,n](1 - \Psi[l,n] + \Psi^r[l,n]))/(2\Psi[l,n])}{1 - \Psi[l,n] + \Psi^r[l,n]\Psi[l,m] + \Psi^r[l,m](1 - \Psi[l,n])};$$

we note that X and Y depend only on the ISFs.

The application of the generalized FCT approximates the impact on the system of the outage of line ℓ_l as a pair of net active power injections. Thus, using superposition, one can easily see that in order to obtain the change in the angle at any bus due to the FCT, we can use (4.2) considering the FCT magnitudes, $\Delta P^c_{l,n}$ and $\Delta P^c_{l,m}$, as an active power perturbation. In particular, we can approximate the change in the angles at the line ℓ_l terminal buses n and m, respectively, with respect to the outage of ℓ_l as

$$\Delta\theta_n \approx \Omega[n,n]\Delta P^c_{l,n} - \Omega[n,m]\Delta P^c_{l,m}, \tag{4.19}$$

and

$$\Delta\theta_m \approx \Omega[m,n]\Delta P^c_{l,n} - \Omega[m,m]\Delta P^c_{l,m}. \tag{4.20}$$

Now, by substituting (4.17) and (4.18) into (4.19) and (4.20), we obtain expressions relating the line ℓ_l terminal bus voltage angles to its pre-outage flow

$$\Delta\theta_n \approx (\Omega[n,n]X - \Omega[n,m]Y)P^f_l = T_n P^f_l, \tag{4.21}$$

and

$$\Delta\theta_m \approx (\Omega[m,n]X - \Omega[m,m]Y)P^f_l = -T_m P^f_l. \tag{4.22}$$

Next, by subtracting the angle change at each terminal node, given by (4.21) and (4.22), we arrive at

$$\Delta\theta_{n\text{-}m} = \Delta\theta_n - \Delta\theta_m \approx (T_n + T_m)P^f_l.$$

Thus, the LOAF for line ℓ_l is given by

$$\Sigma_l = T_n + T_m. \tag{4.23}$$

4.2.3 LOAFs under the Dc Assumptions

In applications for which the dc assumptions are appropriate, e.g., the day-ahead markets, the computation of the LOAFs can be greatly simplified. Consider again a line ℓ_l. With the assumption that the system is lossless, the FCT magnitude for line ℓ_l is identical at both terminal buses and is given by:

$$\Delta P_l^c = P_l^f + \Delta P_l^f. \tag{4.24}$$

Moreover, under the dc assumptions, we can write ΔP_l^f as

$$\Delta P_l^f = (\Psi[l,n] - \Psi[l,m])\Delta P_l^c. \tag{4.25}$$

Substituting (4.25) into (4.24) and rearranging we arrive at the dc-model-based FCT,

$$\Delta P_l^c = \frac{P_l^f}{1 - (\Psi[l,n] - \Psi[l,m])}. \tag{4.26}$$

Then, we can approximate the change in the angles at the line ℓ_l terminal buses n and m, respectively, with respect to the outage of ℓ_l as follows:

$$\Delta\theta_n \approx (\Omega[n,n] - \Omega[n,m])\Delta P_l^c, \tag{4.27}$$

and

$$\Delta\theta_m \approx (\Omega[m,n] - \Omega[m,m])\Delta P_l^c. \tag{4.28}$$

Substituting (4.26) into (4.27) and (4.28), we obtain expressions relating the line ℓ_l terminal bus voltage angles to its pre-outage flow

$$\Delta\theta_n \approx \frac{(\Omega[n,n] - \Omega[n,m])}{1 - (\Psi[l,n] - \Psi[l,m])} P_k^f = T_n^{dc} P_l^f, \tag{4.29}$$

and

$$\Delta\theta_m \approx \frac{(\Omega[m,n] - \Omega[m,m])}{1 - (\Psi[l,n] - \Psi[l,m])} P_l^f = -T_m^{dc} P_l^f. \tag{4.30}$$

Subtracting the angle change at each terminal node, given by (4.29) and (4.30), we arrive at

$$\Delta\theta_{n\text{-}m} = \Delta\theta_n - \Delta\theta_m \approx (T_n^{dc} + T_m^{dc}) P_l^f.$$

Thus, the dc-model-based LOAF for line ℓ_l is given by

$$\Sigma_l^{dc} = T_n^{dc} + T_m^{dc}. \tag{4.31}$$

4.3 LOAF Applications

In this section, we give an overview of two primary online applications for LOAFs, both of which are motivated by the needs expressed in the San Diego blackout after-the-fact assessment report [3]: (i) line outage angle monitoring; and (ii) generator dispatch considering outage angle limits across a set of lines via LOAF-based reliability constraints in the SCED.

4.3.1 Outage Angle Monitoring

The LOAFs can be used to alert operators of the existence of large line outage angles. To this end, the total outage angle between the terminal buses of a line $\ell_l = (n, m)$, which we denote by θ_l^f, can be written in terms of the bus angles and line flows (obtained from a state estimator or from PMU measurements), and the LOAFs as follows:

$$\theta_l^f = \theta_{n\text{-}m} + \Sigma_l P_l^f, \tag{4.32}$$

where $\theta_{n\text{-}m} = \theta_n - \theta_m$.

The outage angles can also be computed with respect to the outage of another line in the system by utilizing the line outage distribution factors (LODFs), which, for any pair of lines, ℓ_l, ℓ_u, provide the proportion of the pre-outage flow on a line ℓ_u that flows on a line ℓ_l in the event of the outage of ℓ_u (see, e.g., [13]). Computing the impact of multiple outages on line outage angles may be of interest for preventing cascading outages. Define $\theta_{l,u}^f$ to be the outage angle on line ℓ_l in the presence of the outage of line ℓ_u and let $\Xi[l, u]$ be the LODF for line ℓ_l with respect to the outage of line ℓ_u. Then, we can compute $\theta_{l,u}^f$ as follows:

$$\theta_{l,u}^f = \theta_{n\text{-}m} + \Sigma_l(P_l^f + \Xi[l, u]P_u^f). \tag{4.33}$$

If an outage angle is shown via (4.32) or (4.33) to exceed a pre-specified limit,

an alarm can be raised and the system operator can, if deemed necessary, take actions to mitigate the angle using LOAF-based dispatch tools, one of which we describe next.

4.3.2 SCED with Angle Constraints

The line outage angles computed online with (4.32) or (4.33) alert operators of potential large outage angles. In order to systematically address identified large outage angles, we propose extending the real-time SCED to include angle constraints.

As stated previously, the real-time SCED is a widely used operational tool that aims to determine the change in the generator dispatch targets, ΔP^g, required to economically meet the forecast change in the load, ΔP^d, plus losses, ΔP^ℓ, and ensure system physical constraints and reliability standards are met [13]. Suppose the system is operating with a load and dispatch (P_0^d, P_0^g) and corresponding line flows P_0^f. Moreover, assume that loads have an infinite willingness to pay. Then, the real-time SCED problem, built on the real-time ED formulated in (2.44), can be stated as follows [26]:

$$\min_{\Delta P^g} \sum_{i \in \mathcal{G}} \mathscr{C}_i(\Delta P_i^g + P_{i,0}^g) \tag{4.34a}$$

$$s.t.$$

$$\mathbb{1}_G^T \Delta P^g - \mathbb{1}_D^T \Delta P^d - \Delta P^\ell = 0 \leftrightarrow \lambda_r \tag{4.34b}$$

$$\underline{P}^g \leq P_0^g + \Delta P^g \leq \bar{P}^g \tag{4.34c}$$

$$\underline{P}^f \leq P_0^f + \Psi \Delta P \leq \bar{P}^f, \qquad \leftrightarrow \underline{\mu}, \bar{\mu} \tag{4.34d}$$

$$\underline{P}^s \leq P_0^f + \Psi^s \Delta P \leq \bar{P}^s, \qquad \leftrightarrow \underline{\mu}^s, \bar{\mu}^s \tag{4.34e}$$

where $\mathscr{C}_i(\cdot)$ is the cost function of generator i (typically a quadratic or piecewise-linear function); Ψ^s is the matrix of post-outage ISFs for lines at risk of overload due to an outage as determined from the results of contingency analysis (see, e.g., [13]); $\underline{P}^s$ ($\bar{P}^s$) is the appropriately dimensioned vector of security constraint lower (upper) limits; and $\underline{\mu}^s$ ($\bar{\mu}^s$) is the vector of dual variables associated of the lower (upper) limiting security constraints. The formulation of the conventional security constraints will be treated in detail in Chapter 5. For now, it suffices to know that the aim of these con-

straints is to prevent transmission equipment overloads.

The primary outcomes of the real-time SCED in (4.34) are generator dispatch instructions, ΔP^g, that ensure $N-1$ reliability, i.e., no piece of equipment is overloaded by a single outage, and the locational marginal prices (LMPs), which we discuss in Section 4.3.3. However, the conventional real-time SCED does not guard against large line outage angles.

To bring outage angle considerations into the SCED, we formulate outage angle-based reliability constraints for each line ℓ_l of interest using the AFs, ISFs, and LOAFs as follows:

$$-\bar{\theta}_l^f \leq \theta_{l,0}^f + (\Omega_n - \Omega_m)\Delta P + \Sigma_l \Psi_l \Delta P \leq \bar{\theta}_l^f \leftrightarrow \underline{\mu}_l^\theta, \bar{\mu}_l^\theta, \tag{4.35}$$

where Ω_n (Ω_m) is the nth (mth) row of Ω; $\theta_{l,0}^f$ is the nominal line ℓ_l outage angle, computed with (4.32); $\bar{\theta}_l^f$ is the maximum allowable line ℓ_l outage angle; and $\underline{\mu}_l^\theta$ ($\bar{\mu}_l^\theta$) are the angle constraint lower (upper) limit dual variables. Those lines deemed to be critical, e.g., lines that must be reclosed quickly in the event of a fault, can have their outage angle restricted in (4.34) by including a constraint (4.35) for each such line.

4.3.3 LMP Angle Component

In current real-time market processes, and as defined in (2.45), the LMPs are typically calculated from the ISFs, the LFs, and the shadow prices [50] as follows:

$$\tilde{\lambda} = \lambda_r \mathbb{1}_N + \begin{bmatrix} \Psi \\ \Psi^s \end{bmatrix}^T \left(\begin{bmatrix} \bar{\mu}^f \\ \bar{\mu}^s \end{bmatrix} - \begin{bmatrix} \underline{\mu}^f \\ \underline{\mu}^s \end{bmatrix} \right) + \Lambda \lambda_r, \tag{4.36}$$

where Λ is the N-dimensional marginal loss factor vector. Now, define

$$\lambda^c = \begin{bmatrix} \Psi \\ \Psi^s \end{bmatrix}^T \left(\begin{bmatrix} \bar{\mu}^f \\ \bar{\mu}^s \end{bmatrix} - \begin{bmatrix} \underline{\mu}^f \\ \underline{\mu}^s \end{bmatrix} \right), \lambda^\ell = \Lambda \lambda_r,$$

and $\lambda^r = \lambda_r \mathbb{1}_N$ to be the N-dimensional vectors representing, respectively, the congestion, loss, and energy components of the so-called three-part LMPs. This conventional three-part LMP incorporates the price impacts of transmission congestion due to network flows and reliability considerations. How-

ever, it does not capture the potential for dispatch limitations due to angle constraints.

To capture the impacts on the LMPs of the introduction of angle reliability constraints in (4.35) we must include an additional LMP component in (4.36). Define λ^θ to be the N-dimensional vector of *angle components* of the LMP and Ψ^θ to be the matrix of angle constraint coefficients, a row of which, corresponding to an angle constraint on a line $\ell_l = (n, m)$, is given by

$$\Psi_l^\theta = (\Omega_n - \Omega_m) + \Sigma_l \Psi_l.$$

Next, using Ψ^θ and the shadow prices of the angle constraints, we compute the angle components of the LMP as follows:

$$\lambda^\theta = (\Psi^\theta)^T \left(\bar{\mu}^\theta - \underline{\mu}^\theta \right). \tag{4.37}$$

Then, the total LMP, including the angle component, is given by

$$\lambda = \lambda^r + \lambda^c + \lambda^\ell + \lambda^\theta. \tag{4.38}$$

The angle components of the LMP capture the cost to deliver the next MW to each bus associated with angle-constraint-driven dispatch limitations.

4.4 Case Studies

In this section, we report the results of case studies carried out on the IEEE 14- and 118-bus test systems to demonstrate the accuracy with which the LOAFs can predict the outage angles, as well as the application of the LOAFs in the SCED.

4.4.1 Case Studies I: The 14-Bus Test System

Here, we present the results of a case study carried out using a modified version of the IEEE 5-generator, 20-line, 14-bus test system [56], the topology of which is shown in Fig. 4.3. The test system has been modified by condensing the parallel lines between buses 1 and 2 into a single, equivalent line.

We first illustrate the accuracy of using the LOAFs to predict outage

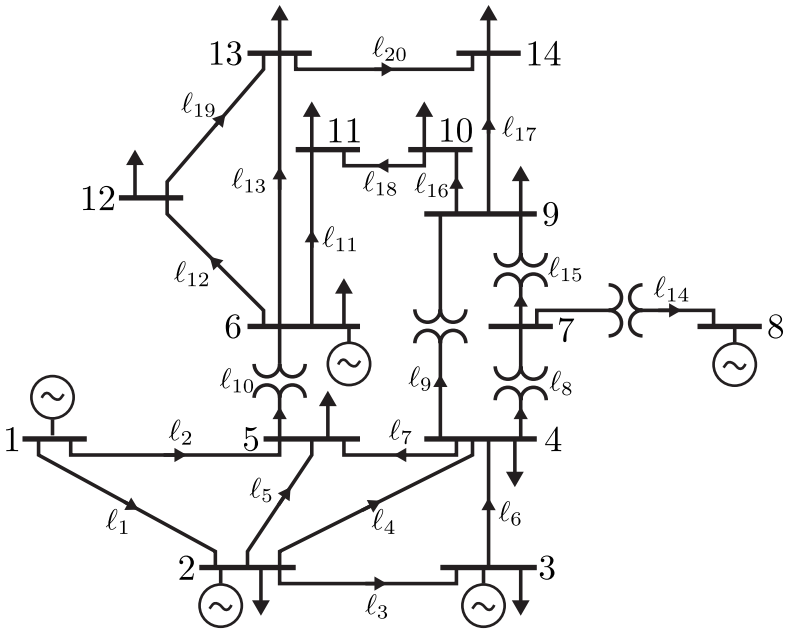

Figure 4.3: The IEEE 14-bus test system.

angles. To do so, we compute the LOAF-predicted outage angles, using (4.32) with LOAFs computed with (4.23) using AFs and ISFs computed with (2.29) and (2.36), respectively, at an ac-OPF solution, which is solved at the nominal load provided with the test case, and nominal voltage angles from the same solution. Then, we compare the LOAF-predicted outage angle to the actual outage angles, which are computed by repeatedly solving the ac power flow around the same ac-OPF solution used to compute the outage angle predictions with a single line removed in each solution and comparing the angles in the outage cases to those in the non-outage case.

As shown in Fig. 4.4a, the outage angles predicted by the LOAFs match well with the actual outage angles; the absolute outage angle error, shown in Fig. 4.4b, is less than 0.5 degrees for the most of the highly impacted lines, with the exception of line ℓ_2, which has an outage angle of 35 degrees and 2 degrees of LOAF-predicted outage angle error. However, as shown in Fig. 4.4c, the percent error of the outage angles at all of the highly impacted lines is less than 6%. Suppose the system operator aimed to keep the outage angles of all lines under a pre-defined threshold, e.g., 30 degrees. Then, LOAF-enabled outage angle monitoring could, in this case, raise an alarm for line ℓ_2 outage angle so that the operator could, if deemed necessary, take action to reduce the outage angle, e.g., by redispatching generation.

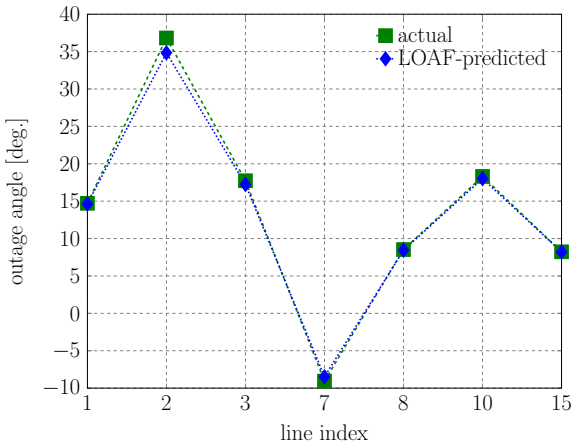

(a) Outage angles.

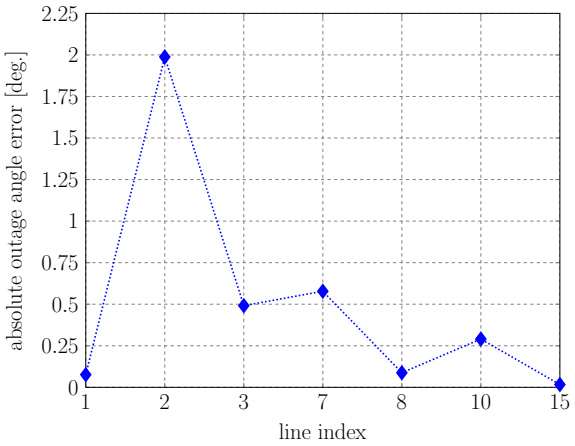

(b) Outage angle absolute errors.

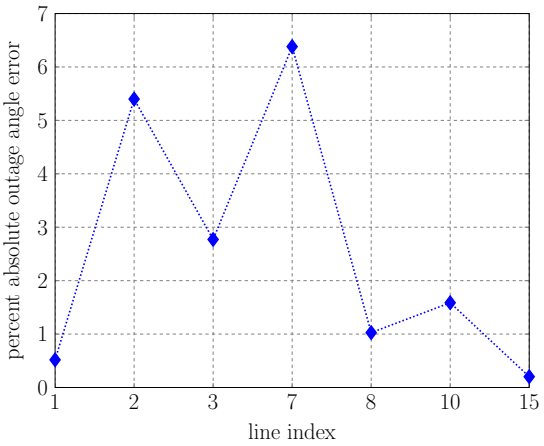

(c) Outage angle percent absolute errors.

Figure 4.4: Model-based LOAF-predicted vs. actual outage angles and errors for lines with outage angle changes ≥ 5 degrees.

Table 4.1: The 118-bus test system modified line limits.

line:	ℓ_8	ℓ_{31}	ℓ_{71}	ℓ_{98}	ℓ_{99}	ℓ_{138}	ℓ_{139}
$\bar{P}_l^f$ (MW):	200	60	50	70	70	70	70

4.4.2 Case Studies II: The 118-Bus Test System

Here, we present the results of case studies carried out using a modified IEEE 54-generator, 186-line, 118-bus test system [56], in which a subset of line limits, shown in Table 4.1, have been reduced so as to introduce transmission congestion; the lower limits on each line in this subset are selected such that $\underline{P}_l^f = -\bar{P}_l^f$. The case studies demonstrate the application of the LOAFs to formulated an angle-constrained SCED. To focus on the impacts of the angle constraints, we assume that there are no potential overloads identified through contingency analysis and thus no conventional security constraints in the SCED. Furthermore, we assume that each load has an infinite willingness to pay, i.e., the demand is inelastic, and each generator $i \in \mathcal{G}$ submits a quadratic offer function of the form $a_i(P_i^g)^2 + b_i P_i^g + c_i$ in the SCED, the parameters of which are taken from the test case.

We demonstrate the execution of the SCED with angle constraints to control the absolute outage angles to within a pre-specified limit and the accuracy of the LOAF-predicted outage angles on a larger-scale system. To do so, we solve two cases of the SCED in (4.34), each computed around an ac-OPF solution computed at the nominal load provided with the test case: (i) SCED with no angle constraints, i.e., the conventional SCED; and (ii) SCED with the angle constraints defined by (4.35) included for each line and a maximum outage angle of 20 degrees, i.e., the angle-constrained SCED. For both the conventional and angle-constrained SCED solutions, we compute the LMPs using (4.36) and (4.38), respectively. Additionally, to demonstrate the accuracy of the LOAFs, we compute the LOAF-predicted and actual outage angles at the conventional SCED solution. As before, the actual outage angles are computed by solving an ac power flow at the SCED solution for the outage of each line individually.

Table 4.2 shows the error statistics for the absolute and percent absolute angle errors between the actual and LOAF-predicted outage angles computed at the conventional SCED solution. As in the 14-bus case described in Section 4.4.1, LOAFs in this case prove to be an accurate predictor of the outage

Table 4.2: LOAF-predicted vs. actual outage angle error statistics at conventional SCED solution in the 118-bus case.

statistic	absolute outage angle error [deg.]	percent absolute outage angle error [%]
MSE:	1.66	6.75
min:	0.02	0.07
mean:	0.29	1.30
max:	1.09	4.13

angles. Indeed, the maximum absolute outage angle error is 1.09 degrees and the mean-squared error (MSE) over all outage angles is 1.66 degrees, while those of the percent absolute error are 4.12% and 6.75%, respectively.

As shown in Fig. 4.5a, the outage angles on lines ℓ_{10} and ℓ_{37} exceed the 20 degree limit at the conventional SCED solution. However, when the angle constraints from (4.35) are include, the outage angles remain within the specified 20 degree limit. The outage angles are maintained within their limits by modifying the generator dispatch, shown in Fig. 4.5b for the conventional and angle-constrained SCED. The redispatch required to bring the outage angles on lines ℓ_{10} and ℓ_{37} within the limits is substantial. For example, generator 5, which resides at bus 10, has its dispatch reduced by more than 1 p.u. in the angle-constrained SCED solution due to its electrical proximity to bus 8, a terminal bus of line ℓ_{37}—in fact, nearly 75% of the active power injected at bus 10 flows over line ℓ_{37}.

Furthermore, the angle-constrained LMPs, shown in Fig. 4.5c, and the angle component of those LMPs, computed with (4.37) and shown in Fig. 4.6, provide an indication of the buses at which active power injections into the system cause increases in the outage angles that are at their limit. Those buses at which the angle component of the LMP is negative, i.e., the LMP decreases in the angle-constrained SCED solution compared to the conventional SCED, e.g., buses 10 and 89, are buses at which active power injections increase the outage angle on binding lines, e.g., line ℓ_{37}, which, in this case, correspond to the buses at which the generators with the largest decrease in dispatch reside (generators 5 and 40). Conversely, those buses at which the angle component of the LMP is positive, i.e., the LMP increases with angle constraints, e.g., buses 4, 6, and 32, are buses at which active power injections reduce the outage angle on binding lines, which, in this case, correspond to the buses at which the generators with the largest increase in dispatch reside

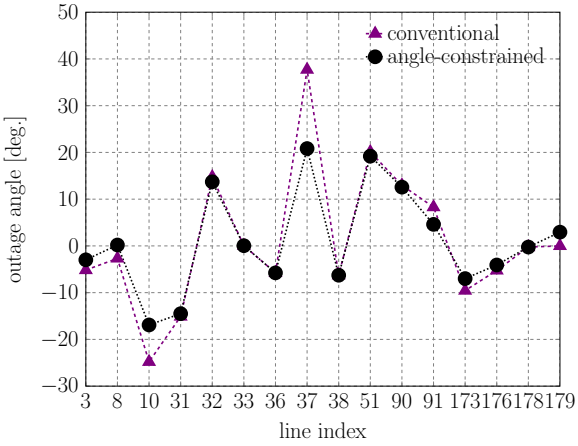

(a) Outage angles.

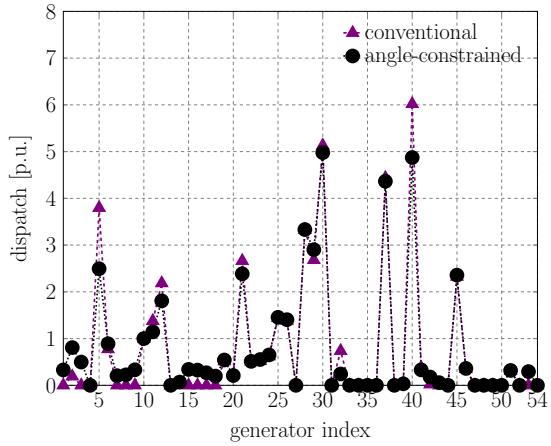

(b) Generator dispatch.

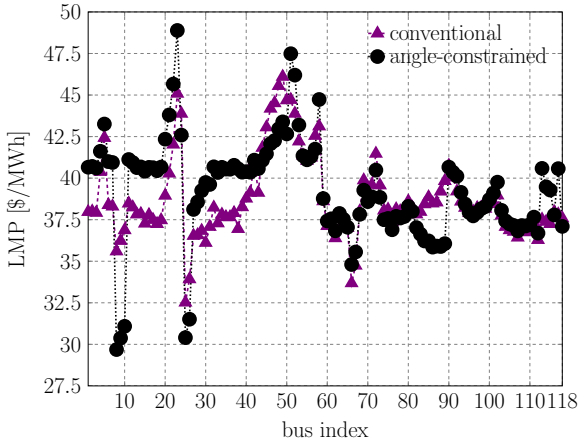

(c) LMPs.

Figure 4.5: Outage angles for lines with outage angle changes greater than 10 degrees, LMPs, and generator dispatch targets obtained with the conventional SCED and the SCED with angle constraints.

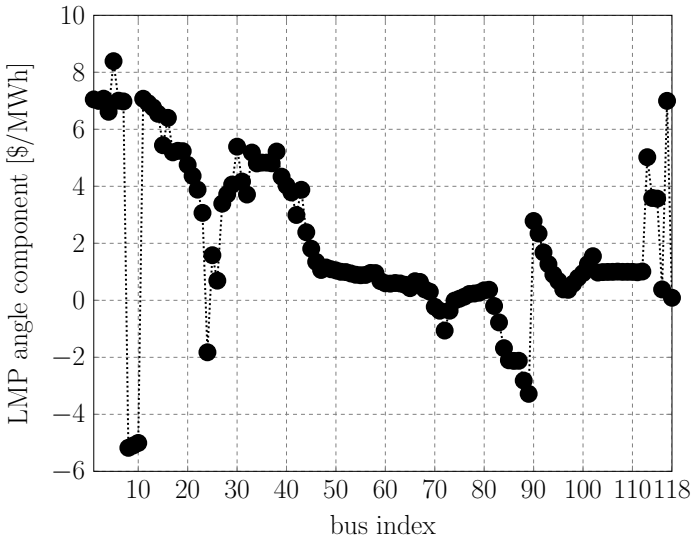

Figure 4.6: Angle component of the LMP for SCED with angle constraints.

(generators 2, 3, and 15).

Thus, the angle-constrained SCED could provide system operators the capability to systematically dispatch generation so as to restrict outage angles to within pre-specified bounds, e.g., those defined by recloser settings or synchrocheck relays. Moreover, the angle component of the LMP gives economic signals that provide a high-level view of the impacts of redispatch decisions on the angles and those buses at which injections may adversely/beneficially impact outage angles that are near their limit.

4.5 Extension: Measurement-Based LOAF Computation

We note that the LOAF defined in (4.23) is computed using ISFs and AFs. As such, it is straightforward to apply the sensitivity estimation approach proposed in Chapter 3 for estimating LFs and that to be presented in Chapter 5 for estimating ISFs to compute a measurement-based LOAF. To do so, we require the additional step of computing a measurement-based estimate of the AFs.

Consider the same power system defined in Section 2.2. Suppose the net active (reactive) power injected into the system at bus n at time t, $P_n(t)$ ($Q_n(t)$), varies by a small amount $\Delta P_n(t)$ ($\Delta Q_n(t)$) from time t to time

$t + \Delta t$, where $\Delta t > 0$ and small. Further, let $\Delta\theta^p_{m,n}(t)$ ($\Delta\theta^q_{m,n}(t)$) be the change in angle of the voltage at bus m due to ΔP_n (ΔQ_n). Then, define the AF for a bus m with respect to an active power injection at bus n as

$$\Omega[m,n] = \frac{\partial\theta_m}{\partial P_n} \approx \frac{\Delta\theta^p_{m,n}}{\Delta P_n}, \tag{4.39}$$

and the AF for bus m with respect to a reactive power injection at bus n as

$$\Omega^q[m,n] = \frac{\partial\theta_m}{\partial Q_n} \approx \frac{\Delta\theta^q_{m,n}}{\Delta Q_n}. \tag{4.40}$$

While $\Delta\theta^p_{m,n}(t)$ and $\Delta\theta^q_{m,n}(t)$ are not directly available through PMU measurements, we can, however, measure $\Delta\theta_m(t)$, the total change in bus m voltage angle due to bus injections at time t. We observe that the variation in the angle of the voltage at bus m is due to variations in the active and reactive power injections at each bus n:

$$\Delta\theta_m = \Delta\theta^p_{m,1}(t) + \cdots + \Delta\theta^p_{m,N}(t) + \Delta\theta^q_{m,1}(t) + \cdots + \Delta\theta^q_{m,N}(t). \tag{4.41}$$

Employing (4.39) and (4.40) in (4.41) we obtain

$$\begin{aligned}\Delta\theta_m \approx & \Delta P_1(t)\Omega[m,1] + \cdots + \Delta P_N(t)\Omega[m,N] \\ & + \Delta Q_1(t)\Omega^q[m,1] + \cdots + \Delta Q_N(t)\Omega^q[m,N].\end{aligned}$$

Now suppose we have $M+1$ sets of synchronized measurements. Let

$$\Delta P_n[k] = P_n[(k+1)\Delta t] - P_n[k\Delta t],$$

$$\Delta Q_n[k] = Q_n[(k+1)\Delta t] - Q_n[k\Delta t],$$

$$\Delta\theta_m[k] = \theta_m[(k+1)\Delta t] - \theta_m[k\Delta t],$$

for $n = 1, \ldots, M$ and define

$$\Delta P_n = \left[\Delta P_n[1] \ \cdots \ \Delta P_n[k] \ \cdots \ \Delta P_n[M]\right]^T,$$

$$\Delta Q_n = \left[\Delta Q_n[1] \ \cdots \ \Delta Q_n[k] \ \cdots \ \Delta Q_n[M]\right]^T,$$

$$\Delta\theta_m = \left[\Delta\theta_m[1] \ \cdots \ \Delta\theta_m[k] \ \cdots \ \Delta\theta_m[M]\right]^T.$$

Furthermore, let

$$\Omega_m = [\Omega[m,1], \ldots, \Omega[m,n], \ldots, \Omega[m,N]],$$

$$\Omega_m^q = [\Omega^q[m,1], \ldots, \Omega^q[m,n], \ldots, \Omega^q[m,N]],$$

$$\Omega_l^s = [(\Omega_m)^T \ (\Omega_m^q)^T]^T.$$

Then, clearly,

$$\Delta\theta_m = [\Delta P_1 \ \cdots \ \Delta P_n \ \cdots \ \Delta P_N \ \cdots \ \Delta Q_1 \ \cdots \ \Delta Q_n \ \cdots \ \Delta Q_N] \, (\Omega_m^s)^T. \tag{4.42}$$

Now, let $\Delta P = [\Delta P_1 \ \cdots \ \Delta P_n \ \cdots \ \Delta P_N]$, $\Delta Q = [\Delta Q_1 \ \cdots \ \Delta Q_n \ \cdots \ \Delta Q_N]$, and $\Delta S = [\Delta P^T \ \Delta Q^T]^T$. Then, the system in (4.42) becomes

$$\Delta\theta_m = \Delta S (\Omega_l^s)^T. \tag{4.43}$$

If $M \geq 2N$, then (4.43) is an overdetermined system. Moreover, assuming the AFs are approximately constant over the $M+1$ measurements,[3] we can obtain an estimate of Ω_m from least-squares error estimation as

$$(\hat{\Omega}_m^s)^T = (\Delta S^T \Delta S)^{-1} \Delta S^T \Delta S_l^f, \tag{4.44}$$

the first N elements of which are the desired measurement-based active power AFs, $\hat{\Omega}_m$, for bus m. Let $\hat{\Omega}$ be the $N \times N$ matrix of measurement-based AF estimates. Then, a measurement-based estimate of the LOAF can be computed using (4.23) with the measurement-based AFs estimated with (4.44) and measurement-based ISFs, which we will derive in Chapter 5.

4.6 Summary

In this chapter, we introduced a formulation of the generalized LOAFs based on the AFs and ISFs computed without the dc assumptions. The proposed LOAFs, together with the AFs and ISFs, provide a means of assessing the impacts of line outage angles using only the non-outage system topology. Additionally, we propose an approach for computing LOAFs from AFs and

[3] We provide an empirical analysis of this assumption in Appendix B.

ISFs estimated from PMU measurements without the need of a system model.

Furthermore, we formulate LOAF-based angle monitoring and dispatch tools, the need of which was identified as critically important by the 2011 San Diego blackout after-the-fact assessment report. As demonstrated above, the angle monitoring, angle-constrained SCED, and angle component of the LMP proposed in this thesis provides a systematic means of controlling outage angles and assessing the costs of maintaining outage angle reliability.

CHAPTER 5

MEASUREMENT-BASED REAL-TIME SECURITY-CONSTRAINED ECONOMIC DISPATCH

In this chapter, we propose a measurement-based approach to the real-time security-constrained economic dispatch (SCED). The real-time SCED is a widely used market scheduling tool that seeks to economically balance electricity system supply and demand and provide locational marginal prices (LMPs). To capture network flows and security considerations, the conventional SCED relies on sensitivities that are typically computed from a model of the system obtained offline. Our approach utilizes power system sensitivities estimated from phasor measurement unit (PMU) measurements.

5.1 Introduction

As described in Chapter 1, independent system operators (ISOs)/regional transmission organizations (RTOs) oversee scheduling procedures consisting of a sequence of forward markets based on security-constrained unit commitment- and economic dispatch-based algorithms (see, e.g., [24], [25]). The goal of these processes is to schedule resources on various time-scales such that the system operator can maintain the supply-demand balance around-the-clock, and satisfy operational and physical constraints imposed by the electricity network and reliability standards. Moreover, the market outcomes include resource dispatch targets and the prices for energy, the locational marginal prices (LMPs), and ancillary services [26], which provide important economic signals to participants. The so-called real-time markets are the final stage in the market scheduling process, and real-time security-constrained economic dispatch (SCED), which relies on accurate contingency selection and analysis, is a key component of that stage. Typically, the real-time SCED is formulated using model-based loss sensitivities—the marginal loss factors (LFs)—to represent system-wide losses, and linear flow sensitivities—

the injection shift factors (ISFs)—to represent active power flows [13].

In order to perform conventional contingency analysis and formulate the real-time SCED, the system operator requires an up-to-date model of the ISO/RTO's electricity system and that of neighboring systems, which is typically derived from the output of a state estimator. As described in Chapter 1, the state estimator-based model is vulnerable to errors due to numerous phenomena, modeling assumptions, and changing ambient operating conditions. Thus, the accuracy of security constraints identified through contingency analysis and the dispatch targets and LMPs determined in the model-based real-time SCED are coupled with the accuracy of the system model and, as such, subject to the same vulnerabilities. Inaccurate contingency analysis, dispatch targets, and LMPs have economic implications, e.g., sending incorrect local price signals and over/under payment to resources, as well as system reliability implications, e.g., unintended equipment overloads and outages [2, 3, 41].

In this chapter, we propose a measurement-based approach to the real-time SCED. Our aim is to overcome the above-described shortcomings of the model-based SCED. To do so, we reformulate the SCED constraints using more accurate data by removing model-based quantities and replacing them with measurement-based estimates of the same quantities. Specifically, we reformulate three types of constraints: (i) the power balance constraint; (ii) network flow constraints; and (iii) security constraints. In the model-based SCED, (i) depends on model-based LFs, whereas (ii) and (iii) depend on model-based ISFs and sensitivities derived from ISFs. Instead of relying on model-based LFs and ISFs, our approach utilizes measurement-based LFs and ISFs computed using the LF estimation approach described in Chapter 3, and a measurement-based method for estimating ISFs similar to that described in [18] and [43]. By removing the model-dependence of the SCED, our approach virtually eliminates the impacts of phenomena such as undetected changes in system topology and erroneous model parameters on the real-time SCED outcomes

Our approach relies on the availability of phasor measurement units (PMUs), the preponderance of which in power systems is facilitating the proliferation of a new generation of operational tools that harness the very high frequency and time synchronicity of their measurements (see, e.g., [7], [58],). Indeed, thousands of PMUs have been installed in North America over the past

decade and many relays come equipped with PMU functionality (see, e.g., [8]). The use of PMU data in real-time operations has been promoted as a means by which to circumvent the shortcomings of the existing telemetry system, and reduce the frequency of occurrence and the magnitude of the impact of preventable outages [3]. As we show, the real-time contingency selection and SCED processes can likewise be enhanced by the deployment of PMU measurements.

5.2 Conventional Real-Time SCED

The SCED is a reliability-enhancing market scheduling tool that is built on the real-time ED formulation presented in Section 2.5. The SCED has four primary components: (i) power flow and network flow constraints obtained from a model of the system; (ii) equipment constraints, e.g., generator power output limits; (iii) the objective, typically the maximization of social surplus or minimization of generator costs, commonly quadratic or piecewise-linear functions; and (iv) reliability-driven constraints, e.g., reserve requirement and security constraints; (see, e.g., [13], [27], [53]). Components (i)-(iii) are precisely the real-time ED, while component (iv) is introduced so as to bring operational reliability considerations into the real-time market scheduling process.

The conventional SCED formulation used in the market setting depends heavily on the ISFs via the network flow and security constraints. Thus, the remainder of this section is dedicated to the discussion of the ISFs in the context of those constraints and their incorporation into the SCED.

5.2.1 Network Flow Constraints

As described in Section 2.5, the ISF matrix, denoted by Ψ, provides the basis of the ISF-based dc-OPF network flow representation. Recall that an entry of Ψ, denoted by $\Psi[l, n]$, provides the sensitivity of the flow on line $\ell_l \in \mathcal{L}$ to an injection at bus n that is withdrawn at the slack bus. Under the dc assumptions, Ψ can be calculated directly from the network connectivity and

parameters using (2.38).[1]

Using the model-based ISFs from (2.38), we may define the vector of incremental line flows in terms of the incremental bus injections as

$$\Delta P^f = \Psi \Delta P, \tag{5.1}$$

which are bounded above and below by the line upper and lower incremental limits, denoted by $\Delta \bar{P}^f = \bar{P}^f - P_0^f$ and $\Delta \underline{P}^f = \underline{P}^f - P_0^f$, respectively.

5.2.2 Security Constraints

Power systems are typically operated with the so-called *"N-1" security criterion*, i.e., no equipment will be overloaded by the outage of a single line, generator, or other facility. To ensure that this requirement is upheld in the solution of the real-time SCED, so-called *security constraints* are added to the formulation. These constraints incorporate the *post-contingency* behavior of the system into the real-time SCED so that the resulting dispatch is secure under such contingencies. In this thesis, we consider a deterministic formulation of the SCED with no corrective actions, i.e., no decision variables for post-contingency reconfiguration of system resources. Such a formulation is a *preventative* approach to ensuring system security, and is consistent with current practice in ISO/RTO-run markets [28]. Alternative SCED formulations, which include the possibility of post-contingency reconfiguration of system resources in response to contingencies, have been proposed (see, e.g., [30], [32], [59]), but, to our knowledge, their deployment in practical real-time operations has so far been limited in scope.

In order to select the contingencies for which security constraints will be formulated, the system operator undertakes contingency selection and contingency analysis so as to ascertain the contingencies, e.g., line and generator outages, that will result in overloads on system equipment should they occur. In practice, operators do not consider the impacts of every possible single out-

[1] As we showed in Section 2.4, the ISFs can also be computed by linearizing the system model around a known ac power flow solution, typically obtained from the state estimator. Thus, if the model of the system is correct, ac-based sensitivities computed in this way are more accurate than the sensitivities computed under the dc assumptions (i.e., those in (2.38)); however, ac-based sensitivities obtained in this fashion might also be inaccurate if the model of the system used to computed them contains errors.

age on every piece of equipment, e.g., line, transformer, in the system, rather they consider a subset of facilities and contingencies via a pre-defined set of so-called *mon-con pairs*—each mon-con pair specifies a monitored facility and the contingency with respect to which it is monitored for overloads.

To be useful in the real-time operational context, real-time contingency analysis (RTCA) must be executed in a timely fashion (on the order of minutes, see, e.g. [60]). As such, RTCA is typically conducted using a contingency list composed of a subset of all possible mon-con pairs, which are selected using a combination of off-line studies, operator discretion, and dc-analysis, e.g., the flow performance index [13]. Ac power flow-based RTCA is used to analyze each mon-con pair on the contingency list, i.e., those mon-con pairs deemed to have significant potential to degrade system security. The outcome of RTCA is a set of mon-con pairs for which the corresponding outages cause overloads and for which security constraints must be included in the SCED.

Sensitivity-based quantities, namely the power transfer distribution factors (PTDFs) and line outage distribution factors (LODFs), which we defined in Section 2.4, are essential to the formulation of security constraints [13]. Recall that the $N \times N$ matrix of PTDFs for a line ℓ_l, which we denote by Φ_l, provides the sensitivity of the flow on line ℓ_l to real-power transactions between buses in the system. Additionally, recall that the $L \times L$ matrix of LODFs, which we denote by Ξ, provides the proportion of the pre-outage flow on each line ℓ_l that flows on each in-service line ℓ_u in the system in the event of the outage of line ℓ_l

Let $\mathcal{C}^g$ and $\mathcal{C}^f$ be the sets of generator and line outage mon-con pairs, respectively, identified by the system operator through contingency analysis as causing overloads. The sets $\mathcal{C}^g$ and $\mathcal{C}^f$ consist of doubles of the form (ℓ_u, c_j^g) and (ℓ_u, c_l^f), respectively, where (ℓ_u, c_j^g) is the mon-con pair for the overload of monitored line ℓ_u with respect to the outage of generator j, and (ℓ_u, c_l^f) is the mon-con pair for the overload of monitored line ℓ_u with respect to the outage of line ℓ_l.

We formulate an incremental security constraint for each line outage mon-con pair, $(\ell_u, c_l^f) \in \mathcal{C}^f$, using the LODFs from (2.40) as follows

$$\Delta \underline{P}^f_{u,c_l^f} \leq \Psi_u \Delta P + \Xi[u,l]\Psi_l \Delta P \leq \Delta \bar{P}^f_{u,c_l^f}, \tag{5.2}$$

where

$$\Delta \underline{P}^f_{u,c^f_l} = \underline{P}^f_u - P^f_{u,0} - \Xi[u,l]P^f_{l,0},$$

$$\Delta \bar{P}^f_{u,c^f_l} = \bar{P}^f_u - P^f_{u,0} - \Xi[u,l]P^f_{l,0},$$

Ψ_u (Ψ_l) is the uth (lth) row of the ISF matrix, and $P^f_{u,0}$ ($P^f_{l,0}$) is the nominal active power flow on line ℓ_u (ℓ_l). Then, define Ψ^f as the matrix of line flow to bus injection sensitivities for all line outages, where each row m corresponds to a mon-con pair $(\ell_u, c^f_l) \in \mathcal{C}^f$ and is given by

$$\Psi^f_m = \Psi_u + \Xi[u,l]\Psi_l. \tag{5.3}$$

The line flow impacts of generator contingencies depends on the response of the remaining generators in the system to such a continency, which is typically approximated by a function of each generator's inertial constant, maximum capacity, or dispatchable range [13]. For the contingency of a generator j, we assume the generators remaining online respond according to pre-specified participation factors corresponding to the outage of generator j. Define the participation factor of each generator i corresponding to the outage of generator j by

$$\alpha^g_i(c^g_j) = \begin{cases} \frac{\bar{P}^g_i}{\sum_{i\in\mathcal{G}, i\neq j}\bar{P}^g_i} & \text{if } i \neq j, i \in \mathcal{G}, \\ -1 & \text{if } i = j, i \in \mathcal{G}, \\ 0 & \text{otherwise.} \end{cases} \tag{5.4}$$

Then, let $\alpha(c^g_j)$ be the N-dimensional vector of nodal generator participation factors corresponding to the outage of generator j, each entry of which is given by

$$\alpha_n(c^g_j) = \sum_{i\in\mathcal{G}_n} \alpha^g_i(c^g_j). \tag{5.5}$$

For notational convenience, and without loss of generality, we assume there are no loads at the generator buses. Then, using the participation factors from (5.5), we formulate an incremental security constraint for each generator outage mon-con pair, $(\ell_u, c^g_j) \in \mathcal{C}^g$, as follows

$$\Delta \underline{P}^f_{u,c^g_j} \leq \Psi_u \Delta P + (\Psi_u \alpha(c^g_j) e^T_j)\Delta P \leq \Delta \bar{P}^f_{u,c^g_j}, \tag{5.6}$$

where

$$\Delta \underline{P}^f_{u,c^g_j} = \underline{P}^f_u - P^f_{u,0} - (\Psi_u \alpha(c^g_j) e^T_j) P_0,$$

$$\Delta \bar{P}^f_{u,c^g_j} = \bar{P}^f_u - P^f_{u,0} - (\Psi_u \alpha(c^g_j) e^T_j) P_0,$$

and e_j is an N-dimensional vector with a one in the jth entry and a zero in each other entry. Define Ψ^g as the matrix of line flow to bus injection sensitivities for the generator outages, where each row m corresponds to a mon-con pair $(\ell_u, c^g_j) \in \mathcal{C}^g$ and is given by

$$\Psi^g_m = \Psi_u + (\Psi_u \alpha(c^g_j)) e^T_j. \tag{5.7}$$

Furthermore, to ensure reliability is not compromised by a generator outage, there must be adequate upward capacity among all generators in the system to respond to the outage. Such limitations are typically captured in the SCED through the provision of reserves—also referred to as ancillary services—via the inclusion of reserve requirement constraints. Though critically important for maintaining reliability, the reserve requirement constraints are not directly impacted by the measurement-based formulation proposed here and so, for the sake of brevity, we do not explicitly represent them in the formulation.

Let $\Delta \underline{P}^s$, $\Delta \bar{P}^s$, be the vectors of lower and upper security constraint incremental limits, respectively, which consist of the incremental line limits corresponding to the potentially overloaded lines of their respective incremental security constraints from (5.2) and (5.6). Then, we can concisely state the collection of incremental security constraints corresponding to those mon-con pairs in $\mathcal{C}^f$ and $\mathcal{C}^g$ and defined in (5.2) and (5.6), respectively, as

$$\Delta \underline{P}^s \leq \Psi^s \Delta P \leq \Delta \bar{P}^s, \tag{5.8}$$

where

$$\Psi^s = \begin{bmatrix} \Psi^f \\ \Psi^g \end{bmatrix}.$$

5.2.3 Model-Based Real-Time SCED Problem Formulation

Combining the ED formulation in (2.44) with the constraints that result from the network flow expression in (5.1) and the security constraints in (5.8), we

formulate the model-based real-time SCED as follows:

$$\max_{\Delta P^g, \Delta P^d} \mathscr{S}(\Delta P^g, \Delta P^d) \tag{5.9a}$$

$$s.t.$$

$$\mathbb{1}_G \Delta P^g - \mathbb{1}_D \Delta P^d - \Delta P^\ell = 0 \;\leftrightarrow \lambda_r \tag{5.9b}$$

$$\underline{P}^g \leq P_0^g + \Delta P^g \leq \bar{P}^g \tag{5.9c}$$

$$\underline{P}^d \leq P_0^d + \Delta P^d \leq \bar{P}^d \tag{5.9d}$$

$$\Delta \underline{P}^f \leq \Psi \Delta P \leq \Delta \bar{P}^f \qquad \leftrightarrow \underline{\mu}^f, \bar{\mu}^f \tag{5.9e}$$

$$\Delta \underline{P}^s \leq \Psi^s \Delta P \leq \Delta \bar{P}^s \qquad \leftrightarrow \underline{\mu}^s, \bar{\mu}^s, \tag{5.9f}$$

where $\underline{\mu}^s, \bar{\mu}^s$ are the dual variables of the security constraints. Note that for clarity of presentation in (5.9), we have left out of the real-time SCED the ramping constraints that are often present in a practical real-time SCED [26]. Ramping constraints are the same regardless of the use of model- or measurement-based sensitivities. Thus, the exclusion of such constraints has no bearing on the formulation of the measurement-based real-time SCED and they may easily be included in our approach. Additionally, such an exclusion does not change the nature of the comparisons we present in the case studies, rather the inclusion of ramping constraints would serve to increase the LMPs in all cases.

The primary outcomes of the real-time SCED are: (i) the optimal generator and load dispatch instructions, which are a direct result of the solution to (5.9); and (ii) the LMPs, which are not a direct result of the solution to (5.9), but may be calculated from the ISFs, the LFs, and the shadow prices [50, 61], along the same lines used in (2.45), as follows:

$$\lambda = \lambda_r \mathbb{1}_N + \begin{bmatrix} \Psi \\ \Psi^s \end{bmatrix}^T \left(\begin{bmatrix} \bar{\mu}^f \\ \bar{\mu}^s \end{bmatrix} - \begin{bmatrix} \underline{\mu}^f \\ \underline{\mu}^s \end{bmatrix} \right) + \lambda_r \Lambda, \tag{5.10}$$

where $\mathbb{1}_N$ is an N-dimensional all-ones vector. Now, define

$$\lambda^c = \begin{bmatrix} \Psi \\ \Psi^s \end{bmatrix}^T \left(\begin{bmatrix} \bar{\mu}^f \\ \bar{\mu}^s \end{bmatrix} - \begin{bmatrix} \underline{\mu}^f \\ \underline{\mu}^s \end{bmatrix} \right) \text{ and } \lambda^\ell = \lambda_r \Lambda,$$

to be the N-dimensional vectors representing the congestion and loss components of the LMPs. The SCED LMPs in (5.10) differ from the ED LMPs

derived in (2.45) owing to the fact that they incorporate the dual variables of the security constraints into the congestion component.

5.3 Measurement-Based Real-Time SCED

It is clear from (5.9) and (5.10) that the dispatch targets and LMPs calculated from the results of the model-based real-time SCED depend heavily on the model-based LFs and ISFs and how accurately these LFs and ISFs reflect the conditions in the system at the time the real-time SCED is formulated. However, due to potential inaccuracies in telemetry and state estimation that may propagate to the underlying system model, these model-based sensitivities may not always reflect the real-time system conditions. We address this shortcoming of the model-based SCED via the deployment of the measurement-based LF estimation approach described in Chapter 3, and a measurement-based ISF estimation approach similar to that proposed in [18].

5.3.1 Measurement-Based ISFs

Consider the same power system defined in Section 2.2. Suppose the net active (reactive) power injected into the system at bus n at time t, $P_n(t)$ ($Q_n(t)$), varies by a small amount $\Delta P_n(t)$ ($\Delta Q_n(t)$) from time t to time $t + \Delta t$, where $\Delta t > 0$ and small. Further, let $\Delta P_{l,n}^{f,p}(t)$ ($\Delta P_{l,n}^{f,q}(t)$) be the change in active power flow on line ℓ_l due to ΔP_n (ΔQ_n). Define the ISF for line ℓ_l with respect to an active power injection at bus n as

$$\Psi[l,n] = \frac{\partial P_l^f}{\partial P_n} \approx \frac{\Delta P_{l,n}^{f,p}}{\Delta P_n}, \tag{5.11}$$

and the ISF for line ℓ_l with respect to a reactive power injection at bus n as

$$\Psi^q[l,n] = \frac{\partial P_l^f}{\partial Q_n} \approx \frac{\Delta P_{l,n}^{f,q}}{\Delta Q_n}. \tag{5.12}$$

While $\Delta P_{l,n}^{f,p}(t)$ and $\Delta P_{l,n}^{f,q}(t)$ are not directly available through PMU measurements, we can, however, measure $\Delta P_l^f(t)$, the total change in active power flow on line ℓ_l due to bus injections at time t. We observe that the

variation in the flow on line ℓ_l is due to variations in the active and reactive power injections at each bus n:

$$\Delta P_l^f = \Delta P_{l,1}^{f,p}(t) + \cdots + \Delta P_{l,N}^{f,p}(t) + \Delta P_{l,1}^{f,q}(t) + \cdots + \Delta P_{l,N}^{f,q}(t). \tag{5.13}$$

Employing (5.11) and (5.12) in (5.13) we obtain

$$\begin{aligned}\Delta P_l^f \approx & \Delta P_1(t)\Psi[l,1] + \cdots + \Delta P_N(t)\Psi[l,N] \\ & + \Delta Q_1(t)\Psi^q[l,1] + \cdots + \Delta Q_N(t)\Psi^q[l,N].\end{aligned}$$

Now suppose we have $M+1$ sets of synchronized measurements. Let

$$\Delta P_n[k] = P_n[(k+1)\Delta t] - P_n[k\Delta t],$$

$$\Delta Q_n[k] = Q_n[(k+1)\Delta t] - Q_n[k\Delta t],$$

$$\Delta P_l^f[k] = P_l^f[(k+1)\Delta t] - P_l^f[k\Delta t],$$

for $n = 1, \ldots, M$ and define

$$\Delta P_n = \left[\Delta P_n[1] \ \cdots \ \Delta P_n[k] \ \cdots \ \Delta P_n[M]\right]^T,$$

$$\Delta Q_n = \left[\Delta Q_n[1] \ \cdots \ \Delta Q_n[k] \ \cdots \ \Delta Q_n[M]\right]^T,$$

$$\Delta P_l^f = \left[\Delta P_l^f[1] \ \cdots \ \Delta P_l^f[k] \ \cdots \ \Delta P_l^f[M]\right]^T.$$

Furthermore, let

$$\Psi_l = [\Psi[l,1], \ldots, \Psi[l,n], \ldots, \Psi[l,N]],$$

$$\Psi_l^q = [\Psi^q[l,1], \ldots, \Psi^q[l,n], \ldots, \Psi^q[l,N]],$$

$$\Psi_l^s = [(\Psi_l)^T \ (\Psi_l^q)^T]^T.$$

Then, clearly,

$$\Delta P_l^f = \left[\Delta P_1 \ \cdots \ \Delta P_n \ \cdots \ \Delta P_N \ \cdots \ \Delta Q_1 \ \cdots \ \Delta Q_n \ \cdots \ \Delta Q_N\right](\Psi_l^s)^T. \tag{5.14}$$

Now, let $\Delta P = [\Delta P_1 \ \cdots \ \Delta P_n \ \cdots \ \Delta P_N]$, $\Delta Q = [\Delta Q_1 \ \cdots \ \Delta Q_n \ \cdots \ \Delta Q_N]$, and $\Delta S = [\Delta P^T \ \Delta Q^T]^T$. Then, the system in (5.14) becomes

$$\Delta P_l^f = \Delta S(\Psi_l^s)^T. \tag{5.15}$$

If $M \geq 2N$, then (5.15) is an overdetermined system. Moreover, assuming the ISFs are approximately constant over the $M+1$ measurements,[2] we can obtain an estimate of Ψ_l^s from least-squares error estimation as

$$(\hat{\Psi}_l^s)^T = (\Delta S^T \Delta S)^{-1} \Delta S^T \Delta S_l^f, \tag{5.16}$$

the first N elements of which are the desired measurement-based active power ISFs, Ψ_l, for line ℓ_l.

Practical Considerations for the ISF Estimation. In the same manner as noted for LFs in Section 3.3.2, the estimation of the measurement-based ISF via (5.16) suffers a number of shortcomings: (i) it requires a complete set of data, i.e., M sets of injection and line flow measurements, where $M > 2N$; and (ii) it gives equal weight to all measurements, regardless of when they were taken. One approach to addressing these shortcomings is the deployment of a weighted least squares (WLS) formulation of (5.16) given by

$$(\hat{\Psi}_l^s)^T = (\Delta S^T W \Delta S)^{-1} \Delta S^T W \Delta P_l^f, \tag{5.17}$$

where W is the weighting matrix, which can be selected to give more weight to recent measurements (see, e.g., [18]). Additional improvements in the speed of computation and the number of required measurement sets can be made, respectively, through the application of recursive least-squares (see, e.g., [18]) and methods from compressed sensing (see, e.g., [43]). In this chapter, we adopt the WLS approach in (5.17) with a diagonal weighting matrix W, where $W[k,k] = f^{M-k}$ and $f \in (0,1]$, for the purpose of demonstrating the benefits of our measurement-based SCED formulation. Additionally, we analyze the appropriate selection of the parameters M and f in Section 5.4.1.

[2]We provide an empirical analysis of this assumption in Appendix B.

5.3.2 Measurement-Based SCED Constraints

Our primary goal in this chapter is to leverage the measurement-based LF estimation approach described in Chapter 3 and the measurement-based ISF estimation approach described above to remove the dependence on a system model of the SCED in (5.9). To this end, we reformulate the SCED power balance, network, and security constraints, (5.9b), (5.9e), and (5.9f), respectively.

Power Balance Constraint. As described in Chapter 3, we may deploy the measurement-based LFs from (3.20) to reformulate the losses in (5.9b) as

$$\Delta \hat{P}^{\ell} = \hat{\Lambda}^T \Delta P^g. \tag{5.18}$$

Doing so ensures that the losses resulting from incremental increases in the generation at each bus to meet the load are accurately computed, which will in turn ensure the accurate dispatch of units to meet the load, including losses.

Network Constraints. Let $\hat{\Psi}$ be the $L \times N$ matrix of the measurement-based active power ISF estimates, each row of which is obtained by taking the first N entries of the vector estimated with (5.17). As described in Section 5.2, model-based ISFs form the basis of the network description in the real-time SCED. To remove the model dependence of (5.9), we deploy $\hat{\Psi}$ to re-formulate the network constraints (5.9e) as

$$\Delta \underline{P}^f \leq \hat{\Psi} \Delta P \leq \Delta \bar{P}^f. \tag{5.19}$$

With these reformulated network constraints, the real-time SCED constraints will be based on pre-contingency line flows that accurately reflect real-time conditions. The measurement-based ISFs are also instrumental to measurement-based contingency analysis and the formulation of security constraints.

Sensitivity-Based Contingency Screening. The measurement-based ISFs can also be used to compute the LODFs and PTDFs, which may subsequently be used to perform contingency selection and formulate security constraints. Contingency selection is the process of choosing the contingencies for which

it is critical to perform contingency analysis from the set of all possible contingencies (i.e., to construct what is often referred to as the *priority list*) [13]. This process is typically a coarse assessment of the severity of contingencies in order to select only those with a high impact for more detailed study in RTCA and thus reduce the computational burden associated with assessing all possible contingencies. As mentioned in Section 5.2.2, in practice, contingency selection occurs by a combination of operator discretion and systematic approaches. One such approach involves using ISFs to assess the approximate impact of every possible contingency on every other element—similar to performing dc contingency analysis—in order to ascertain the most severe among them. The application of the measurement-based ISFs in this context offers several substantial enhancement to the SCED. The adaptive nature of the measurement-based ISFs reduces or eliminates the impacts of model accuracies (e.g., erroneous model data or undetected changes in system topology) on: (i) the identification of contingencies and their relative severity during contingency selection; (ii) the identification, through contingency analysis, of those facilities in the system that will be overloaded by a given outage (by providing an accurate contingency list); and (iii) the formulation of security constraints that accurately reflect the impacts of outages and injections.

To conduct online measurement-based contingency selection, the system operator could deploy the measurement-based ISFs and LODFs to compute the impacts of all potential contingencies (or a pre-determined subset of all potential contingencies composed of a set larger than the current contingency list). For each potential outage of a line ℓ_l, the operator analyzes the flow impacts on each non-outage line ℓ_u as follows:

$$|\hat{\Psi}_u \Delta P + \hat{\Xi}[u,l]\hat{\Psi}_l \Delta P| \leq \Delta \bar{P}^f_{u,c_l^f}, \tag{5.20}$$

where $\hat{\Xi}[u,l]$ is the measurement-based estimate of the LODF of line ℓ_u with respect to the outage of line ℓ_l. Similarly, for each potential outage of a generator j, the operator analyzes the flow impacts on each line ℓ_u as follows:

$$|\hat{\Psi}_u \Delta P + (\hat{\Psi}_u \alpha(c_j^g) e_j^T) \Delta P| \leq \Delta \bar{P}^f_{u,c_l^g}. \tag{5.21}$$

If a generator or line contingency is found to cause an overload via (5.20)

or (5.21), respectively, a mon-con pair for the contingency and each corresponding overloaded element is added to the contingency list, which is subsequently assessed in ac contingency analysis and, if necessary, populated into $\mathcal{C}^f$ and $\mathcal{C}^g$.

Additionally, if the post-contingency flows computed with (5.20) or (5.21) conflict substantially with those computed using ac contingency analysis, e.g., if a flow difference of more than 40% is identified (greater than the flow error between the various ac and dc models studied in [54]), the system operator could flag a potential error in the ac system model, which could be investigate using methods such as "parity checking", which is used in fault detection (see, e.g., [62]). Furthermore, on such occasions, the system operator could use the results of the online measurement-based contingency selection in (5.20) and (5.21) in addition to, or in lieu of, such (potentially erroneous) ac contingency analysis results to formulate the security constraints in the SCED.

Security Constraints. We reformulate the line outage security constraints for each line outage mon-con pair, $(\ell_u, c_l^f) \in \mathcal{C}^f$, to reflect the utilization of the measurement-based ISFs as

$$\Delta \underline{P}^f_{u,c_l^f} \leq \hat{\Psi}_u \Delta P + \hat{\Xi}[u,l]\hat{\Psi}_l \Delta P \leq \Delta \bar{P}^f_{u,c_l^f}. \tag{5.22}$$

Additionally, we reformulate the security constraints for each generator outage mon-con pair $(\ell_u, c_j^g) \in \mathcal{C}^g$ as

$$\Delta \underline{P}^f_{u,c_j^g} \leq \hat{\Psi}_u \Delta P + (\hat{\Psi}_u \alpha(c_j^g) e_j^T) \Delta P \leq \Delta \bar{P}^f_{u,c_j^g}. \tag{5.23}$$

With the reformulated network and security constraints in (5.19) and in (5.22) and (5.23), respectively, the real-time SCED no longer relies on a system model. Instead, the system operator continuously updates the estimate of $\hat{\Lambda}$ via (3.21) and (3.20), $\hat{\Psi}$ via (5.17), and recomputes $\hat{\Xi}$ via (2.39) and (2.40), as new PMU measurements become available and uses the most up-to-date estimates to perform contingency selection/analysis, identify and formulate the necessary security constraints, and formulate the real-time SCED. This measurement-based real-time SCED is adaptive to changing system conditions, such as detected or undetected topology changes, variations in bus injections, and even changes in line and other system parameters due to

loading or extreme temperature conditions. As such, the dispatch targets and LMPs resulting from the measurement-based SCED process will reflect real-time system conditions.

A key strength of our proposed measurement-based SCED approach is its consistency with the current real-time SCED framework; the structure of the SCED formulation is left largely unchanged, but more appropriate data is used as the basis for that structure and the process by which that data is obtained is made more flexibility to changing real-time conditions. The result is an enhanced and adaptive real-time SCED. The following case studies demonstrate the adaptability of our measurement-based approach to the real-time SCED.

5.4 Case Studies

In the following case studies, we compare the model-based, measurement-based, and actual ISFs and sensitivities derived from the ISFs, e.g., PTDFs and LODFs, and the impacts when utilizing them to determine the generator dispatch and LMPs via the real-time SCED. To focus on the impacts of incorrect ISFs on the SCED outcomes in the following case studies, we assume the LFs are known—the impacts on the SCED outcomes of erroneous LFs are thoroughly described in Chapter 3.

We deploy (2.38) to compute the conventional, model-based ISFs. Furthermore, we calculate the actual ISFs used in our studies by (i) increasing the net active power injection at each bus by 0.01 p.u., and (ii) computing the change in line active power flows via a solution to the full nonlinear ac power flow with the appropriate system model, and assuming the net load injection change is balanced according to distributed load slack weights, α^d, defined $\forall n \in \mathcal{N}$ by

$$\alpha_n^d = \frac{\sum_{v \in \mathcal{D}_n} P_{v,0}^d}{\sum_{v \in \mathcal{D}} P_{v,0}^d}, \tag{5.24}$$

where $P_{v,0}^d$ is the case nominal load injection for load v; to compute the actual ISFs, for each net injection increase and ac-power flow solution, we take the ratio of the ac-power-flow-calculated change in the line active power flows and the change in the net active power injection.

We compute the measurement-based ISF estimates with (5.17), and carry

out the estimation procedures with simulated PMU measurements (assumed to be collected at a measurement frequency of 30/s) of the random fluctuations in each load injection $v \in \mathcal{D}$, which are generated according to

$$P_v^d[k] = P_{v,0}^d[k] + \sigma_1 P_{v,0}^d[k]\nu_1 + \sigma_2\nu_2, \tag{5.25}$$

where $P_{v,0}^d[k]$ is nominal load injection for load v at instant k, and ν_1 and ν_2 are pseudorandom values drawn from a normal distribution with zero mean and standard deviations $\sigma_1, \sigma_2 = 0.01$, respectively ($\sigma_1 P_{v,0}^d[k]\nu_1$ represents random load fluctuations, whereas $\sigma_2\nu_2$ represents measurement noise). We compute simulated PMU measurements of generator injections, $P_i^g[k]$, for each generator $i \in \mathcal{G}$, and line active power flows, $P_l^f[k]$ for each line $\ell_l \in \mathcal{L}$, corresponding to the loads at instant k by solving (2.9) with pre-allocation generation outputs $P^g[k-1]$, and loads $P^d[k]$, nominal bus reactive power injections Q_0 and voltages V_0 and distributed generator slack weights, α^g, defined $\forall n \in \mathcal{N}$ by

$$\alpha_n^g = \frac{\sum_{i\in\mathcal{G}_n} \bar{P}_i^g}{\sum_{i\in\mathcal{G}} \bar{P}_i^g}. \tag{5.26}$$

We compute the fluctuations in net active power injection at each bus, ΔP_n, at each time instant, k, using (2.1). For simplicity, we again assume no variation in the load reactive power injections, i.e., $\Delta Q_v^d[k] = 0$, $\forall v \in D$. We emphasize, however, that this assumption does not impact the nature of the results presented.

5.4.1 Case Studies I: The 6-Bus Test System

We demonstrate the proposed measurement-based real-time SCED using a modified version of the 3-generator, 6-bus test system, the topology of which is shown in Fig. 3.1, which is provided in the simulation package MATPOWER [56]. When solving the SCED, we assume each load has an infinite willingness to pay, i.e., the demand is inelastic, and each generator, i, submits a quadratic offer function of the form $a_i(P_i^g)^2 + b_i P_i^g + c_i$, the parameters of which are provided in Table 3.1.

On the Selection of M and f. The WLS estimation procedure in (5.17) has two degrees of degrees of freedom: (i) the selection of the number of

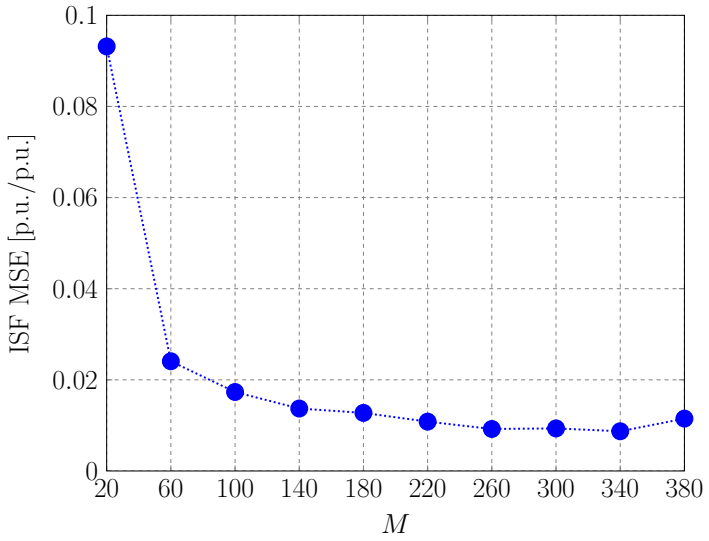

Figure 5.1: Sensitivity of the ISF estimation error to the selection of M under steady-state operating conditions with $f = 1$.

sample sets, M, to include in the estimation, i.e. the size of the measurement window; and (ii) the selection of $f \in (0, 1]$ so as to specify the diagonal weighting matrix W. A larger measurement window, M, increases the accuracy of the estimation and decreases its susceptibility to noise when the system is in steady state at the expense of increased error when the operation point changes [63]. The selection of f impacts the weight given to the measurements from each measurement instant in the measurement window and choosing $f < 1$ can improve the tracking of the estimator under changing operating conditions at the expense of steady-state accuracy [64]. Furthermore, the selection of M and f must be balanced so as to ensure the regressor matrix is full column rank. We demonstrate the impacts of the selection of M and f on the ISF estimation with the following series of examples and provide some guidelines for their selection.

To illustrate the impacts on the ISF mean-squared error (MSE) of the selection of M under steady-state conditions, we simulate 500 PMU measurements using the process outlined above at the nominal 6-bus power flow solution. Then, we compute the ISFs using (5.17) with $f = 1$ and with M varied from 20 to 380 measurement instants in increments of 20. The ISF estimates are compared to the actual ISFs, which are computed by repeatedly solving the ac power flow equations around the operating point at each measurement instant with a 0.01 p.u. increase in the net injection at each

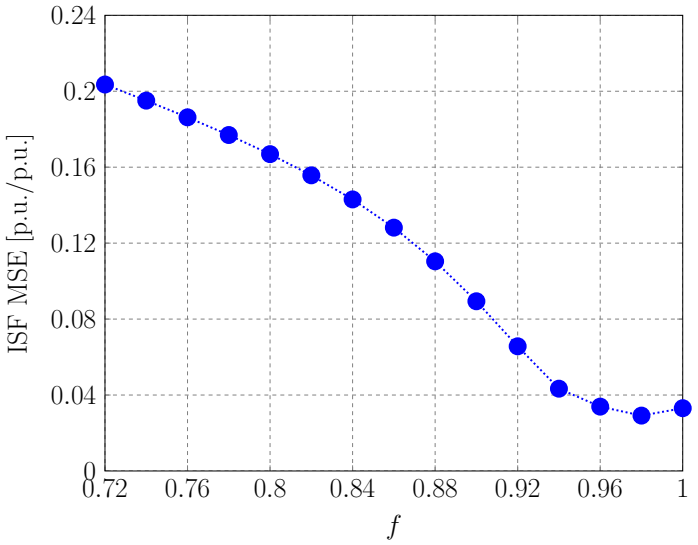

Figure 5.2: Sensitivity of the ISF estimation error at instant 350 to the selection of f under changing operating conditions with $M = 120$.

bus and taking the ratio of line flow changes to the net injection change.

As shown in Fig. 5.1, as we increase the value of M, the MSE between the estimated and actual ISFs decreases—substantially between $M = 20$ and $M = 100$ and then slowly for $M > 120$. This finding suggests that one should select as large an M as is computationally feasible. However, as we show below, when performing the estimation under changing operating conditions, the ISF MSE may not decrease with increasing M. Furthermore, the ISF MSE can be improved under changing conditions by selecting $f < 1$.

To demonstrate the impacts on the ISF MSE of the selection of f and M under changing operating conditions, we again simulate 500 PMU measurements, however now we increase the load at bus 4 linearly by 100% between measurement instants 300 and 400, assuming the load increase is balanced by the generators in the system according to the distributed slack policy defined in (5.26). We then compute four cases of the ISF estimation using (5.17) with estimation parameters f and M: (i) executed at measurement instance 350 with $M = 120$ and f varied from 0.72 to 1 measurement instants in increments of 0.02; (ii) $f = 1$ and M varied from 140 to 500 measurement instants in increments of 20 and executed at each measurement instance; (iii) with $f = 1$ and $M = 120$ executed at measurement instants 140 to 500 in increments of 20; and (iv) with $f = 0.98$ and $M = 120$ executed at measurement instants 140 to 500 in increments of 20. We select $M = 120$ in these cases

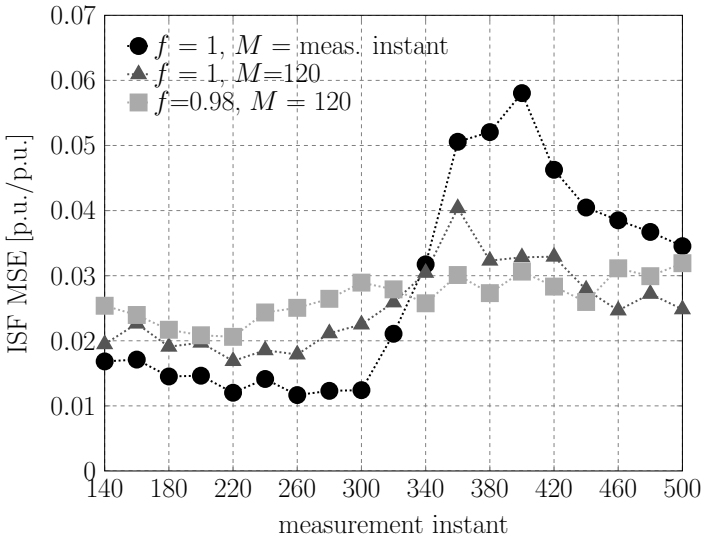

Figure 5.3: Impacts on ISF estimation error under changing operating conditions of the selection of M and f.

based on the the relatively low steady-state ISF MSE found in the above sensitivity study for this value of M. For each case, we compare the ISF estimates to the actual ISFs computed at the corresponding measurement instant.

As is clear from Fig. 5.2, the ISF MSE in case (i) is minimized during the operating point change for a fixed M by selecting a value of f close to 1 (or, alternatively, by selecting a value of f such that the weights for the oldest measurements in the measurement window do not decay to near zero rendering the measurements ineffectual and the regressor matrix nearly singular). As shown in Fig. 5.3, in case (ii), the MSE increases considerably during the operating point change between measurement instants 300 and 400, due to the inclusion of pre-operating point change data from measurement instants 140 through 300 in the estimation. However, in case (iii), in which we select $f = 1$ and a sliding measurement window of $M = 120$, the MSE is decreased compared to case (ii) during the operating point change as fewer pre-operating point measurements are included in the measurement window throughout the change. Finally, in case (iv), in which we select $f = 0.98$, the ISF MSE when adapting to the operating point change is improved further still due to the bias introduced toward the most recently obtained measurements in the measurement window. However, the ability to track the operating point change in cases (iii) and (iv) comes at the expense

Table 5.1: LMPs with undetected topology change.

	model-based LMP [$/MWh]		measurement-based LMP [$/MWh]	
bus	undetected outage	detected outage	pre-outage	post-outage
1	19.54	17.41	19.54	17.65
2	19.48	13.99	19.48	13.91
3	20.04	30.92	20.04	31.18
4	20.26	20.91	20.25	20.77
5	20.40	52.73	20.40	53.12
6	19.63	30.04	19.63	29.91

of additional steady-state MSE, as illustrated by the MSE from measurement instants 140 through 300 for those cases. Thus, as expected, there is a tradeoff between the estimator's ability to accurately track changing operating conditions and the steady-state accuracy. Our observations from a number of tests carried out on IEEE test systems of varying sizes suggest that for larger-scale systems $M \approx 4N$ and $f \approx e^{\frac{-2.4}{M}}$ are appropriate for balancing tracking and steady-state error, and to ensure the regressor matrix is non-singular.

Undetected Line Outage. In this study, we simulate 600 PMU measurements using the approach outlined above and assume there is an undetected outage of line ℓ_3 at measurement instant 300 and that the real-time SCED is executed at measurement instant 500. We compute the ISFs at each measurement instant beginning with instant 120 using (5.17) and with $M = 120$ and $f = 0.98$, and execute the SCED every 20 measurement instants. For buses 1, 2, and 6 (generator buses) and buses 3 through 5 (load buses), and at measurement instants 120 (pre-outage) and 500 (post-outage), Table 5.1 shows: (i) the undetected-outage, model-based LMPs, which are the LMPs that would be realized in the presence of the undetected outage; (ii) the detected-outage, model-based LMPs, which are the LMPs that would be realized if the outage was detected; and (iii) the measurement-based estimates of the LMPs. Unsurprisingly, there is a large discrepancy between the undetected and detected outage model-based LMPs, more than $30/MWh at bus 5. The measurement-based LMPs, however, closely track the correct model-based LMPs regardless of whether or not the outage is detected.

Furthermore, the measurement-based LMPs converge quickly to the cor-

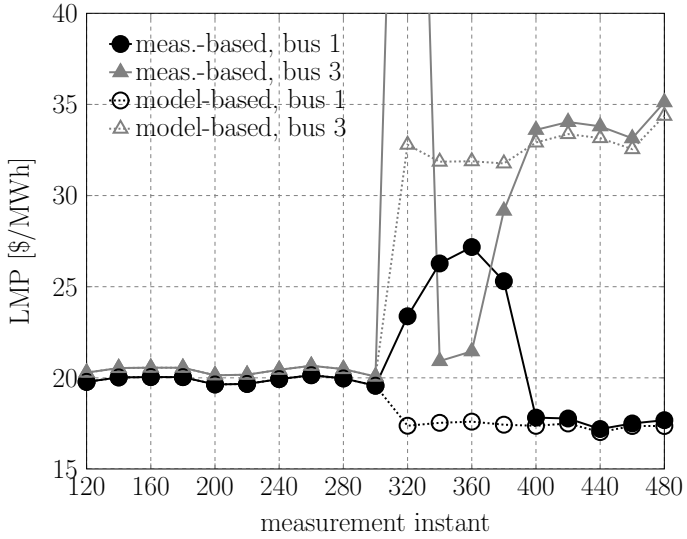

Figure 5.4: Measurement- and correct-model-based LMP evolution at a subset of buses with outage of line ℓ_3.

rect values following the outage of line ℓ_3. Figure 5.4 shows the evolution of the measurement-based and correct-model-based LMPs at buses 1 and 3 (a generator and load bus, respectively) before, during, and after the outage. As shown Fig. 5.4, the measurement-based LMPs at both buses are nearly coincident with the correct-model-based LMPs prior to the contingency at measurement instant 300, after which there is a period of 100 measurements during which the measurement-based LMPs diverge. However, as the measurement window moves past the pre-outage measurement period, starting at measurement instant 400, the measurement-based LMPs again track the correct-model-based LMP values.

Incorrect Data Impacts on Security Analysis. In this study, we simulate 600 PMU measurements using the approach described above and assume the line ℓ_5 impedance data in the model is incorrectly thought to be 20% higher than its true value. The ISFs are again estimated at each measurement instant beginning with instant 120 using (5.17) and with $M = 120$ and $f = 0.98$. We run ac contingency analysis with sensitivity-based contingency selection and the real-time SCED at measurement instant 400. Table 5.2 shows the overloads identified and SCED LMPs with: (i) the model-based contingency selection and SCED run with incorrect line data; (ii) the model-based contingency selection and SCED run with correct line data; and (iii)

Table 5.2: Identified overloads and LMPs with incorrect model data.

	model-based		
	incorrect data	correct data	measurement-based
identified overload	–	(ℓ_5, c_6^f)	(ℓ_5, c_6^f)
bus	LMP [$/MWh]		
1	19.86	20.99	21.09
2	19.80	19.02	18.96
3	20.36	20.29	20.28
4	20.57	23.62	23.99
5	20.73	21.57	21.66
6	19.95	19.83	19.81

the measurement-based contingency selection and SCED.

The model-based contingency selection run with the model-based ISFs finds no potential overloads and so no security constraints are added to the model-based SCED formulation. As a result, the model-based SCED with incorrect line data LMPs are similar at all buses, except for differences due to losses. However, with correct line impedance data, contingency selection identifies a potential overload with respect to (ℓ_5, c_6^f), which is confirmed by contingency analysis. As such, a security constraint is added in the model-based SCED formulation with correct line data, which binds on execution producing significantly different LMPs than in the incorrect data case. The measurement-based contingency selection identifies the overload (ℓ_5, c_6^f) and the resulting SCED with the measurement-based security constraints produces LMPs that track those in the model-based case with correct line data.

5.4.2 Case Studies II: The 118-Bus Test System

In this section, we present the results of case studies carried out using a modified version of the IEEE 54-generator, 186-line, 118-bus test system [57]. The test system has been modified by reducing the thermal limits on a subset of tranimssion lines, reported in Table 4.1, so as to introduce transmission congestion in the SCED. As before, we assume each load has an infinite willingness to pay, i.e., the demand is inelastic, and each generator, i, submits a quadratic offer function of the form $a_i(P_i^g)^2 + b_i P_i^g + c_i$, the parameters of which we take from the test case [57].

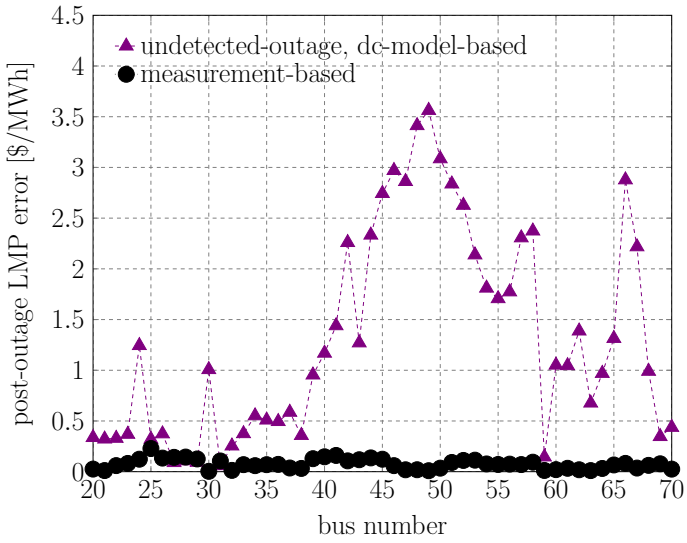

Figure 5.5: LMP errors at a highly impacted subset of buses due to the undetected outage of double-circuit ℓ_{98}, ℓ_{99}.

Undetected Line Outage. In this study, we simulate 1500 PMU measurements of load active power consumption and generator active power production according to the procedure outlined above. Further, we assume there is an undetected outage of the double circuit consisting of lines ℓ_{98} and ℓ_{99} at measurement instant 500 and that the real-time SCED is executed at measurement instant 1400. We compute estimates of the ISFs at each measurement instant beginning with instant 240 using (5.17) and with $M = 236$ and $f = 0.99$.

Figure 5.5 shows the absolute LMP errors for the model-based SCED with an undetected outage and the measurement-based SCED compared to the model-based SCED with the detected outage at a highly impacted subset of buses. The undetected changes in system topology have a significant impact on the prices realized with the real-time SCED process, especially at those buses close to transmission lines at their limit, e.g., buses 49 and 50 or buses 66 and 67. The LMP MSE with the undetected outage in the dc-model-based SCED with respect to the detected-outage, dc-model-based LMPs is \$14.4/MWh across all buses. In contrast, the measurement-based LMPs track the detected-outage, model-based LMPs well resulting in an LMP MSE of \$0.90/MWh.

Table 5.3: Identified line outage overloads common to all cases and those unidentified due to incorrect data.

overloaded line #	overload w.r.t. outage of line #
identified overloads common to all cases	
8	33,36,37,51,54
31	16,33,34,36,38,51,54,104,116
71	16,33,34,36,37,38,54,70,74,82,93,94,97,107,116,119
98,99	16,33,34,36,37,38,51,54,74,82,93,94,96,97,104,116,119
138,139	16,33,34,36,37,38,51,54,70,74,82,93,94,96,97,104,107,116,119
overloads unidentified due to bad data	
31	70,74,82,119

Inaccurate System Model Data. In this study, we simulate the real-time SCED in the presence of erroneous model data. To this end, we perturb the line impedance on each of the top 30% of loaded lines by a random multiple in $[0.7, 1.3]$ drawn from a uniform distribution. We simulate 600 measurements using the same simulated load PMU data used in the previous case and compute the line flows with the incorrect and correct data. Further, we compute estimates of the ISFs at each measurement instant beginning with instant 240 using (5.17) and with $M = 236$ and $f = 0.99$ and assume the real-time SCED is executed at measurement instant 500.

We perform sensitivity-based contingency selection on the 20 and 10 most impactful line and generator contingencies, respectively, to identify overloads. The contingencies that resulted in overloads during contingency analysis (and, in the measurement-based SCED, those that were identified as causing overloads by measurement-based contingency selection) and thus necessitate the formulation of security constraints are reported in Tables 5.3 and 5.4. As reported in Table 5.3, the incorrect model data results in the failure of model-based contingency selection/analysis to identify line contingency pairs (ℓ_{31}, c^f_{70}), (ℓ_{31}, c^f_{74}), (ℓ_{31}, c^f_{82}), and (ℓ_{31}, c^f_{119}). Furthermore, as shown in Table 5.4, the inaccurate model data results in the incorrect identification of generator contingency pair (ℓ_{71}, c^g_{40}). The unidentified (mis-identified) overloads translate into fewer (additional) constraints in the SCED that subsequently impact the market outcomes. The measurement-based contingency selection, on the other hand, identifies the appropriate contingency overloads and results in the formulation of the correct security constraints.

Cases of omission and commission in the selection of contingency constraints, along with erroneous data model data can significantly impact the

Table 5.4: Identified generator outage overloads common to all cases and those mis-identified due to incorrect data.

overloaded line #	overload w.r.t. outage of generator #
identified overloads common to all cases	
8	1,6
31	10,21,22,23,24,25,37,40
71	1,6,10,22,23,24,25,37
98,99	1,6,10,21,22,23,24,25
138,139	1,6,10,21,22,23,24,25,37
overloads mis-identified due to bad data	
71	40

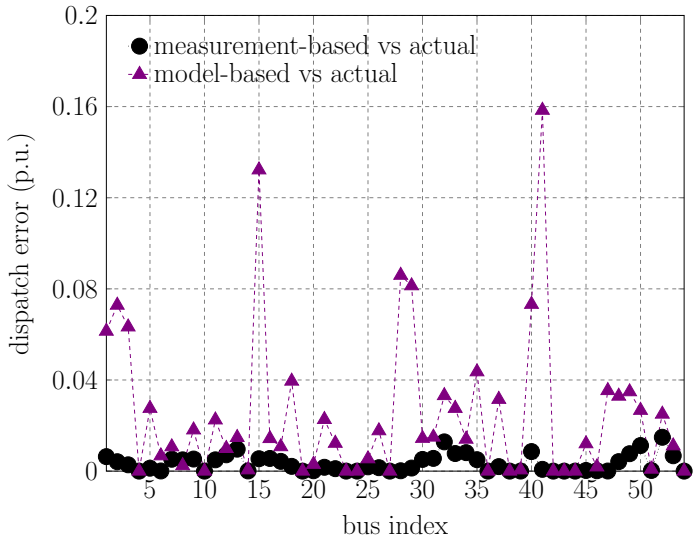

Figure 5.6: Measurement- and model-based dispatch errors resulting from incorrect model data.

generator dispatch determined by the SCED. Figure 5.6 compares the difference between the measurement- and model-based dispatches and the actual dispatch when the SCED is solved with the security constraints for each respective case identified above. Clearly, the existence of erroneous model data and the follow-on effects such data has on the constraints in the SCED have a serious impact on the incorrect-model-data-based dispatch that can be mitigated by eradicating the model dependence with the proposed measurement-based approach.

An incorrect dispatch itself is not problematic from the perspective of maintaining reliability; however, the misrepresentation of the physical system due to erroneous model data may result in an insecure dispatch, i.e., a

Table 5.5: Base and outage case line flows on limited lines due to dispatch from SCED solved with actual, incorrect-data-model-, and measurement-based ISFs.

		line flow [p.u.]								
		base case (no outages)			ℓ_{36} outage			ℓ_{96} outage		
line	limit (p.u.)	actual	model-based	meas.-based	actual	model-based	meas.-based	actual	model-based	meas.-based
ℓ_8	2.0	1.61	1.74	1.60	2.00	**2.16**	2.00	1.58	1.71	1.58
ℓ_{31}	0.5	0.194	0.197	0.193	0.330	0.342	0.331	0.008	0.017	0.006
ℓ_{71}	0.6	0.381	0.379	0.380	0.379	0.377	0.379	0.340	0.332	0.340
ℓ_{98}, ℓ_{99}	1.4	1.00	1.06	1.00	1.015	1.07	1.01	1.43	**1.55**	1.43
ℓ_{138}, ℓ_{139}	1.4	1.40	**1.52**	1.40	1.40	1.52	1.40	1.40	1.52	1.40

dispatch in which at least one transmission element is overloaded in the base case (no outages) or in the event of a contingency. To illustrate this effect, we present in Table 5.5 a comparison of the line flows computed for lines near their thermal limit for a sample of outages with the actual, incorrect data model-based, and measurement-based dispatches on the system model with correct data. The reported flows represent the flows that would arise in the system for each of the respective cases if the dispatch for that case were implemented. As can be seen in the table, the incorrect model data results in an insecure dispatch in the base case as well as in the reported contingency cases—the overloaded lines are shown in bold in the table. In the base case, the double circuit consisting of lines ℓ_{138} and ℓ_{139} is overloaded by 8.6%. Moreover, for contingencies shown, lines ℓ_8 and the double circuit consisting of lines ℓ_{98} and ℓ_{99} are respectively overload by 8.0% and 10.7%. However, the measurement-based SCED results in a secure dispatch further illustrating the benefits of our proposed approach.

Dispatch errors also have economic impact via the LMPs computed at the SCED solution, which will be used to settle the market. Figure 5.7a shows the deviations between the dc-model-based LMPs with correct line impedance data and the incorrect data dc-model-based LMPs and measurement-based LMPs. Overall, the measurement-based SCED approach results in LMPs close to those found with the correct line data, the MSE over all buses is \$1.67/MWh compared to \$5.25/MWh for the incorrect data dc-model. However, there are some deviations between the LMPs computed with dc-model-based with correct data and measurement-based approaches. To give some insight into the nature of these differences, Fig. 5.7b shows the correct-data, dc-model-based LMPs and measurement-based LMPs compared to LMPs computed with the actual ISFs, which recall are computed by repeatedly

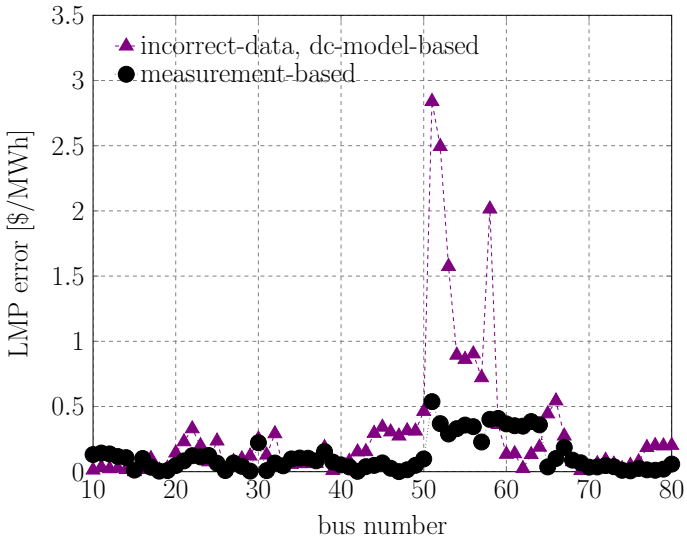

(a) LMP errors w.r.t. dc-model with correct data LMPs.

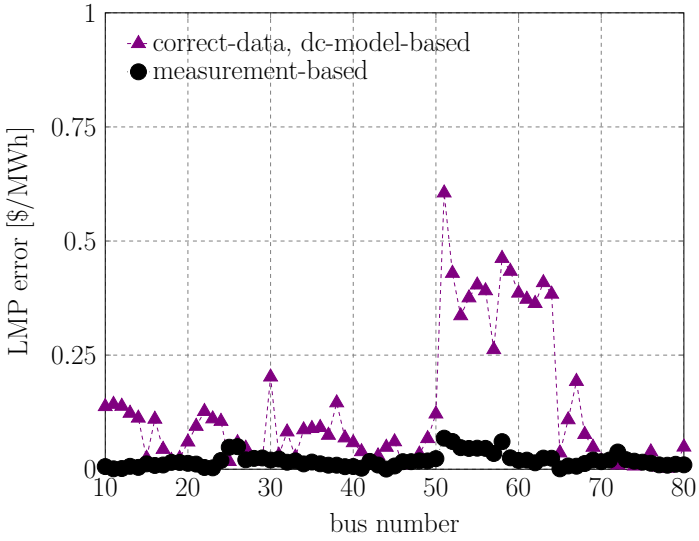

(b) LMP errors w.r.t. linearized ac-model with correct data LMPs.

Figure 5.7: Model-based and measurement-based absolute LMP errors due to the incorrect model data for heavily loaded lines with respect to correct data, dc-model and actual LMPs at a highly impacted subset of buses.

solving the ac power flow.

When compared to the actual model-based LMPs, the measurement-based LMPs perform much better than the dc-model-based LMPs, the MSE is \$0.23/MWh compared to the \$1.78/MWh for the correct-data, dc-model-based LMPs. This finding suggests that the measurement-based SCED approach is able to capture information that the dc-model-based SCED ap-

proach does not, e.g., the impacts of reactive power and voltage changes in response to active power injection changes on active power flows, which is subsequently reflected in the LMPs. As such, the differences between the measurement-base LMPs and correct-data, dc-model-based LMPs, reported in Fig. 5.7a, may actually be indicative of errors in the correct-data, dc-model-based LMPs related to the underlying dc assumptions; the measurement-based approach requires the assumption that the relationship between active power injections and active power flows is linear, however it does not require the dc assumptions and thus is not impacted by the error introduced by those assumptions.

5.5 Summary

In this chapter, we proposed a measurement-based approach to the real-time SCED. Our approach leverages sensitivities estimated from PMU measurements to perform contingency selection and formulate security constraints, as well as to reformulate the model-based power balance and network flow constraints of the model-based real-time SCED. As shown in our case studies, the measurement-based real-time SCED is robust to undetected system disturbances and inaccurate model data and results in market outcomes that more accurately reflect real-time system conditions.

CHAPTER 6

CONCLUDING REMARKS

In this chapter, we give a brief recap of the thesis, and highlight the key contributions. Then, we conclude with some insights gained by undertaking the work presented herein.

6.1 Thesis Summary and Contributions

Maintaining operational reliability has been and will continue to be for the foreseeable future the primary goal of power system operators. Moreover, the swelling tide of renewable resource additions to the electricity system, both at the transmission and distribution level, and the additional operational challenges posed by the uncertainty they add to the system will push current operational strategies and tools to the limit of their effectiveness. To keep up with the growing complexity of the system, operators will require new analysis tools that harness the vast number of measurements that are beginning to be collected and the economy of computational resources that have become available in the past decade.

In this thesis, we proposed a set of operational reliability tools that can be integrated into the existing real-time market framework used by ISOs/RTOs, mainly the SCED, with two main goals in mind: (i) to remove the model dependence of the primary tools used by system operators in real-time operations; and (ii) to address the challenge of assessing and mitigating large outage angles, such as that which contributed to the 2011 San Diego blackout. To these ends, we developed the measurement-based LFs (Chapter 3), derived a sensitivity-based LOAF using our generalization of the FCT (Chapter 4), and demonstrated the use of measurement-based ISFs and LFs for contingency selection, and in the formulation of the measurement-based SCED (Chapter 5).

Our tools and the case studies carried out with them demonstrate the potential gains that can be made, both reliability and economic, by adopting tools that harness sensitivities estimated from real-time measurements, rather than those computed from an offline model. Furthermore, our LOAF-based tools further emphasize the prominent role that power flow sensitivities play in achieving operational reliability and, more specifically, the improved detection and mitigation of large outage angle that can be achieved by their application.

6.2 Conclusions

Advances in measurement availability and quality via the expanded installation of PMUs is certain to continue opening doors to more effective and adaptive power system operational tools. Our hope is that the tools presented in this thesis will be used to enhance existing operational reliability processes, as well as become a jumping off point for this new generation of tools, which will begin to illustrate to system operators the high value of PMU measurement data, and of measurement-based analysis tools for effective, efficient, and reliable power system operations.

APPENDIX A

SUPPLEMENTAL POWER FLOW SENSITIVITY DERIVATION

In Chapter 2, we derived the fundamental power flow sensitivities under the assumption that the voltages are constant at voltage-controlled buses, i.e., $\Delta V^c = 0$, and that the active power mismatch, Δp_m, is zero after the distributed slack policy has been imposed. In this appendix, we furnish proof that the derivation provided indeed results in $\Delta V_c = 0$ and $\Delta p_m = 0$, as claimed.

Recall from Chapter 2 that we partition the inverse of the Jacobian as follows:

$$J^{-1} = \begin{bmatrix} -F & -M \\ -E & -H \\ -r^T & -w^T \end{bmatrix}, \tag{A.1}$$

and further partitioned those partitions as follows:

$$E = \begin{bmatrix} E_{cc} & E_{cu} \\ E_{uc} & E_{uu} \end{bmatrix}, \; H = \begin{bmatrix} H_{cc} & H_{cu} \\ H_{uc} & H_{uu} \end{bmatrix},$$

$$\text{and } M = \begin{bmatrix} M_{cc} & M_{cu} \\ M_{uc} & M_{uu} \end{bmatrix}.$$

Additionally, recall that

$$U = -H_{cc}^{-1}(E_c + E_c \alpha r^T), \tag{A.2}$$

and

$$W = -H_{cc}^{-1}(H_c + E_c \alpha w^T). \tag{A.3}$$

A.1 Proof That $\Delta V_c = 0$

Recall that

$$\Delta V \approx \Pi \Delta P' + \Pi^q \Delta Q', \tag{A.4}$$

where

$$\Pi = E + E\alpha r^T + H_{c^*} U, \tag{A.5}$$

$$\Pi^q = H + E\alpha w^T + H_{c^*} W, \tag{A.6}$$

By substituting (A.2), (A.3), (A.5), and (A.6) into (A.4) we obtain

$$\begin{aligned} \Delta V \approx & (E + E\alpha r^T + H_{c^*}(-H_{cc}^{-1}(E_c + E_c\alpha r^T)))\Delta P' \\ & + (H + E\alpha w^T + H_{c^*}(-H_{cc}^{-1}(H_c + E_c\alpha w^T)))\Delta Q', \end{aligned} \tag{A.7}$$

where $E_c = [E_{cc}\ E_{cu}]$ and $H_c = [H_{cc}\ H_{cu}]$.

From (A.7), we conclude that

$$\begin{aligned} \Delta V_c \approx & (E_c + E_c\alpha r_c^T + H_{cc}(-H_{cc}^{-1}(E_c + E_c\alpha r^T)))\Delta P' \\ & + (H_c + E_c\alpha w_c^T + H_{cc}(-H_{cc}^{-1}(H_c + E_c\alpha w^T)))\Delta Q', \end{aligned} \tag{A.8}$$

where $w = [w_c^T\ w_u^T]^T$ and $r = [r_c^T\ r_u^T]^T$. Noting that $H_{cc}(-H_{cc}^{-1}) = -I_{cc}$, where $I_{cc} \in \mathbb{R}^{N_c \times N_c}$ is an identity matrix, (A.8) can be simplified to obtain

$$\begin{aligned} \Delta V_c \approx & (E_c + E_c\alpha r_c^T - E_c - E_c\alpha r^T)))\Delta P' \\ & + (H_c + E_c\alpha w_c^T - H_c - E_c\alpha w^T)))\Delta Q', \end{aligned}$$

the right-hand side of which is identically zero, as claimed.

A.2 Proof That $\Delta p_m = 0$

Now, recall that

$$\Delta p_m \approx \gamma^T \Delta P' + (\gamma^q)^T \Delta Q', \tag{A.9}$$

where

$$\gamma^T = r^T + r^T \alpha r^T + w_c^T U, \tag{A.10}$$

$$(\gamma^q)^T = w^T + r^T \alpha w^T + w_c^T W, \tag{A.11}$$

By substituting (A.2), (A.3), (A.10), and (A.11) into (A.9) we obtain

$$\begin{aligned}\Delta p_m \approx &(r^T + r^T \alpha r^T + w_c^T(-H_{cc}^{-1}(E_c + E_c \alpha r^T)))\Delta P' \\ &+(w^T + r^T \alpha w^T + w_c^T(-H_{cc}^{-1}(H_c + E_c \alpha w^T)))\Delta Q',\end{aligned} \tag{A.12}$$

which we simplify as follows:

$$\begin{aligned}\Delta p_m \approx &((r^T - w_c^T H_{cc}^{-1} E_c) + (r^T - w_c^T H_{cc}^{-1} E_c)\alpha r^T)\Delta P' \\ &+((w^T - w_c^T H_{cc}^{-1} H_c) + (r^T \alpha w^T - w_c^T H_{cc}^{-1} E_c \alpha w^T))\Delta Q'.\end{aligned} \tag{A.13}$$

By the definition of the inverse Jacobian and our defined partitions in (A.1), we have that $r = \frac{\partial p_m}{\partial \tilde{P}}$, $w = \frac{\partial p_m}{\partial \tilde{Q}}$, $w_c = \frac{\partial p_m}{\partial \tilde{Q}_c}$, $H_{cc}^{-1} = \frac{\partial \tilde{Q}_c}{\partial V_c}$, $E_c = \frac{\partial V_c}{\partial \tilde{P}}$, and $H_c = \frac{\partial V_c}{\partial \tilde{Q}}$, from which we have that

$$\begin{aligned}w_c^T H_{cc}^{-1} E_c &= \left[\frac{\partial p_m}{\partial \tilde{Q}_c}\right]^T \left[\frac{\partial \tilde{Q}_c}{\partial V_c}\right] \left[\frac{\partial V_c}{\partial \tilde{P}}\right] \\ &= \left[\frac{\partial p_m}{\partial \tilde{P}}\right]^T \\ &= r^T,\end{aligned} \tag{A.14}$$

and

$$\begin{aligned}w_c^T H_{cc}^{-1} H_c &= \left[\frac{\partial p_m}{\partial \tilde{Q}_c}\right]^T \left[\frac{\partial \tilde{Q}_c}{\partial V_c}\right] \left[\frac{\partial V_c}{\partial \tilde{Q}}\right] \\ &= \left[\frac{\partial p_m}{\partial \tilde{Q}}\right]^T \\ &= w^T.\end{aligned} \tag{A.15}$$

Now, by substituting (A.14) and (A.15) into (A.16), we obtain

$$\begin{aligned}\Delta p_m \approx &((r^T - r^T) + (r^T - r^T)\alpha r^T)\Delta P' \\ &+((w^T - w^T) + (r^T \alpha w^T - r^T \alpha w^T))\Delta Q',\end{aligned} \tag{A.16}$$

the right-had side of which is identically zero, as claimed.

APPENDIX B

CASE STUDY: POWER FLOW SENSITIVITY VARIATION WITH OPERATING POINT

The measurement-based sensitivity estimation approach harnessed throughout this thesis rests on two fundamental assumptions:

A1. The regressor matrix is nonsingular.

A2. The sensitivity we estimate remains constant over all measurements in the measurement window.

In this appendix, we present some illustrative examples that provide empirical evidence in support of assumption A2—ensuring the validity of assumption A1 depends on the selection of the estimation parameters M and f discussed in Section 5.4.1. Our aim is to show that many of the power flow sensitivities remain relatively constant over a wide range of operating conditions, i.e., the range of operating conditions that would arise during the measurement window in a practical measurement-based sensitivity estimation. Primarily, we focus on the ISFs, which are used to formulate network and security constraints in the SCED, as well as AFs used with the ISFs to formulate the LOAFs. In addition, we show that the LFs vary approximately linearly with the operating point, which conforms to our assumption in Chapter 4 that the line losses on a line are approximately quadratic with respect to the active power flow on the line.

We conduct the simulations presented in these examples on the 6-bus test system shown in Fig. 3.1 around the nominal power flow solution provided with the case (see Section 3.5 for details). To demonstrate the variation of the sensitivities with changes in the operating point, we vary the active and reactive power withdrawn at bus 4, a non-voltage controlled bus, around the nominal operating point by ± 0.5 p.u. in increments of 0.1 p.u; the active and reactive power variations are conducted independently. We solve the ac power flow using the single slack bus, bus 1, at each active or reactive power increment. The sensitivities are estimate by taking the difference of

the relevant quantity at increment $i+1$ and that at increment i divided by the change in active or reactive power, i.e. 0.1 p.u. For example, the ISF for a line ℓ_l at the operating point for increment i was estimated as $\Psi_i[l,4] \approx (P_l^f(i+1) - P_l^f(i))/0.1$.

B.1 Active Power Injection Variation Impacts on Power Flow Sensitivities

In this section, we illustrate the sensitivity of the ISFs, AFs, and LFs to changes in the active power consumed at bus 4. In Fig. B.1, we show the empirical ISFs computed at each active power increment. As shown in the figure, the ISFs are approximately constant over the range of active power consumption.

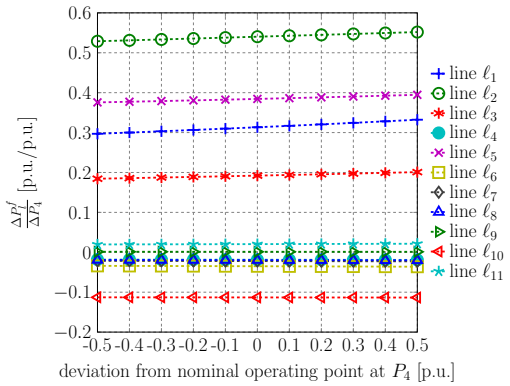

Figure B.1: Variation in the ISFs with respect to the bus 4 active power injection, P_4.

The changes that do appear in the ISFs, e.g. on lines ℓ_1, ℓ_2, and ℓ_4, are due to increases in the system-wide active power losses as we increase P_4, which as we show in Fig. B.2, are quadratic in the active power injection at bus 4.

The relationship of the line losses on a line ℓ_l due to the flow on the line is of interest in the derivation of the LOAFs. In Fig. B.3, we show the line losses on line ℓ_1 plotted against the line flows on line ℓ_1 at each increment in the active power consumption at bus 4. Moreover, we show in the figure a second-order polynomial fit between the line losses and line flow for line ℓ_1. The accuracy of the fit lends credence to the validity of the assumption of a

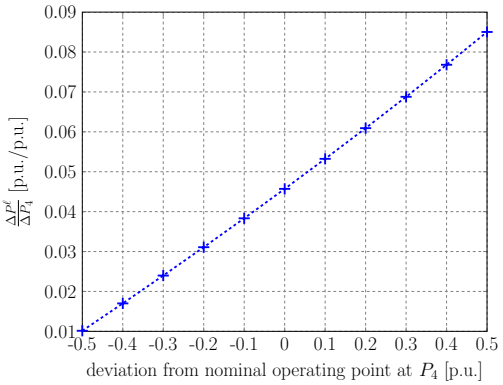

Figure B.2: Variation in the bus 4 LF with respect to the bus 4 active power injection, P_4.

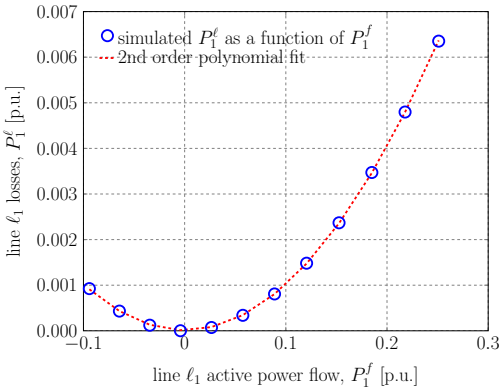

Figure B.3: Line ℓ_1 losses as a function of line ℓ_1 active power flow due to deviation in bus 4 active power injection, P_4 away from nominal operating point.

quadratic relationship between P_l^ℓ and P_l^f used in the LOAF derivation in Chapter 4. The relationship shown in Fig. B.3 makes intuitive sense as the losses on line ℓ_1 are quadratically related to the current flowing through the line.

Finally, in Fig. B.4 we show the variation in the active power AFs with respect to the bus 4 active power variation. As in the case of the ISFs, the AFs are relatively constant across the range of active power consumption. The relative invariance of the AFs and ISFs to changes in active power consumptions is a major contributing factor to the high accuracy of the LOAFs when used to predict outage angles.

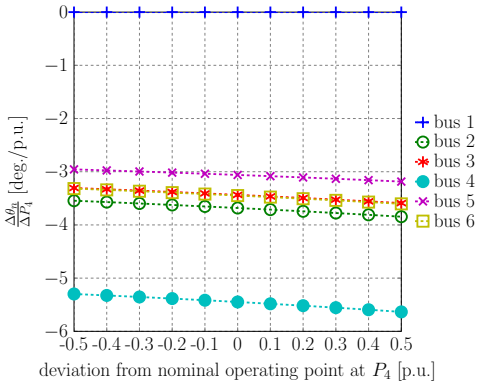

Figure B.4: Variation in the AFs with respect to the bus 4 active power injection, P_4.

B.2 Reactive Power Injection Variation Impacts on Power Flow Sensitivities

In this section, we illustrate the sensitivity of the ISFs, AFs, and LFs to changes in the reactive power consumed at bus 4. In Fig. B.5, we show the empirical ISFs computed at each reactive power increment. As shown in the

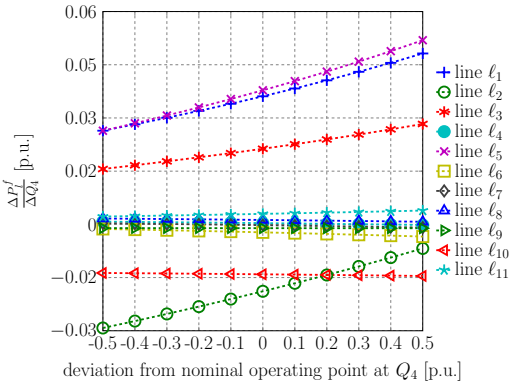

Figure B.5: Variation in the reactive ISFs with respect to the bus 4 reactive power injection, Q_4.

figure, the ISFs are vary considerably on lines ℓ_1, ℓ_2, ℓ_3, and ℓ_5, which are the lines that connect bus 4 to the voltage controlled buses which supply reactive power to the system. This variation, which is largely linear, is due to the variation in the active power losses, shown in Fig. B.6, that occur due to variations in the reactive power consumed at bus 4. Unlike in the case of the active power variation shown in Fig. B.1, for which the losses account only for a small proportion of the active power transfers on the lines due to changes

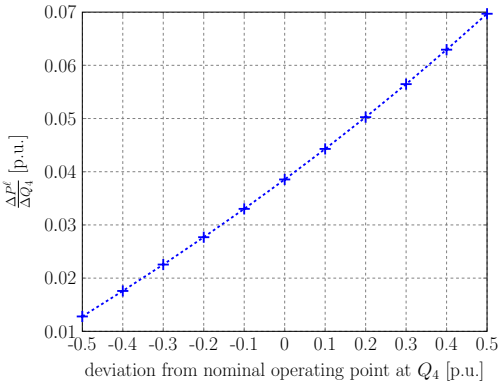

Figure B.6: Variation in the bus 4 reactive LF with respect to the bus 4 reactive power injection, Q_4.

in active power consumption, in the case of the reactive power variation, the active power flow changes on the lines are due entirely to changes in the losses. Thus, the reactive power ISFs exhibit the same characteristics as the reactive power LFs in response to reactive power injection changes.

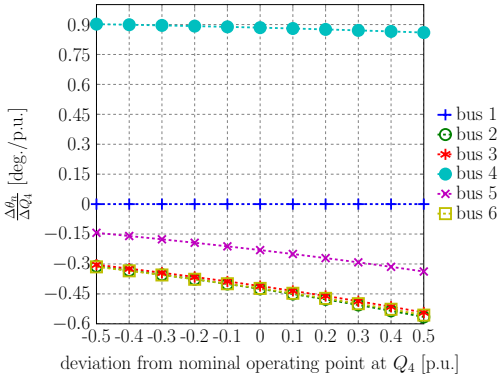

Figure B.7: Variation in the reactive AFs with respect to the bus 4 reactive power injection, Q_4.

Figure B.7 shows the variation in the reactive power AFs with respect to changes in the bus 4 reactive power injection. As in the case of the reactive ISFs, the reactive AFs exhibit linear change with the reactive power consumption variation due to the dependence of those changes on the active power losses. We also note that the reactive power ISFs and AFs are roughly an order of magnitude less than their active power counterparts.

REFERENCES

[1] NERC, "Reliability concepts v 1.0.2," 2007, Accessed: Dec. 9, 2014. [Online]. Available: http://www.nerc.com/files/concepts_v1.0.2.pdf

[2] U.S.-Canada Power System Outage Task Force, "Final report on the August 14, 2003 blackout in the United States and Canada: Causes and recommendations," 2004, accessed Feb 12, 2015.

[3] NERC and FERC, "Arizona-Southern California outages on September 8, 2011," 2012, accessed Nov. 4, 2014.

[4] A. Monticelli, *State Estimation in Electric Power Systems: A Generalized Approach*. Kluwer Academic Publishers, 1999.

[5] NASPI, "Synchrophasor technical fact sheet," 2014, accessed Feb. 12, 2015. [Online]. Available: https://www.naspi.org/File.aspx?fileID=1326

[6] A. Silverstein, "Diagnosing equipment health & mis-operations with PMU data," North American SynchroPhasor Initiative, Tech. Report, May 2015.

[7] Y. Chen, A. Domínguez-García, and P. Sauer, "Generalized injection shift factors and application to estimation of power flow transients," in *Proc. of North American Power Symposium*, Pullman, Wa, 2014.

[8] General Electric, "Multilin L90 line current differential system," 2013, accessed Aug. 25, 2015. [Online]. Available: http://www.gedigitalenergy.com/products/brochures/l90.pdf

[9] L. Kirchmayer, *Economic Operation of Power Systems*. Wiley, 1958.

[10] L. Kirchmayer and G. Stagg, "Analysis of total and incremental losses in transmission systems," *Trans. Amer. Inst. of Elec. Eng.*, vol. 70, no. 2, pp. 1197–1205, 1951.

[11] F. Alvarado, "Penalty factors from Newton's method," *IEEE Trans. Power App. Syst.*, vol. PAS-97, no. 6, pp. 2031–2040, Nov. 1978.

[12] D. Kothari and J. Dhillon, *Power System Optimization*, 1st ed. PHI Learning Private Limited, 2011.

[13] B. Wood, B. Wollenberg, and G. Sheblé, *Power Generation, Operation, and Control*, 3rd ed. John Wiley and Sons, Inc., 2014.

[14] E. Litvinov, T. Zheng, G. Rosenwald, and P. Shamsollahi, "Marginal loss modeling in LMP calculation," *IEEE Trans. Power Syst.*, vol. 19, no. 2, pp. 880–888, May 2004.

[15] Midcontinent Independent System Operator, "MISO tariff, module C—Energy and operating reserve markets," 2014, accessed Jan. 10, 2014. [Online]. Available: https://www.misoenergy.org/Library/Tariff/Pages/Tariff.aspx

[16] California Indendent System Operator, "CAISO tariff, appendix c: Locational marginal prices," 2014, accessed Jan. 10, 2015. [Online]. Available: http://www.caiso.com/Documents/AppendixC_LocationalMarginalPrice_Nov19_2014.pdf

[17] Monitoring Analytics, "PJM state of the market," 2014, Accessed: Feb. 2, 2015. [Online]. Available: http://www.monitoringanalytics.com/reports/PJM_State_of_the_Market/2014.shtml

[18] Y. Chen, A. Domínguez-García, and P. Sauer, "Measurement-based estimation of linear sensitivity distribution factors and applications," *IEEE Trans. Power Syst.*, vol. 29, no. 3, pp. 1372–1382, May 2014.

[19] Y. Chen, J. Wang, A. Domínguez-García, and P. Sauer, "Measurement-based estimation of the power flow jacobian matrix," submitted for publication.

[20] NERC, "NERC training document: Synchronizing islands overview," 2002, Accessed: February 28, 2015. [Online]. Available: http://icourseplayer.360training.com/courses/course1156/pdf/04_nerc_si01_sync_island_training01r.pdf

[21] N. Srinivasan, K. Prakasa, C. Indulkar, and S. Venkata, "On-line compuation of phase shifter distribution factors and lineload alleviation," *IEEE Trans. Power App. Syst.*, vol. PAS-104, no. 7, pp. 1656–1662, July 1985.

[22] P. Sauer, K. Reinhard, and T. Overbye, "Extended factors for linear contingency analysis," in *Proc. of Hawaii International Conference on System Sciences*, Jan. 2001, pp. 697–703.

[23] "2009 state of the markets report," ISO/RTO Council, Tech. Rep., 2010.

[24] California Indendent System Operator, "CAISO markets and processes," 2014, accessed Nov. 4, 2014. [Online]. Available: http://www.caiso.com/Documents/Section27CAISOMarketsAndProcessesOct12014.pdf

[25] Independent System Operator of New England, "M-11 market operations," 2014, accessed Nov. 4, 2014. [Online]. Available: http://www.iso-ne.com/participate/rules-procedures/manuals

[26] A. Ott, "Experience with PJM market operations, system design, and implementation," *IEEE Trans. Power Syst.*, vol. 18, no. 2, pp. 528–534, May 2003.

[27] O. Alsaç and B. Stott, "Optimal load flow with steady-state security," *IEEE Trans. Power App. Syst.*, vol. PAS-93, no. 3, pp. 745–751, May 1974.

[28] F. Capitanescu, J. Martinez Ramos, P. Panciatici, D. Kirschen, A. Marano Marcolini, L. Platbrood, and L. Wehenkel, "State-of-the-art, challenges, and future trends in security constrained optimal power flow," *Electric Power Systems Research*, vol. 81, no. 8, pp. 1731–1741, 2011.

[29] A. Ardakani and F. Bouffard, "Identification of umbrella contraints in dc-based security-constrained optimal power flow," *IEEE Trans. Power Syst.*, vol. 28, no. 4, pp. 3924–3934, Nov. 2013.

[30] Y. Liu, M. Ferris, and F. Zhao, "Computational study of security constrained economic dispatch with multi-stage rescheduling," *IEEE Trans. Power Syst.*, vol. 30, no. 2, pp. 920–929, Mar. 2015.

[31] Y. Chen and P. Gribik, "Incorporating post zonal reserve deployment transmission constraints into energy and ancillary service co-optimization," *IEEE Trans. Power Syst.*, vol. 29, no. 2, pp. 537–549, Mar. 2014.

[32] F. Bouffard, F. Galiana, and A. Conejo, "Market-clearing with stochastic security—Part I: Formulation," *IEEE Trans. Power Syst.*, vol. 20, no. 4, pp. 1818–1826, Nov. 2005.

[33] A. Sakis Meliopoulos, B. Fardanesh, and S. Zelingher, "Power system state estimation: Modeling error effects and impacts on system operation," in *Proc. of the Hawaii International Conference on System Sciences*, Jan. 2001.

[34] K. Poon, R. Emami, A. Bose, and A. Abur, "External data exchange issues for state estimation in power systems," *IEEE Trans. Power Syst.*, vol. 27, no. 2, pp. 849–856, May 2012.

[35] IEEE Working Group D6, "AC transmission line model parameter validation," Prepared for the Line Protection Subcommittee of the Power System Relay Committee of the IEEE Power & Energy Society, Tech. Rep., 2014.

[36] M. Bŏkarjova and A. Göran, "Transmission line conductor temperature impact on state estimation accuracy," in *Proc. of the IEEE POWERTECH Conference*, July 2007.

[37] K. Clements and P. Davis, "Detection and identification of topology errors in electric power systems," *IEEE Trans. Power Syst.*, vol. 3, no. 4, pp. 1748–1753, Nov. 1988.

[38] H. Singh and F. Alvarado, "Network topology determination using least absolute value state estimation," *IEEE Trans. Power Syst.*, vol. 10, no. 3, pp. 1159–1165, Aug. 1995.

[39] F. Wu and W. Liu, "Detection of topology erros by state estimation [power systems]," *IEEE Trans. Power Syst.*, vol. 4, no. 1, pp. 176–183, Jan. 1989.

[40] California Indendent System Operator, "Business practice manual for manging full network model," 2014, accessed Jan. 4, 2015. [Online]. Available: http://bpmcm.caiso.com/Pages/BPMDetails.aspx?BPM=Managing%20Full%20Network%20Model

[41] NERC, "Lesson learned: Real-time contingency analysis failure due to a modeling error," June 2015.

[42] T. Güller, G. Gross, and M. Liu, "Generalized line outage distribution factors," *IEEE Trans. Power Syst.*, vol. 22, no. 2, pp. 879–881, May 2007.

[43] Y. Chen, A. Domínguez-García, and P. Sauer, "A sparse representation approach to online estimation of power system distribution factors," *IEEE Trans. Power Syst.*, vol. 30, no. 4, pp. 1727–1738, July 2015.

[44] K. Van Horn, A. Domínguez-García, and P. Sauer, "Measurement-based loss factor estimation," submitted for publication.

[45] Midcontinent Independent System Operator, "MISO phase angle differences monitoring and control," Whitepaper, May 2014.

[46] K. Van Horn, A. Domínguez-García, and P. Sauer, "Sensitivity-based line outage angle factors," in *Proc. of North American Power Symposium*, 2015.

[47] K. Van Horn, A. Domínguez-García, and P. Sauer, "Generalized line outage angle factors," submitted for publication.

[48] K. Van Horn, A. Domínguez-García, and P. Sauer, "Measurement-based real-time economic dispatch," in *Proc. of IEEE Power and Energy Society General Meeting*, 2015.

[49] K. Van Horn, A. Domínguez-García, and P. Sauer, "Measurement-based real-time security-constrained economic dispatch," *IEEE Trans. Power Syst.*, to be published.

[50] T. Orfanogianni and G. Gross, "A general formulation for LMP evaluation," *IEEE Trans. Power Syst.*, vol. 22, no. 3, pp. 1163–1173, Aug. 2007.

[51] G. Strang, *Linear Algebra and its Applications*, 3rd ed. Harcourt, Brace, Jovanovich, Publishers, 1988.

[52] P. Krugman and R. Wells, *Microeconomics*. Worth, 2005.

[53] D. Kirschen and G. Strbac, *Fundamentals of Power System Economics*. West Sussex, England: John Wiley and Sons Ltd., 2004.

[54] B. Stott, J. Jardim, and O. Alsaç, "DC power flow revisited," *IEEE Trans. Power Syst.*, vol. 24, no. 3, pp. 1290–1300, Aug. 2009.

[55] Electric Power Group, "Synchro-phasor data conditioning and validation project phase 1, task 3 report: Algorithms and methods for data validation and conditioning," 2014, accessed June 1, 2015. [Online]. Available: https://www.naspi.org/File.aspx?fileID=1306

[56] R. Zimmerman, C. Murillo-Sanchez, and R. Thomas, "Matpower: Steady-state operations, planning and analysis tools for power systems research and education," *IEEE Trans. Power Syst.*, vol. 26, no. 1, pp. 12–19, Feb. 2011.

[57] University of Washington, "Power systems test case archive," 1993, accessed Nov. 20, 2014. [Online]. Available: http://www.ee.washington.edu/research/pstca/pf118/pg_tca118bus.htm

[58] E. Makram, M. Vutsinas, A. Girgis, and Z. Zhao, "Contingency analysis using synchrophasor measurements," *Electric Power Systems Research*, vol. 88, pp. 64–68, 2012.

[59] A. Monticelli, M. Pereira, and S. Granville, "Security-constrained optimal power flow with post-contingency corrective rescheduling," *IEEE Trans. Power App. Syst.*, vol. 2, no. 1, pp. 175–180, Feb. 1987.

[60] J. Dondeti, P. Addepalle, C. Yang, and B. Buescher, "MISO experiences of network model maintenance—State estimator and contingency analysis accuracy," in *Proc. of IEEE Power and Energy Society General Meeting*, 2014.

[61] X. Cheng and T. Overbye, "An energy reference bus independent LMP decomposition algorithm," *IEEE Trans. Power Syst.*, vol. 21, no. 3, pp. 1041–1049, Aug. 2006.

[62] R. Isermann, *Fault-Diagnosis Systems: An Introduction from Fault Detection to Fault Tolerance.* Springer, 2006.

[63] S. Haykin, *Adaptive Filter Theory.* Prentice Hall, 1996.

[64] L. Ljung and T. Söderström, *Theory and Practice of Recursive Identification.* MIT Press, 1983.